

ผลกระทบของ MCM-41 ที่ถูกปรับปรุงด้วยโบรอนต่อตัวเร่งปฏิกิริยา Co/MCM-41
สำหรับปฏิกิริยาคาร์บอนมอนอกไซด์ ไฮโดรจิเนชัน



นายพิมพ์ชนก ทุกะบุตร

สถาบันวิทยบริการ

จุฬาลงกรณ์มหาวิทยาลัย

วิทยานิพนธ์นี้เป็นส่วนหนึ่งของการศึกษาตามหลักสูตรปริญญาวิศวกรรมศาสตรมหาบัณฑิต

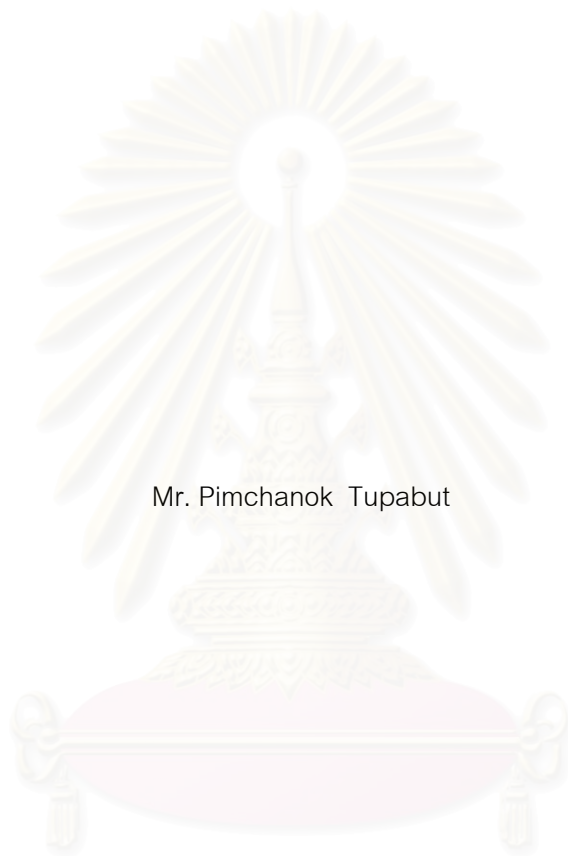
สาขาวิชาวิศวกรรมเคมี ภาควิชาวิศวกรรมเคมี

คณะวิศวกรรมศาสตร์ จุฬาลงกรณ์มหาวิทยาลัย

ปีการศึกษา 2549

ลิขสิทธิ์ของจุฬาลงกรณ์มหาวิทยาลัย

EFFECT OF BORON-MODIFIED MCM-41 ON COBALT/MCM-41 CATALYST FOR
CARBON MONOXIDE HYDROGENATION



Mr. Pimchanok Tupabut

สถาบันวิทยบริการ
A Thesis Submitted in Partial Fulfillment of the Requirements
for the Degree of Master of Engineering Program in Chemical Engineering
Department of Chemical Engineering
Faculty of Engineering
Chulalongkorn University
Academic Year 2006


Thesis Title EFFECT OF BORON-MODIFIED MCM-41 ON COBALT/MCM-41
CATALYST FOR CARBON MONOXIDE HYDROGENATION

By Mr. Pimchanok Tupabut

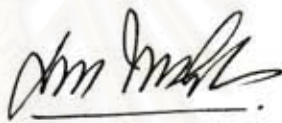
Field of Study Chemical Engineering

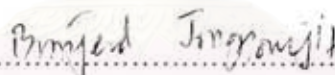
Thesis Advisor Assistant Professor Bunjerd Jongsomjit, Ph.D

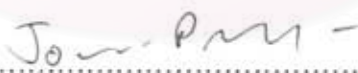
Accepted by the Faculty of Engineering, Chulalongkorn University in Partial
Fulfillment of the Requirements for the Master's Degree



..... Dean of the Faculty of Engineering
(Professor Direk Lavansiri, Ph.D.)

THESIS COMMITTEE


..... Chairman
(Associate Professor ML Suppakano Thongyai)


..... Thesis Advisor
(Assistant Professor Bunjerd Jongsomjit, Ph.D.)


..... Member
(Assistant Professor Joongjai Panpranot, Ph.D.)


..... Member
(Assistant Professor Muenduen Phisalaphong, Ph.D.)


..... Member
(Assistant Professor Okorn Mekasuwandamrong, Ph.D.)

พิมพ์ชนก ทุกะบุตร:ผลกระทบของ MCM-41 ที่ถูกปรับปรุงด้วยโบรอนต่อตัวเร่งปฏิกิริยา Co/MCM-41 สำหรับปฏิกิริยาคาร์บอนมอนอกไซด์ ไฮโดรจิเนชัน (EFFECT OF BORON-MODIFIED MCM-41 ON COBALT/MCM-41 CATALYST FOR CARBON MONOXIDE HYDROGENATION) อ. ที่ปรึกษา : ผศ. ดร. บรรเจิด จงสมจิตร, 106 หน้า

วิทยานิพนธ์นี้ศึกษาถึงคุณลักษณะและความว่องไวในการเร่งปฏิกิริยา ไฮโดรจิเนชันของคาร์บอนมอนอกไซด์ที่แตกต่างกันระหว่าง ตัวเร่งปฏิกิริยาโคบอลต์ที่กระจายตัวอยู่บนตัวรองรับ MCM-41 ที่ถูกปรับปรุงด้วยโบรอนในอัตราส่วนต่างๆ โดยอัตราส่วนระหว่าง MCM-41 ต่อโบรอนถูกเตรียมขึ้นที่อัตราส่วนต่างๆกันโดยน้ำหนัก ด้วยวิธีฝังเกลือ MCM-41 ด้วยโบรอนแล้วนำไปเผาในอากาศ หลังจากนั้นนำไปฝังเกลืออีกครั้งด้วยโคบอลต์อัตราส่วนต่างๆกันโดยน้ำหนัก หลังจากการเผาในอากาศ ตัวอย่างต่างๆจะถูกนำไปตรวจสอบคุณลักษณะ โดยใช้การดูดซับทางกายภาพด้วยไนโตรเจน การกระเจิงรังสีเอ็กซ์ การส่องผ่านด้วยกล้องจุลทรรศน์อิเล็กตรอน การวัดการกระจายตัวของโลหะ การส่องกราดด้วยกล้องจุลทรรศน์อิเล็กตรอน การวัดกัมมันตภาพรังสี และการดูดซับด้วยไฮโดรเจน ปฏิกิริยาไฮโดรจิเนชันของคาร์บอนมอนอกไซด์ (มีอัตราส่วนของไฮโดรเจนต่อคาร์บอนมอนอกไซด์=10/1) ถูกใช้เพื่อทดสอบความว่องไวของตัวเร่งปฏิกิริยาและการเลือกเกิดของผลิตภัณฑ์ ผลการศึกษาแสดงให้เห็นว่าขนาดของโคบอลต์ออกไซด์ขึ้นอยู่กับปริมาณ โบรอนที่ปรับปรุงทั้งนี้ตัวแปรที่มีผลกระทบต่อกลไกของการวัดกัมมันตภาพรังสี ได้แก่ ขนาดอนุภาค, อันตรกิริยาของตัวรองรับ และปริมาณของโบรอน โดยพบว่าตัวเร่งปฏิกิริยาที่กระจายตัวอยู่บนตัวรองรับ MCM-41 จะมีความว่องไวลดลงเนื่องจากความสามารถในการรีดิวที่ลดลง เมื่อปริมาณโบรอนที่สูงขึ้นและยังพบว่า ความว่องไวของตัวเร่งปฏิกิริยาจะลดลงเมื่อปริมาณโคบอลต์ลดลงทำให้ความสามารถในการรีดิวลดลง ส่วนสามารถในการเกิดไฮโดรคาร์บอนที่โมเลกุลใหญ่สูงขึ้นเล็กน้อยเมื่อปริมาณโบรอนสูงขึ้น

สถาบันวิทยบริการ จุฬาลงกรณ์มหาวิทยาลัย

ภาควิชา.....วิศวกรรมเคมี..... ลายมือชื่อผู้นิสิต.....
สาขาวิชา.....วิศวกรรมเคมี..... ลายมือชื่ออาจารย์ที่ปรึกษา.....
ปีการศึกษา.....2549.....

##4870405921: MAJOR CHEMICAL ENGINEERING

KEY WORD: COBALT CATALYST/ MCM-41/ SUPPORT/ BORON
MODIFICATION/ CO HYDROGENATION

PIMCHANOK TUPABUT: EFFECT OF BORON-MODIFIED MCM-41 ON
COBALT/MCM-41 CATALYST FOR CARBON MONOXIDE
HYDROGENATION. THESIS ADVISOR: BUNJERD JONGSOMJIT,
Ph.D., 106 pp.

In the present study, differences in characteristics and catalytic activity towards CO hydrogenation of Co catalysts dispersed on various boron-modified MCM-41 supports were investigated. The various weight ratios of MCM-41/B were prepared by incipient wetness impregnation method, then calcined them in air. Then, consequently impregnated with the cobalt precursor. After calcination, the various samples were characterized using N₂ physisorption, XRD, SEM/EDX, TEM, TPR and H₂ chemisorption. CO hydrogenation (H₂/CO = 10/1) was also performed to determine the overall activity and selectivity. It revealed that the size of Co oxide species depends on the boron content on modification support. A wide range of variables including particle size, support interaction, and the boron content can affect the kinetics of reduction. It was found that for the boron modified MCM-41 catalyst, the catalyst dispersed on the high boron content support exhibited low activities due to low reducibility. With small amount of cobalt loading, activity decreased due to a decrease in reducibility. Selectivity to C₂-C₄ products slightly increased with increasing boron loading.

สถาบันวิทยบริการ
จุฬาลงกรณ์มหาวิทยาลัย

Department.....Chemical Engineering... Student's signature.....*Pimchanok Tupabut*
Field of study...Chemical Engineering... Advisor's signature.....*Bunjerd Jongsomjit*
Academic year.....2006.....

ACKNOWLEDGEMENTS

The author would like to express his greatest gratitude and appreciation to his advisor, Dr, Bunjerd Jongsomjit for his invaluable guidance, providing value suggestions and his kind supervision throughout this study. In addition, he is also grateful to Associate Professor ML Suppakankong Thongyai, as the chairman, Assistant Professor Muenduen Phisalaphong, Assistant Professor Joongjai Panpranot and Assistant Professor Okorn Mekasuwandamrong as the members of the thesis committee. The financial supports from the Thailand Reserch Fund (TRF) and the graduate school of Chulalongkorn University (90th Anniversary of CU under the Golden Tubilee Fund) are also gratefully acknowledged.

Many thanks for kind suggestions and useful help to Miss Sujittra Kittiruangrayub, Mr. Narakorn Chanprasert, Miss Nitinart Chitpong, and many friends in the petrochemical laboratory who always provide the encouragement and co-operate along the thesis study.

Most of all, the author would like to express his greatest gratitude to his parents and his family who always pay attention to his all the times for suggestions, support and encouragement.

สถาบันวิทยบริการ
จุฬาลงกรณ์มหาวิทยาลัย

CONTENTS

	page
ABSTRACT (IN THAI).....	iv
ABSTRACT (IN ENGLISH).....	v
ACKNOWLEDGMENTS.....	vi
CONTENTS.....	vii
LIST OF TABLES.....	x
LIST OF FIGURES.....	xi
CHAPTER	
I INTRODUCTION.....	1
II LITERATER REVIEWS.....	3
2.1 Silica supported cobalt catalysts.....	3
2.2 MCM-41 supported cobalt catalysts	9
2.3 Boron-modified supported cobalt catalyst.....	12
III THEORY.....	16
3.1 Fischer-Tropsch synthesis (FTS)	16
3.1.1 The surface carbide mechanism.....	19
3.1.2 The hydroxycarbene mechanism.....	21
3.1.3 The CO insertion mechanism.....	22
3.2 Cobalt.....	24
3.2.1 General.....	24
3.2.2 Physical properties.....	24
3.2.3 Cobalt oxides.....	27
3.3 Cobalt-based catalysts.....	27
3.4 Cobalt-support compound formation (Co-SCF).....	28
3.4.1 Co-Silicate Formation.....	28
3.5 Silicon dioxide	29
3.5.1 General feature of silica.....	29
3.6 MCM-41.....	33
3.6.1 General feature of MCM-41.....	33
IV EXPERIMENTS.....	39
4.1 Catalyst preparation.....	39

	page
4.1.1 Chemicals.....	39
4.1.2 Preparation of MCM-41 supports.....	40
4.1.3 Preparation of the boron-modified MCM-41.....	40
4.1.4 Preparation of the supported Co samples	40
4.1.5 Sample nomenclature	41
4.2 Catalyst characterization.....	41
4.2.1 N ₂ physisorption.....	41
4.2.2 X-ray diffraction (XRD).....	42
4.2.3 Temperature programmed reduction (TPR).....	42
4.2.4 Scanning Electron Microscopy.....	43
4.2.5 Transmission Electron Microscopy (TEM).....	43
4.2.6 Hydrogen chemisorption	43
4.3 Reaction study in CO hydrogenation.....	43
4.3.1 Materials.....	43
4.3.2 Apparatus.....	44
4.3.3 Procedures.....	45
V RESULTS AND DISCUSSION	49
5.1 Various boron loading of 20 wt% cobalt on boron-modified MCM-41 supported catalyst.....	49
5.2 Various Co loading of 3 wt% boron-modified MCM-41 supported catalyst.....	71
VI CONCLUSIONS AND RECOMMENDATIONS.....	89
6.1 Conclusions.....	89
6.2 Recommendations.....	90
REFERENCES.....	91
APPENDICES.....	96
APPENDIX A: CALCULATION FOR CATALYST PREPARATION.....	97
APPENDIX B: CALCULATION FOR TOTAL H ₂ CHEMISORPTION AND DISPERSION.....	99
APPENDIX C: CALIBRATION CURVES.....	101
APPENDIX D: CALCULATION OF CO CONVERSION, REACTION RATE AND SELECTIVITY.....	104

	page
APPENDIX E: LIST OF PUBLICATIONS.....	105
VITAE	106



สถาบันวิทยบริการ
จุฬาลงกรณ์มหาวิทยาลัย

LIST OF TABLES

Table	page
3.1 Physical properties of cobalt	25
3.2 Physical properties of silica	29
4.1 Chemicals used in the preparation of catalysts.....	39
4.2 Operating condition for gas chromatograph.....	45
5.1 BET surface area measurement of 20 wt% cobalt on boron-modified supported cobalt catalyst.....	49
5.2 Results of H ₂ chemisorption, steady-state rate and selectivity to products.....	70
5.3 BET surface area measurement of 3 wt% boron-modified supported cobalt catalyst.....	71
5.4 Results of H ₂ chemisorption, steady-state rate and selectivity to product.....	88
B.1 H ₂ chemisorption results for various boron-modified supported Co catalysts samples.....	99
C.1 Conditions use in Shimadzu modal GC-8A and GC-14B.....	100



 สถาบันวิทยบริการ
 จุฬาลงกรณ์มหาวิทยาลัย

LIST OF FIGURES

Figure	page
3.1 Two hexagonal channels of MCM41, linked to its 3D structural pdb file.....	33
3.2 Methane and ethane inside one of the hexagonal pores of molecular sieve MCM-41.....	34
4.1 Flow diagram of CO hydrogenation system.....	47
5.1 XRD patterns of the boron-modified supports before impregnation with the cobalt precursor.....	51
5.2 XRD patterns of the boron-modified-supported Co catalyst.....	52
5.3 SEM micrograph and EDX mapping for 20-Co/SiB-0 catalyst granule	54
5.4 SEM micrograph and EDX mapping for 20-Co/SiB-1 catalyst granule	55
5.5 SEM micrograph and EDX mapping for 20-Co/SiB-3catalyst granule	56
5.6 SEM micrograph and EDX mapping for 20-Co/SiB-5 catalyst granule	57
5.7 SEM micrograph and EDX mapping for 20-Co/MB-0 catalyst granule	58
5.8 SEM micrograph and EDX mapping for 20-Co/MB-1 catalyst granule	59
5.9 SEM micrograph and EDX mapping for 20-Co/MB-3 catalyst granule	60
5.10 SEM micrograph and EDX mapping for 20-Co/MB-5 catalyst granule.....	61
5.11 TEM micrographs of pure silica, pure MCM-41 and 3 wt% of boron- modified supports.....	63
5.12 TEM micrographs of boron-modified MCM-41 supports and 5 wt% of boron-modified MCM-41 supported Co catalyst structure.....	64
5.13 TEM micrographs for all cobalt dispersed on the boron-modified silica supports.....	65
5.14 TEM micrographs for all cobalt dispersed on the boron-modified MCM-41 supports.....	66
5.15 TPR profiles for the boron-modified-supported Co catalyst.....	68
5.16 XRD patterns of the 3 wt% of boron-modified-supported Co catalyst.....	72
5.17 SEM micrograph and EDX mapping for 5-Co/SiB-3 catalyst granule.....	74
5.18 SEM micrograph and EDX mapping for 10-Co/SiB-3 catalyst granule.....	75
5.19 SEM micrograph and EDX mapping for 15-Co/SiB-3 catalyst granule.....	76
5.20 SEM micrograph and EDX mapping for 20-Co/SiB-3 catalyst granule.....	77

LIST OF FIGURES

Figure	page
5.21 SEM micrograph and EDX mapping for 5-Co/MB-3 catalyst granule.....	78
5.22 SEM micrograph and EDX mapping for 10-Co/MB-3 catalyst granule.....	79
5.23 SEM micrograph and EDX mapping for 15-Co/MB-3 catalyst granule.....	80
5.24 SEM micrograph and EDX mapping for 20-Co/MB-3 catalyst granule.....	81
5.25 TEM micrographs of all cobalt dispersed on 3 wt% of boron-modified silica supports.....	83
5.26 TEM micrographs of all cobalt dispersed on 3 wt% of boron-modified MCM-41 supports.....	84
5.27 TPR profiles for the 3 wt% of boron-modified-supported Co catalyst.....	86
C.1 The calibration curve of methane.....	101
C.2 The calibration curve of ethylene.....	101
C.3 The chromatograms of catalyst sample from thermal conductivity detector, gas chromatography Shimadzu model 8A (Molecular sieve 5A column).....	102
C.4 The chromatograms of catalyst sample from flame ionization detector, gas chromatography Shimadzu model 14B (VZ10 column).....	102

CHAPTER I

INTRODUCTION

In general, a catalyst usually consists of three components; (i) a catalytic phase, (ii) a promoter, and (iii) a support or carrier. As known, the catalytic properties apparently depend upon the components as mentioned above. The catalytic phase can be metal, metal oxide, metal carbide and etc. The active form of the catalytic phase definitely depends on the specific reaction within the catalyst is applied. It is known that the performance of catalysts could be improved using a promoter such as noble metals. However, besides the consideration only in a catalytic phase and a promoter, it should be noted that a support could play a crucial role, especially as a dispersing medium for the catalytic phase. Hence, the nature of support can affect the catalytic properties based on the fact that the dispersion and interaction between a support and a catalytic phase can be altered with different supports.

It was reported that many inorganic supports such as SiO₂ (R. Oukaci *et al.*, 1999; R. Riva *et al.*, 2000; G.R. Moradi *et al.*, 2003; M. Shinoda *et al.*, 2004), MCM-41 (S. Suvanto *et al.*, 2000; J. Panpranot *et al.*, 2002; P. Concepción *et al.*, 2004; V. Cortés Corberán *et al.*, 2004), B (J. Li *et al.*, 2001; J. Li *et al.*, 2002; N.J. Coville *et al.*, 2002; Y. Brik *et al.*, 2002) have been extensively studied for many years. In particular, the use of modified support was also mentioned as one of the promising ways to obtain a suitable support. In the recent year, a significant development in zeolites has been tremendous. Therefore, many zeolites have brought much attention to the research in this field (J. Panpranot *et al.*, 2002). However, only few studies have been done on using a boron-modified support for a catalytic phase. In addition, it would be of great benefits to compare differences in characteristics between the catalytic phase dispersed on the silica support and MCM-41 support. This will lead to a significant development in a catalyst design.

In the present study, the properties of cobalt (Co) catalysts dispersed on various boron-modified MCM-41 supports for carbon monoxide (CO) hydrogenation reaction were investigated and compared with boron-modified silica supports. The study was scoped as follows:

1. Preparation of MCM-41 modified boron 1, 3, and 5 wt% catalysts support.
2. Preparation of MCM-41 modified boron 1, 3, and 5 wt% supported Co catalyst (5, 10, 15 and 20 wt% Co) using the incipient wetness impregnation method.
3. Preparation of silica modified boron 1, 3, and 5 wt% catalysts support.
4. Preparation of silica modified boron 1, 3, and 5 wt% supported Co catalyst (5, 10, 15 and 20 wt% Co) using the incipient wetness impregnation method.
5. Characterization of the catalyst samples using nitrogen physisorption, X-ray diffraction (XRD), temperature programmed reduction (TPR), hydrogen chemisorption, scanning electron microscopy (SEM) and energy dispersive X-ray spectroscopy (EDX) and transmission electron spectroscopy (TEM).
6. Reaction study of the catalyst samples in carbon monoxide (CO) hydrogenation at 220°C and 1 atm and a H₂/CO ratio of 10.

CHAPTER II

LITERATURE REVIEWS

There are several studies of silica, MCM-41 and boron-modified supported catalysts. Many researchers have found better knowledge about silica especially supported cobalt catalyst in Fischer-Tropsch synthesis. These reports are very useful and will use to develop works for the future.

2.1 Silica supported cobalt catalysts

R.C. Reuel and C.H. Bartholomew (1984) studied the effect of support and dispersion on the CO hydrogenation activity/selectivity properties of cobalt. They found that the specific activity and selectivity of cobalt in CO hydrogenation is a function of support, dispersion, metal loading and preparation. The order of decreasing CO hydrogenation activity at 1 atm and 225°C for catalysts containing 3wt% cobalt is $\text{Co/TiO}_2 > \text{Co/SiO}_2 > \text{Co/Al}_2\text{O}_3 > \text{Co/C} > \text{Co/MgO}$. The specific activity of cobalt best correlated with dispersion and extent of reduction. In the $\text{Co/Al}_2\text{O}_3$ system, activity and selectivity for high molecular weight hydrocarbons increase very significantly with increasing cobalt loading.

A. Feller *et al.* (1995) studied the addition of zirconium oxide chloride to the catalyst formulation of Co/SiO_2 . It leads to a higher reducibility of cobalt, due to the formation of a cobalt zirconium species, which can be reduced at lower temperatures than cobalt silicate. Furthermore, the metal particle size of cobalt is increased, but the size of cobalt clusters is reduced. The Co-Zr/SiO_2 catalysts were tested for their activity in the Fischer-Tropsch synthesis. The steady-state activity increased with increasing zirconium loading, which was attributed to the resistance against reoxidation of the larger cobalt particles and thus to the larger amounts of surface cobalt metal present at steady-state in the zirconium promote catalysts. Based on the assumption that the intrinsic activity of cobalt in these catalysts remains unchanged, the observed changes in selectivity could be explained on the basis of secondary reactions in the Fischer-Tropsch system. With increasing zirconium content the number of surface

metal atoms at steady-state conditions increases, leading to a higher extent of secondary reactions, but the size of the cobalt clusters decreases, leading to a decrease in the extent of secondary reactions. With increasing zirconium content the extent of secondary hydrogenation of olefins (e.g., ethene) passes a minimum, and the C_{5+} -selectivity passes a maximum due to readsorption of small, reactive organic product compounds, which can be incorporated in larger product compounds. Double bond isomerization increases with increasing zirconium content. This might be attributed to the catalytic activity of zirconia.

A. Kogelbauer *et al.* (1995) studied the formation of cobalt silicates on Co/SiO_2 under hydrothermal conditions. Hydrothermal treatment at $220^\circ C$ led to a catalyst with lower reducibility due to the formation of both reducible and nonreducible (at temperatures $< 900^\circ C$) Co silicates. They also showed that silicate was formed in catalysts which had been used for FT synthesis. No significant change occurred upon hydrothermal treatment of calcined catalyst. The presence of air during the hydrothermal treatment inhibited the formation of silicate and they proposed that the formation of silicate was linked to the presence of metallic cobalt.

J. Choi *et al.* (1995) investigated the reduction of cobalt catalysts supported on Al_2O_3 , SiO_2 and TiO_2 and the effect of metal loading on the reduction. He reported that the activation energy of reduction increased in the following order: $Co/SiO_2 > Co/Al_2O_3 > Co/TiO_2$. For different metal loading, the catalyst with the higher loading is more readily reducible than with the lower metal loading.

S. Ali *et al.* (1995) investigated the influence of Zr promotion of 20 wt% Co/SiO_2 on Fischer-Tropsch synthesis using catalysts prepared in different ways and having different loadings of Zr (up to 8.5 wt%). The catalysts were investigated using FTS ($H_2/CO=2$), H_2-D_2 exchange, and CO dissociation to provide insight into how Zr modifies the Co properties. The Zr-promoted exhibited higher overall rates of FTS compared to unpromoted Co/SiO_2 . The sequentially impregnated $Co/Zr/SiO_2$ catalysts appeared to be the most active. However, the co-impregnation method of preparation appeared to result in higher cobalt dispersion. While Zr promotion did not appear to promote or inhibit H_2 activation, hydrogen spillover may have been partly responsible

for enhancing the activity of the sequentially impregnated Zr/Co/SiO₂ catalysts. Zr also possibly created an active interface with Co that increased catalyst activity by facilitating Co dissociation. Although high levels of promotion tended to increase the selectivity for higher hydrocarbon, Zr appears to be primarily an excellent rate promoter for Co/SiO₂.

R. Oukaci *et al.* (1999) studied the catalyst support in both promoted and non-promoted cobalt catalysts was found to play a major role in influencing the overall hydrocarbon production rate with little or no effect on catalyst selectivity (except for titania) in both the fixed-bed and the slurry bubble column reactor. Zr oxide had a similar effect on the activity of Co/silica. Addition of ZrO₂ to the support prior to the impregnation of cobalt probably serves somewhat to hinder the formation of cobalt silicates. ZrO₂ was found, thus, to be an excellent F–T synthesis rate promoter for SiO₂-supported Co catalysts without any effect, negative or positive, on catalyst selectivity. However, the long-term protecting effect of the zirconia remains to be determined. It is also important to note the differences observed in the two reaction systems, i.e. fixed-bed versus slurry bubble column reactors.

V. Curtis *et al.* (1999) synthesized TiO₂- and SiO₂-supported cobalt Fischer-Tropsch catalysts load with low concentration of sulfur (100-2000 ppm) from different sources ((NH₄)₂S, (NH₄)₂SO₄, and (NH₄)₂SO₃) and characterized using diffuse reflectance infrared fourier transform spectroscopy (DRIFTS) and TPR. They reported that, for the IR data, sulfur inhibits CO adsorption onto the surface of Co catalysts for a sulfur concentration studied possibly due to (i) site blockage and (ii) inhibited reduction of the catalysts. They also found that sulfur also affects the TiO₂- and SiO₂-supported cobalt catalysts during the Fischer-Tropsch reaction. The *in situ* F-T reactions, monitored by DRIFTS, further suggest that lower concentrations of sulfur (100 ppm) on TiO₂-supported cobalt catalysts improves catalysts activity. Besides, the surface of the silica supported catalysts decreased the intensity of the TPR peak related to reducible silicate.

R. Riva *et al.* (2000) studied the interaction of cobalt with two different kinds of support: silica and titania and their effect on the dispersion and reducibility by XPS, TPR, TPO, XRD and TEM. They also showed that the interaction is much stronger in the case of titania. The different reactivity of cobalt with silica and titania explains why reducing and reoxidizing treatments have opposite effects on the dispersion of cobalt depending on whether it is supported on SiO₂ or TiO₂. The low reactivity of cobalt with silica favors sintering effects. Conversely, due to the high reactivity of cobalt with titania, the coverage of TiO₂ by cobalt tends to increase after the same treatments.

S.L. Sun *et al.* (2000) prepared by mixed impregnation of cobalt(II) nitrate and cobalt(II) acetate displayed higher activity than the catalysts prepared from either mono-precursor at mild reaction conditions (1MPa total pressure, H₂/CO=2, TD513 K) of Fischer–Tropsch synthesis (FTS). X-ray diffraction (XRD) indicated that highly dispersed cobalt metal provided the main active sites on the catalyst prepared by mixed impregnation method. Through the mixed impregnation, different cobalt species were formed and their reduction performances were detected by the temperature-programmed reduction (TPR) and thermal gravimetric analysis. Transmission electronic microscopy (TEM) and FT-IR spectroscopy of adsorbed CO as probe molecule revealed that the presence of different sites associated with cobalt after the reduction of the catalysts with hydrogen at 673 K. It was assumed that the metal readily reduced from cobalt nitrate promoted the reduction of Co²⁺ to metallic state in cobalt acetate by H₂ spillover mechanism during catalyst reduction process. The reduced cobalt from cobalt acetate was highly dispersed and remarkably enhanced the catalytic activity.

G. Jacobs *et al.* (2002) investigated the effect of support, loading and promoter on the reducibility of cobalt catalysts. They have reported that significant support interactions on the reduction of cobalt oxide species were observed in the order Al₂O₃ > TiO₂ > SiO₂. Addition of Ru and Pt exhibited a similar catalytic effect by decreasing the reduction temperature of cobalt oxide species, and for Co species where a significant surface interaction with the support was present, while Re impacted mainly the reduction of Co species interaction with the support. They also suggested that, for catalysts prepared with a noble metal promoter and reduced at the same temperature,

the increase in the number of active sites was due mainly to improvements in the percentage reduction rather than the actual dispersion (cluster size). Increasing the cobalt loading, and therefore the average Co cluster size, was found to exhibit improved reducibility by decreasing interactions with the support.

M. Voß *et al.* (2002) investigated the structural, chemical and electronic properties of Co and Co/Mn catalysts supported on Al₂O₃, SiO₂ and TiO₂ by a combination of different methods such as TEM, XRD, XPS, TPR and TPO. They reported that temperature-programmed reduction and oxidation reveal the formation of various oxides in dependence on temperature. In case of the alumina- and titania-supported cobalt catalysts, the formation of high-temperature compounds CoAl₂O₄ and CoTiO₃, respectively. Moreover, these compounds are not reducible under the applied conditions, the degrees of reduction are only 18-20% (Co/Al₂O₃) and 77% (Co/TiO₂).

G.R. Moradi *et al.* (2003) studied the effect of zirconia addition at various loading ratios on the performance of 10 wt% Co/SiO₂ catalysts for the so-called reaction of Fischer–Tropsch synthesis. The catalysts were prepared through a new pseudo sol–gel method which permits a uniform distribution of the incorporated components and a low deviation from theoretical composition. By increasing zirconia, Co–SiO₂ interaction decreases and is replaced by Co–Zr interaction which favours reduction of the catalysts at lower temperatures. The activity and selectivity toward higher hydrocarbons of the promoted catalysts increase with increasing zirconium loading ratios. No appreciable decrease in activity was observed when all catalysts were employed under H₂/CO at 230 °C and 8 bar for 240 h.

L.S. Sales *et al.* (2003) prepared silica embedded with transition metals exhibits adequate properties for applications in catalysis, sensors and optics. Cobalt–silica (Co–SiO₂) nanocomposites were prepared by the sol–gel method and thermally treated at 700, 900, 1100 and 1250 °C. Characterization of the samples was performed by XRD and BET nitrogen adsorption. The performance of the nanocomposites was investigated by catalysis reactions of oxidation. These catalysts were found to be recyclable showing a catalytic activity even after a third recovering. The results indicate that thermal

treatment of sol–gel nanocomposites at temperatures higher than 900 °C is essential for the preparation of active heterogeneous catalysts.

K. Okabe *et al.* (2004) investigated Fischer–Tropsch synthesis was carried out in slurry phase over uniformly dispersed Co–SiO₂ catalysts prepared by the sol–gel method. When 0.01–1 wt.% of noble metals were added to the Co–SiO₂ catalysts, a high and stable catalytic activity was obtained over 60 h of the reaction at 503K and 1MPa. The addition of noble metals increased the reducibility of surface Co on the catalysts, without changing the particle size of Co metal significantly. High dispersion of metallic Co species stabilized on SiO₂ was responsible for stable activity. The uniform pore size of the catalysts was enlarged by varying the preparation conditions and by adding organic compounds such as *N,N*-dimethylformamide and formamide. Increased pore size resulted in decrease in CO conversion and selectivity for CO₂, a byproduct, and an increase in the olefin/paraffin ratio of the products. By modifying the surface of wide pore silica with Co–SiO₂ prepared by the sol–gel method, a bimodal pore structured catalyst was prepared. The bimodal catalyst showed high catalytic performance with reducing the amounts of the expensive

A. K. Dalai *et al.* (2005) studied The effect of water on the performance of narrow and wide-pore silica-supported cobalt catalysts was investigated during Fischer–Tropsch synthesis in a continuously stirred tank reactor (CSTR). In these studies the added water replaced an equivalent amounts of inert gas so that all other reaction conditions remained the same before, during and after water addition. A low cobalt loading of 12.4 wt.% on wide-pore silica exhibited a beneficial effect on CO conversion with the addition of water up to 25 vol.% of the total feed. In contrast, the addition of up to 20 vol.% water to a 20 wt.% Co on narrow- or wide-pore silica did not significantly alter the CO conversion. It appears that the CO conversion mainly increases when cobalt clusters are small enough to fit inside the silica pores.

2.2 MCM-41 supported cobalt catalysts

P. Concepción *et al.* (2004) reported cobalt catalysts (ca. 20 wt% Co) supported on all-silica delaminated ITQ-2 and ITQ-6 zeolites have been prepared by impregnation with aqueous $\text{Co}(\text{NO}_3)_3$ solutions. The catalysts have been characterized by X-ray diffraction (XRD), nitrogen adsorption, transmission electron microscopy (TEM), temperature-programmed reduction (TPR), and infrared spectroscopy of adsorbed CO. The catalytic properties for the Fischer–Tropsch synthesis (FTS) reaction under typical FTS conditions (493 K, 20 bar, $\text{H}_2/\text{CO} = 2$) have been evaluated, and the results compared with those obtained over a conventional Co/SiO_2 and a mesoporous $\text{Co}/\text{MCM-41}$ catalyst with comparable cobalt loading. $\text{Co}/\text{ITQ-6}$ was the most active catalyst, with a FTS reaction rate which was about 1.5 and 1.8 times higher than that of $\text{Co}/\text{MCM-41}$ and Co/SiO_2 , respectively. The high activity of $\text{Co}/\text{ITQ-6}$ is ascribed both to a relatively good dispersion (as observed by TEM) and to a high reducibility (determined by TPR) of the supported Co_3O_4 particles. The dispersion and reducibility of cobalt particles in $\text{Co}/\text{ITQ-2}$ were very close to those in Co/SiO_2 . Consequently, both catalysts presented similar FTS reaction rates. In addition, $\text{Co}/\text{ITQ-6}$ and $\text{Co}/\text{ITQ-2}$ presented a higher selectivity toward the formation of C_{5+} hydrocarbons than Co/SiO_2 and $\text{Co}/\text{MCM-41}$. The higher C_{5+} selectivity of the catalysts based on the delaminated zeolites was ascribed to a higher concentration of coordinatively unsaturated Co^0 sites which are characterized by a band at 1897 cm^{-1} in the infrared spectrum of adsorbed CO. This type of site having an enhanced electron density might stabilize surface hydrocarbon intermediates favoring chain growth processes.

V. Cortés Corberán *et al.* (2004) reported cobalt-containing mesoporous silicates with MCM-41-like structure, with $\text{Si}/\text{Co} \geq 49$, are active and selective catalysts for the oxidative dehydrogenation (ODH) of isobutane. The formation of dehydrogenation products is analysed in terms of the nature of the cobalt species, tetrahedral $\text{Co}(\text{II})$, and heterogeneously initiated gas-phase reactions inside the mesopores.

J. Panpranot *et al.* (2002) studied of CO hydrogenation on MCM-41 and SiO_2 -supported Ru-promoted Co catalysts has been performed using both global rate

measurements and steady-state isotopic transient kinetic analysis (SSITKA). A significant increase in CO hydrogenation was observed when MCM-41 was used as the support in the order $M1 > M2 > SiO_2$ at methanation conditions, where M1 and M2 are small pore ($d_p = 3$ nm) and larger pore ($d_p = 7$ nm) MCM-41, respectively. TOFH based on H_2 chemisorption can be misleading since any suppression of hydrogen chemisorption, as probably occurred for CoRu/M1, results in larger values of TOFH being calculated. SSITKA results, on the other hand, provide a measure of the “true” intrinsic CO hydrogenation activity of the Co sites. SSITKA studies indicated that the higher CO hydrogenation rates for MCM-41-supported catalysts are due to their greater number of active sites, not to a change in the intrinsic site activity. N_2 physisorption and XRD results reveal that the structure of MCM-41 became less ordered and the surface area decreased after standard reduction and 24 h of FTS, probably due to an effect of water vapor produced during metal reduction and reaction. However, the Co surface was still accessible since there was no significant loss of activity with TOS. The extent of deactivation during the initial reaction period was similar for MCM-41- and SiO_2 -supported CoRu catalysts. By providing high activity and unrestricted diffusion of FT reactants and products, CoRu/MCM-41 may be potentially useful for FTS as well as for other catalytic applications, although modified forms of MCM-41 will probably be required in order to increase its hydrothermal stability.

S. Suvanto et al. (2000) reported high surface area MCM-41 with mesoporous structure and conventional SiO_2 ; containing micropores were used as support materials for $Co_2(CO)_8$ in a gas phase preparation of supported cobalt samples. Two different kinds of preparation methods were used: direct deposition, with continuous adsorption of cobalt carbonyl on to the support over an extended period of time; and a pulsing method with successive deposition/decarbonylation cycles. Since the reduced metal is usually the active phase in catalytic reactions, the aim of the preparation of heterogeneous catalysts is to produce samples in which the supported metal is easily reducible. The effects of the support materials, the gas phase deposition methods and decarbonylation atmospheres on the reactivity of the Co/ SiO_2 and Co/MCM-41 samples toward oxygen and hydrogen treatments were compared. According to the results, reducibility of the samples decreased in the order: MCM-41 pulsing method > SiO_2 pulsing method > SiO_2 direct method > MCM-41 direct method. Oxygen/hydrogen consumptions of the samples decreased in the decarbonylation atmosphere inert >

oxidising > reducing. Co/SiO₂ and Co/MCM-41 samples prepared via pulsing method indicated a good stability during oxidation/reduction treatments.

A. Jentys et al. (1995) reported highly dispersed Co particles in MCM-41 were prepared by direct addition of CoCl₂ to the synthesis gel. The small clusters of Co did not sinter during reduction and sulfidation. Incorporation of Co into the MCM-41 lattice was not observed. The addition of Co to the synthesis gel did not alter the structural characteristics of the MCM-41 samples.

J. Panpranot et al. (2002) prepared supported CoRu catalysts with ordered mesoporous silica (MCM-41) as the support using the incipient wetness impregnation method in order to study the effect of ordered mesoporous silica and pore size on cobalt dispersion, reduction behavior, and catalytic properties for the Fischer–Tropsch synthesis (FTS). Metal loadings of 2, 5, 8, and 14 wt.% Co with 0.5 wt.% Ru were investigated, as well as two different mesoporous silicas having average pore diameters of 3 and 7 nm. For comparison purposes, conventional amorphous silica (SiO₂) supported CoRu catalysts were also prepared using the same procedure. Due probably to higher concentration of water vapor in the small pores of MCM-41 during metal reduction, CoRu/MCM-41 catalysts showed stronger interaction of Co with the support than CoRu/SiO₂ as manifested by lower reducibilities of the catalysts during standard reduction. The Co dispersions were similar on MCM-41 to that on amorphous silica for a given Co loading. MCM-41 supported catalysts exhibited similar selectivities for FTS as to the SiO₂ supported ones; however, they had in general greater activities. There was an absence of any obvious pore size effect on product selectivity, probably due to the pores being sufficiently large for the reaction to easily proceed at 1 atm and 220 °C, the reaction conditions used. Thus, MCM-41 supported CoRu catalysts appear to be suitable for application to FTS. Their unique and tailored properties offer interesting possibilities for catalyst design and application in particular cases.

2.3 Boron-modified supported cobalt catalyst

M. A. Stracknick *et al.* (1987) reported the influence of boron on the chemical state and dispersion of Co/Al₂O₃ catalysts has been investigated by bulk and surface spectroscopic techniques. Three series of Co/Al₂O₃ catalysts were studied: one containing a constant Co loading of 3 wt% and boron loadings of 0.3 to 3 wt% and two series containing 0.7 to 10 wt% Co and constant boron loadings of either 0 or 3 wt% Co. In the absence of boron, Co dispersion decreased with increasing Co loading above 1.5 wt% Co. The presence of boron had little effect on Co dispersion at low Co loadings, while catalysts with Co loadings in excess of 1.5 wt% exhibited an increase in Co dispersion compared to boron-free catalysts. X-ray photoelectron spectroscopy, diffuse reflectance spectroscopy, and gravimetric analysis were used to quantify the Co species present on the catalysts as a function of both Co and boron loading. In the absence of boron, Co exists as tetrahedral and octahedral Co²⁺ at low Co loadings, while Co₃O₄ is the primary phase at higher Co loadings. In the presence of boron, Co₃O₄ formation is suppressed for catalysts with Co loadings less than 8 wt% in favor of octahedral Co²⁺ and minor amounts of Co borate. The formation of Co₃O₄ occurs at Co loadings greater than 6 wt% for boron-containing catalyst. A mechanism is described to account for the effect of boron on the dispersion and chemical state of Co.

N.J. Coville *et al.* (1999) reported the effect of boron (as H₃BO₃) on the CO hydrogenation ability of Co/TiO₂ catalysts was investigated using XRD, LRS, TGA, DRIFTS and a fixed bed reactor. The introduction of boron (0.02±1.5%) into a 10 wt% Co/TiO₂ catalyst decreased the Co₃O₄ crystallite size (26±16 nm) in the oxidic catalysts (calcined at 300°C) and decreased the hydrogen uptake (0.35±0.9 ml/g cat) in the reduced catalyst. Reduction of the Co/TiO₂ catalyst was made more difficult by the presence of boron. The CO conversion and overall hydrogenation rate decreased with decreasing ease of reducibility and decreasing cobalt dispersion caused by boron. Turnover frequency, however, remained constant throughout and was independent of the extent of reduction and dispersion of the catalysts. This provides further evidence of the structure-insensitivity of supported Co Fischer-Tropsch catalysts. Addition of small amounts of B (<0.1%) do, however, result in an increase in α , less CH₄ production and an increase in the olefin/paraffin ratio. This suggests an increase in the monomer

propagation to termination ratio. At higher B loadings, product selectivity shifted to the lower molecular weight hydrocarbons and CO₂ selectivity increased (0±2.5%).

N.J. Coville et al.(2001) reported TiO₂ was treated with boron (0.05, 0.1%; boric acid source) to give B/TiO₂. Co(NO₃)₂.6H₂O (10% Co) was then added to both TiO₂ and B/TiO₂ (incipient wetness) and the materials were then sulfided with 100, 200 and 500 ppm (NH₄)₂S. The sulfided Co/TiO₂ catalysts with and without boron were characterised by TPR and O₂ titration and evaluated for Fischer–Tropsch synthesis. Low-level sulfur addition (100, 200 ppm S) did not significantly influence the activity and selectivity of the catalysts. The addition of a higher-level loading of sulfur (500 ppm S) resulted in severe sulfur poisoning of catalysts (80% decrease in reaction rate), but the modification of Co/TiO₂ by boron retarded this poisoning (35% decrease in reaction rate). A shift in the product distribution to light molecular weight hydrocarbons was observed for the 500 ppm S loaded catalyst (no boron addition) while boron addition retarded this shift. The effect of boron on the sulfur poisoning resistance of the Co/TiO₂ catalysts is discussed.

J. Li *et al.* (2002) studied the effect of the addition of small amounts of boron, ruthenium and rhenium on the Fischer–Tropsch (F–T) catalyst activity and selectivity of a 10wt.% Co/TiO₂ catalyst has been investigated in a continuously stirred tank reactor (CSTR). A wide range of synthesis gas conversions has been obtained by varying space velocities over the catalysts. The addition of a small amounts of boron (0.05 wt.%) onto Co/TiO₂ does not change the activity of the catalyst at lower space times and slightly increases synthesis gas conversion at higher space times. The product selectivity is not significantly influenced by boron addition for all space velocities investigated. Ruthenium addition (0.20 wt.%) onto Co/TiO₂ and CoB/TiO₂ catalysts improves the catalyst activity and selectivity. At a space time of 0.5 h-g cat./NL, synthesis gas conversion increases from 50–54 to 68–71% range and methane selectivity decreases from 9.5 to 5.5% (molar carbon basis) for the promoted catalyst. Among the five promoted and non-promoted catalysts, the rhenium promoted Co/TiO₂ catalyst (0.34 wt.% Re) exhibited the highest synthesis gas conversion, and at a space time of 0.5 h-g cat./NL, synthesis gas conversion was 73.4%. In comparison with the results obtained in a fixed bed reactor, the catalysts displayed a higher F–T catalytic activity in the CSTR.

G. Jacobs *et al.* (2002) Temperature programmed reduction (TPR) and hydrogen chemisorption combined with reoxidation measurements were used to define the reducibility of supported cobalt catalysts. Different supports (e.g. Al_2O_3 , TiO_2 , SiO_2 , and ZrO_2 modified SiO_2 or Al_2O_3) and a variety of promoters, including noble metals and metal cations, were examined. Significant support interactions on the reduction of cobalt oxide species were observed in the order $\text{Al}_2\text{O}_3 > \text{TiO}_2 > \text{SiO}_2$. Addition of Ru and Pt exhibited a similar catalytic effect by decreasing the reduction temperature of cobalt oxide species, and for Co species where a significant surface interaction with the support was present, while Re impacted mainly the reduction of Co species interacting with the support. For catalysts reduced at the same temperature, a slight decrease in cluster size was observed in H_2 chemisorption/pulse reoxidation with noble metal promotion, indicating that the promoter aided in reducing smaller Co species that interacted with the support. On the other hand, addition of non-reducible metal oxides such as B, La, Zr, and K was found to cause the reduction temperature of Co species to shift to higher temperatures, resulting in a decrease in the percentage reduction. For both Al_2O_3 and SiO_2 , modifying the support with Zr was found to enhance the dispersion. Increasing the cobalt loading, and therefore the average Co cluster size, resulted in improvements to the percentage reduction. Finally, a slurry phase impregnation method led to improvements in the reduction profile of $\text{Co}/\text{Al}_2\text{O}_3$.

N.J. Coville *et al.* (2002) studied a series of $\text{Co}/\text{B}/\text{TiO}_2$ (B = ammonium borate, boric acid, *o*-carborane, 0.01–1.5 wt.% B) catalysts were synthesized. The addition of boron decreased the reducibility of the Co as determined from temperature-programmed reduction studies and H_2 reduction/ O_2 back titration studies. This in turn decreased the FT activity but not the turnover frequency of the Co catalyst.

Y. Brik *et al.* (2002) studied cobalt- and cobalt–boron-loaded TiO_2 (anatase) catalysts were prepared and characterized before and after catalytic tests by XRD, HRTEM, IR, UV–visible, and laser Raman spectroscopy. Their activity was investigated in oxidative dehydrogenation (ODH) of ethane. In the absence of boron, the best performances were exhibited by the sample containing 7.6 wt% Co, which was selected for further investigations. At 550°C , it displayed a stationary state with a conversion of 22.2% and an ethylene selectivity around 60%. This catalyst also showed in the first 3 h on stream a 30% decay in activity that was attributed to a concomitant

loss of specific surface area and the formation of CoTiO_3 and Co_2TiO_4 phases. The addition of 0.25 wt% boron to this $\text{Co}(7.6)/\text{TiO}_2$ sample improved the ethane conversion and the ethylene selectivity, which attained 28.4 and 67%, respectively. Boron concentrations superior to 0.25 wt% negatively affected the catalysts performances, probably because at high loadings it profoundly modified the acid–base properties of the surface. XRD and HRTEM analyses showed that at the same time the size of Co_3O_4 crystallites decreased. IR investigations confirmed the increase in acidity upon boron addition and the decrease in strength of the basic sites which were involved in the dehydrogenation processes. The catalytic behavior and the acid–base properties of $\text{Co}(7.6)/\text{TiO}_2$ loaded with different amounts of boron were also studied using butan-2-ol conversion. Boron addition enhanced the dehydration and the dehydrogenation reactions. However, above 0.25 wt% it decreased the dehydrogenation activity, confirming the modifications of the properties of the acid–base centers revealed by the IR studies. For this optimal concentration of boron, the activity and the selectivity in butan-2-ol dehydrogenation exhibited a maximum that coincided with the one observed in the ethane ODH, which suggests that both reactions possibly involved the same type of active centers.

CHAPTER III

THEORY

3.1 Fischer-Tropsch synthesis (FTS)

Fisher and Tropsch (1925) reported the catalytic hydrogenation of carbonmonoxide over iron-based catalysis at atmospheric pressure to produce a Flory Schulz distribution of alkanes and olefin. The process was originally intended for the production of synthetic liquid fuels followed by cracking the proper fraction of the olefins; or by direct conversion of synthesis gas to lower olefins by applying the proper reaction conditions (Catalysts, temp, pressure, CO/H₂ ratio, reactor design etc.) The process has been developed over several decades and many improvements has been introduced in the various components of the system.

By manipulation of the reaction conditions, the process may be designed to produce heavier saturated hydrocarbons or lower olefins or oxygenated hydrocarbons as we shall see in the following discussion.

Metals that have significant activity for Fischer-Tropsch synthesis include iron, cobalt, nickel and ruthenium. Iron has proved so far to be the best. It is superior to cobalt with respect to conversion rate, selectivity and flexibility. Nickel has disadvantage of producing appreciable amounts of methane. Ruthenium enhance the formation of high molecular weight alkanes and catalyzes polymerization to polymethane. Other group VIII metals are of low activity. Copper does not catalyze Fischer-Tropsch synthesis.

The catalyst is usually prepared by fusion or precipitation over a silica, alumina or kieselguhr support. Small amounts of promoters such as alkali metal or copper salts are included in the catalytic mix. Copper is believe to facilitate the reduction of the catalyst, alkali metal salt, particularly K₂O₂ enhance activity and olefins selectivity. The support increased the surface area of the catalyst metal thus extremely increasing in dispersion.

Sulfur compounds generally poison the catalyst and they must be removed from the synthesis gas feed stream. However, partial sulfur poisoning may have favorable effects. Thus, it has been found that deliberate slight sulfur poisoning of the iron/manganese catalyst enhances selectivity to short chain olefins.

Three main types of reactors are currently in use in the Fischer-Tropsch processes: Fixed-bed, fluidized-bed and slurry bed reactors. Fixed-bed reactors are usually tubular, each tube having 50 mm ID and 12 m length. A single reactor may contain as many as 2000 such tubes. Fluidized-bed reactors provide for better heat transfer and continuous regeneration of the catalyst. The catalyst used in fluidized-bed reactors must have high physical stability. SASOL (in South Africa), uses fluidized-bed reactors 46 m high, 230 cm in diameter with reaction temperature of 320-360°C and pressure. In the slurry-bed reactors the feed gas is bubbled through a suspension of finely divided catalyst particles. It has the advantage of good temperature control thus providing greater flexibility of reaction conditions.

Each type of reactor is better suited for certain product composition. Fixed-bed reactors, for example, produce high boiling straight-chain hydrocarbons consisting, typically, of 33% gasoline hydrocarbons (C₅-C₁₁), 17% diesel and 40% heavy paraffins and higher waxes. The gasoline fraction is of low octane value and requires further treatment (isomerization or blending) before use. Fluidized-bed reactors are the best when lighter hydrocarbons are desired. A typical product composition is 72% lower molecular weight gasoline-range hydrocarbons rich in olefins and 14% oxygenated hydrocarbons. However, the product is low in diesel. Thus two or more different reactors may be operated in parallel to provide an integrated fuel plant.

The demands on selectivity of Fischer-Tropsch reactions are ever-increasing. In the earlier days of the process the concern was to improve selectivity with respect to better gasoline grade and/or diesel oil chemicals. With the realization of feasible route of converting synthesis gas to industrial intermediates, more stringent conditions are being imposed on the reaction parameters to make the process more selective.

Selectivity improvement is sought with respect to product properties such as chain length, chain branching, olefin content, alcohol content and methane content.

Reaction conditions that particularly eliminate or minimize carbon deposition are desirable. In order to achieve and improve product selectivity the optimization of the following reaction parameters has been investigated: reaction temperature and pressure, H_2/CO ratio, conversion, space velocity, amount and type of promoters, nature of the catalyst, size of catalyst particles and mode of its deposition, type of support, and type of reactor.

We have already seen examples of how the choice of the metal catalyst and support affects the product distribution. The effect of the choice of the reactor type on the nature of the reaction products has also been demonstrated.

Selectivity to olefins may be enhanced by addition of promoters such as K_2O , Ti, Mn or V. Selectivity of greater than 70% to C_2 - C_4 olefins at high conversion rate has been achieved.

The search for selectivity to lower olefins by controlling the chain growth and inhibiting hydrogenation has been followed in three directions:

- (a) The use of highly dispersed catalyst either by improving the method of deposition or using special dispersing supports.
- (b) The use of bimetallic catalyst eg. With Mn/Fe ratio of 9:1 at 330 °C up to 90% olefin selectivity has been achieved. However, the activity of the catalyst and its life-time are low.
- (c) The use of shape-selective catalyst.

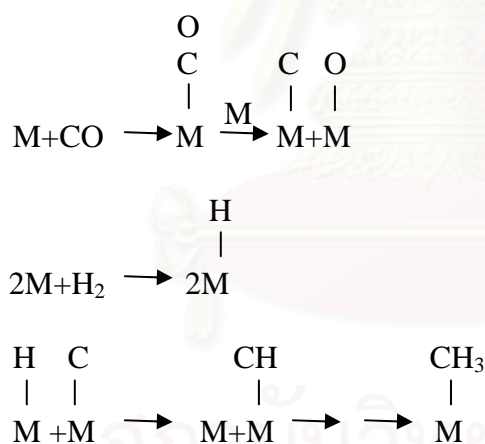
Since the Fischer-Tropsch process was originally intended for the production of hydrocarbons, little attention was paid in the early phases of the application of the process to the oxygenated products obtained as co-products. With the search for more economical sources of the oxygenated hydrocarbons, the possibility of tuning the Fischer-Tropsch process for the production such as oxygenates has been investigated. It has been found that with a nitrated iron catalyst, selectivity for alcohols may exceed 80%. A Rh/Hg/SiO₂ catalyst system gave 75% selectivity with respect to ethanol. The major side products are olefins.

The Fischer-Tropsch process may be defined as being the hydrogenative oligomerization of CO over heterogeneous catalyst to produce alkanes, alkenes oxygenated hydrocarbons and water. A complete mechanism must account for the formation of all products observed. The first attempt at elucidating the mechanism of the process was made by the inventors of the process themselves, Fischer and Tropsch.

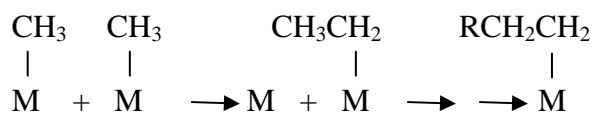
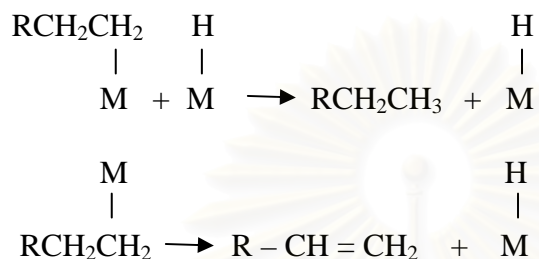
3.1.1 The surface carbide mechanism

Fischer and Tropsch apparently were trying to explain the formation of alkanes and alkenes rather than introduce a mechanism for whole line of the products that could be formed from the process. They observed that hydrocarbon formation occurred with heterogeneous metal catalysts (Ni, Fe, Co, Ru) that tend to absorb CO dissociatively to form surface carbide species. Their mechanism consists of the following steps:

(i) Initiation:

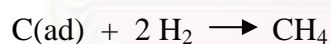


Note: M-X means species X chemisorbed on the metal surface atom M. The hyphen has no implication with respect to the strength of the M-X interaction or the order of the bond. More recently it has been suggested, based spectroscopic evidence, that in order to for an absorbed CO to undergo dissociation it must be bonded side-on to the metal, not end-on.

(ii) Propagation:**(iii) Termination:**

The carbide mechanism has survived the several decades since its introduction. Several items of evidence arising from recent investigation support this mechanism e.g.

(a) In the hydrogenation of CO over clean Ni surface it has been observed that CO₂ evolution proceeds that CH₄ thus



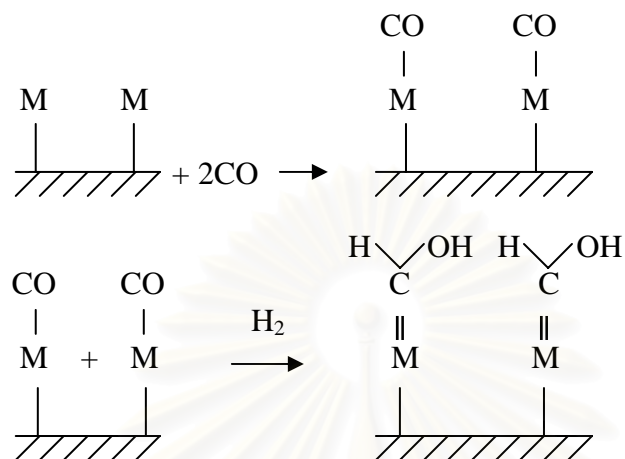
(b) Decomposition of diazomethane(CH₂N₂) at 200°C in the presence of H₂ over Co, Fe and Ru catalysts gives linear alkanes and olefins with distribution similar to that obtained from CO/H₂ reaction over the same catalyst.

(c) Distribution of ¹³C in CH₂=CH formed when ¹³CO, H₂- and ¹²CH₂N₂ were reacted under Fischer-Tropsch conditions is consistent with the distribution predicted based on the carbided mechanism and inconsistent with other proposed mechanism.

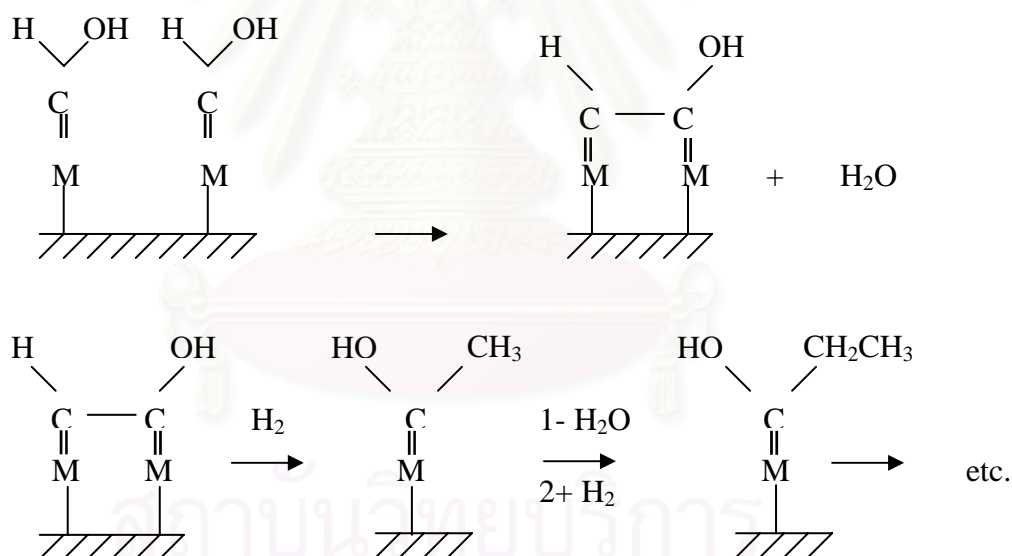
However, a drawback of this mechanism is that it does not explain the formation of oxygenated products.

3.1.2 The hydroxycarbene mechanism

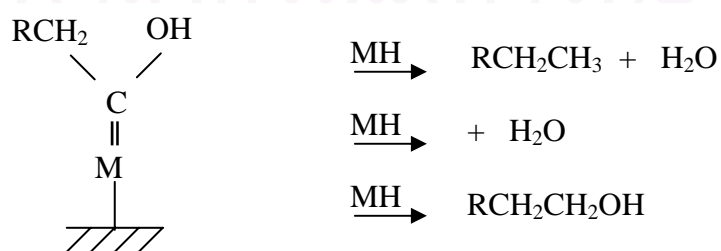
(i) Initiation:



(ii) Propagation:



(iii) Termination:

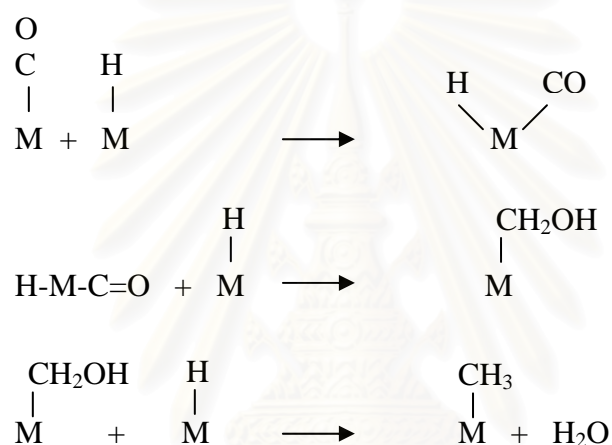


This mechanism explains the formation of alkanes, and olefins as well as oxygenated hydrocarbons. However, it precludes the dissociation of CO, which is not consistent with many experimental observations.

3.1.3 The CO insertion mechanism.

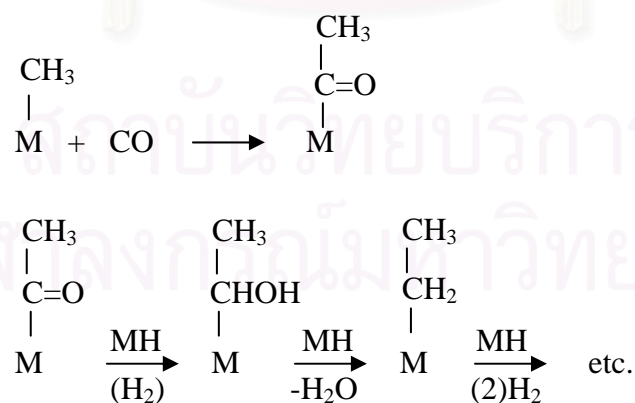
(i) initiation :

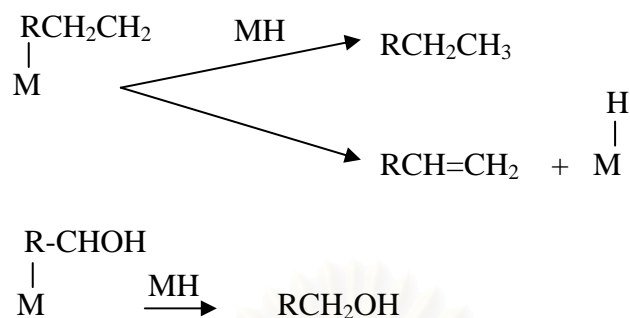
The initiation of active species is similar to that of the carbide mechanism although the mechanism of its formation is different.



(ii) Propagation:

propagation proceeds via CO insertion rather than $-\text{CH}_2-$ insertion.



(iii) Termination:

Normally, catalysts used for FTS are group VIII metals. By nature, the hydrogenation activity increases in order of $\text{Fe} < \text{Co} < \text{Ni} < \text{Ru}$. Ru is the most active. Ni forms predominantly methane, while Co yields much higher ratios of paraffins to olefins and much less oxygenated products such as alcohols and aldehydes than Fe does.

The current main goal in FTS is to obtain high molecular weight, straight chain hydrocarbons. However, methane and other light hydrocarbons are always present as less desirable products from the synthesis. According to the Anderson-Schulz-Flory (ASF) product distribution, typically 10 to 20% of products from the synthesis are usually light hydrocarbon ($\text{C}_1\text{-C}_4$). These light alkanes have low boiling points and exist in the gas phase at room temperature, which is inconvenient for transportation. Many attempts have been made to minimize these by-products and increase the yield of long chain liquid hydrocarbons by improving chain growth probability. It would be more efficient to be able to convert these less desirable products into more useful forms, rather than re-reforming them into syngas and recycling them (Farrauto and Bartholomew, 1997). Depending upon the type of catalyst used, promoters, reaction conditions (pressure, temperature and H_2/CO ratios), and type of reactors, the distribution of the molecular weight of the hydrocarbon products can be noticeably varied.

3.2 Cobalt (Young 1960; Othmer, 1991)

3.2.1 General

Cobalt, a transition series metallic element having atomic number 27, is similar to silver in appearance.

Cobalt and cobalt compounds have expanded from use colorants in glasses and ground coat fits for pottery to drying agents in paints and lacquers, animal and human nutrients, electroplating materials, high temperature alloys, hard facing alloys, high speed tools, magnetic alloys, alloys used for prosthetics, and used in radiology. Cobalt is also as a catalyst for hydrocarbon refining from crude oil for the synthesis of heating fuel.

3.2.2 Physical Properties

The electronic structure of cobalt is $[\text{Ar}] 3d^7 4s^2$. At room temperature the crystalline structure of the α (or ϵ) form, is close-packed hexagonal (cph) and lattice parameters are $a = 0.2501$ nm and $c = 0.4066$ nm. Above approximately 417°C , a face-centered cubic (fcc) allotrope, the γ (or β) form, having a lattice parameter $a = 0.3554$ nm, becomes the stable crystalline form

The scale formed on unalloyed cobalt during exposure to air or oxygen at high temperature is double-layered. In the range of 300 to 900°C , the scale consists of a thin layer of mixed cobalt oxide, Co_3O_4 , on the outside and cobalt (II) oxide, CoO , layer next to metal. Cobalt (III) oxide, Co_2O_3 , may be formed at temperatures below 300°C . Above 900°C , Co_3O_4 decomposes and both layers, although of different appearance, are composed of CoO only. Scales formed below 600°C and above 750°C appear to be stable to cracking on cooling, whereas those produced at 600 - 750°C crack and flake off the surface.

Cobalt forms numerous compounds and complexes of industrial importance. Cobalt, atomic weight 58.933, is one of the first transition series of Group 9 (VIII B). There are thirteen known isotopes, but only three are significant: ^{59}Co is the only stable and naturally occurring isotope; ^{60}Co has a half-life of 5.3 years and is a common source of γ -source for Mössbauer spectroscopy.

Cobalt exists in the +2 or +3 valance states for the major of its compounds and complexes. A multitude of complexes of the cobalt (III) ion exists, but few stable simple salt are know. Octahedral stereochemistries are the most common for cobalt (II) ion as well as for cobalt (III). Cobalt (II) forms numerous simple compounds and complexes, most of which are octahedral or tetrahedral in nature; cobalt (II) forms more tetrahedral complex than other transition-metal ions. Because of the small stability difference between octahedral and tetrahedral complexes of cobalt (II), both can be found equilibrium for a number of complexes. Typically, octahedral cobalt (II) salts and complexes are pink to brownish red; most of the tetrahedral Co (II) species are blue.

Table 3.1 Physical properties of cobalt (Othmer, 1991)

Property	Value
atomic number	27
atomic weight	58.93
transformation temperature, °C	417
heat of transformation, J/g ^a	251
melting point, °C	1493
latent heat of fusion, ΔH_{fus} J/g ^a	395
boiling point, °C	3100
latent heat of vaporization at bp, ΔH_{vap} kJ/g ^a	6276
specific heat, J/(g°C) ^a	
15-100°C	0.442
molten metal	0.560
coefficient of thermalexpansion, °C ⁻¹	
cph at room temperature	12.5
fcc at 417°C	14.2
thermal conductivity at 25 °C, W/(m·K)	69.16
thermal neutron absorption, Bohr atom	34.8
resistivity, at 20 °C ^b , 10 ⁻⁸ Ω·m	6.24
Curie temperature, °C	1121

Table 3.1 Physical properties of cobalt (cont.)

Property	Value		
saturation induction, $4\pi I_s$, T ^c	1.870		
permeability, μ			
initial	68		
max	245		
residual induction, T ^c	0.490		
coercive force, A/m	708		
Young's modulus, Gpac	211		
Poisson's ratio	0.32		
Hardness ^f , diamond pyramid, of %Co	99.9 99.98 ^e		
At 20 °C	225 253		
At 300 °C	141 145		
At 600 °C	62 43		
At 900 °C	22 17		
strength of 99.99 %cobalt, MPa ^g	as cast	annealed	sintered
tensile	237	588	679
tensile yield	138	193	302
compressive	841	808	
compressive yield	291	387	

^aTo convert J to cal, divided by 4.184.

^bconductivity = 27.6 % of International Annealed Copper Standard.

^cTo convert T to gauss, multiply by 10^4 .

^dTo convert GPa to psi , multiply by 145,000.

^eZone refined.

^fVickers.

^gTo convert MPa to psi , multiply by 145.

3.2.3 Cobalt Oxides

Cobalt has three well-known oxides:

Cobalt (II) oxide, CoO , is an olive green, cubic crystalline material. Cobalt (II) oxide is the final product formed when the carbonate or the other oxides are calcined to a sufficiently high temperature, preferably in a neutral or slightly reducing atmosphere. Pure cobalt (II) oxide is a difficult substance to prepare, since it readily takes up oxygen even at room temperature to re-form a higher oxide. Above about 850°C , cobalt (II) oxide form is the stable oxide. The product of commerce is usually dark gray and contains 77-78 wt % cobalt. Cobalt (II) oxide is soluble in water, ammonia solution, and organic solvents, but dissolves in strong mineral acids. It is used in glass decorating and coloring and is a precursor for the production of cobalt chemical.

Cobalt (III) oxide, Co_2O_3 , is formed when cobalt compounds are heated at a low temperature in the presence of an excess of air. Some authorities told that cobalt (III) oxide exists only in the hydrate form. The lower hydrate may be made as a black powder by oxidizing neutral cobalt solutions with substances like sodium hypochlorite. Co_2O_3 or $\text{Co}_2\text{O}_3 \cdot \text{H}_2\text{O}$ is completely converted to Co_3O_4 at temperatures above 265°C . Co_3O_4 will absorb oxygen in a sufficient quantity to correspond to the higher oxide Co_2O_3 .

Cobalt oxide, Co_3O_4 , is formed when cobalt compounds, such as the carbonate or the hydrated sesquioxide, are heated in air at temperatures above approximately 265°C and not exceeding 800°C .

3.3 Co-based catalysts

Supported cobalt (Co) catalysts are the preferred catalysts for the synthesis of heavy hydrocarbons from natural gas based syngas (CO and H_2) because of their high Fischer-Tropsch (FT) activity, high selectivity for linear hydrocarbons, and low activity for the water gas shift reaction. It is known that reduced cobalt metal, rather than its oxides or carbides, is the most active phase for CO hydrogenation in such catalysts. Investigations have been done to determine the nature of cobalt species on various supports such as alumina, silica, titania, magnesia, carbon, and zeolites. The influence of various types of cobalt precursors used was also investigated. It was found that the

used of organic precursors such as Co (III) acetyl acetate resulting in an increase of CO conversion compared to that of cobalt nitrate (Kraum and Baerns, 1999).

3.4 Cobalt-Support Compound Formation (Co-SCF)

Compound formation between cobalt metal and the support can occur under pretreatment and/or reaction conditions, leading to catalyst deactivation. The compound formation of cobalt metal with support materials, however, is difficult to predict because of the lack of sufficient thermodynamic data. Co-support compound formation can be detected evidentially.

3.4.1 Co-Silicate Formation

The formation of cobalt silicates on Co/SiO₂ under hydrothermal conditions has been extensively studied by Kogelbauer *et al.* (1995). Hydrothermal treatment at 200°C led to a catalyst with lower reducibility due to the formation of both reducible and non-reducible (at temperature ≤ 900°C) cobalt silicates. It was found that hydrothermal treatment of the reduced catalyst or hydrothermal treatment of the calcination catalyst in the presence of hydrogen produces cobalt silicates, while hydrothermal treatment of the calcined catalyst in air does not result in their formation. Hydrothermal treatment of the calcined catalyst in inert gas also has little effect.

3.5 Silicon dioxide (Patnaik,2002)

3.5.1 General feature of silica

Table 3.2 Physical properties of silica

Properties	
Other names	Silica
Molecular formula	SiO ₂
Molar mass	60.1 g/mol
Appearance	white or colourless solid (when pure)
Density and phase	2.6 g/cm ³ , solid
Solubility in water	insoluble
Melting point	1610 °C
Boiling point	2230 °C

In its many forms, silica has been used in all stages of civilization, from the ancient flints of the Stone Age to the modern silica laboratory ware. Because of its many uses, and of the many varied forms in which it occurs, silica has been called by more names than any other mineral. Many of the older names of flint are now so obsolete that repetition is needless, but many of the present-day names for quartz gems are unknown save to a few jewellers. Then, too, the exact research of the modern laboratory has shown several distinct crystallographic varieties of silica; some of which are closely connected with the temperatures experienced in their life-history.

The many different names, and their different connotations, which are now in use for silica minerals, call for a classification and arrangement in a more ample, yet more concise manner than is to be found in the usual discussion of the varieties of silica. This article is written with the hope of making a scientific

classification of these names, so that the use of the different terms will no longer be a cause for tedious searching for definitions.

These varieties are named in the order formed with descending temperatures. Recrystallization changes occur at the temperatures noted when ample time is allowed for the action, often in the laboratory only in the presence of catalysts. Besides the changes at these critical temperatures, there are probably similar changes from unstable forms towards quartz at atmospheric temperatures, especially after long time intervals. With fairly rapid cooling or heating intermediate forms may not occur in their stable zone, but a direct change from one to another without the intermediate product may take place. Most of the recrystallization changes noted are found to occur at both ascending and descending temperatures.

(A) SILICA GLASS - amorphous, a true non-crystalline glass, stable below the melting point and above the "gc" temperature. Quartz Glass, Fused Silica, Fused Quartz, are other names for this supercooled liquid. In most forms at atmospheric temperatures there are traces of cristobalite.

(B) CRISTOBALITE - isometric, or pseudo-isometric, "gc" range is at 1710° where Cristobalite changes to glass as temperatures rise, or glass to cristobalite as they fall. Cristobalite, an alternate spelling. Beta Cristobalite, also called High Cristobalite, is the high temperature product, forming in the "gc" range in cooling. It is isometric, and in cooling recrystallizes to Alpha Cristobalite, or Low Cristobalite, at 200-275°, providing cooling through the "ct" and "tq" ranges has been too rapid for recrystallization. It is tetragonal.

(C) TRIDYMITE - hexagonal, bipyramidal. "ct" range is at 1470°, where cristobalite changes to tridymite on cooling. Glass may crystallize as tridymite at 1670° if the cooling was too rapid through the "gc" range. Beta Second Tridymite, or Upper High Tridymite, is the high temperature product, forming in the "ct" range in cooling, and which recrystallizes to Beta First Tridymite, also called Lower High Tridymite, at 163° if cooling was too rapid for the "tq" transformation. This in turn alters to Alpha Tridymite, or Low Tridymite, at 117°, which is the usual tridymite of nature.

- Asmanite - a meteoric tridymite, related to the above series.
 Vestan - a doubtful silica mineral, probably to be ascribed to tridymite.
 Granuline - a doubtful pulverescent mineral which seems allied to tridymite on optical grounds.

(D) QUARTZ - hexagonal, forms from tridymite in the "tq" range at 870° in cooling. Glass may change to crystalline quartz at about 1400° providing cooling was too rapid for the "gc", "gt" and "ct" transformations. Beta Quartz, or High Quartz, is the high temperature product, forming at the "tq" point. It is hemihedral. On cooling it recrystallizes to Alpha Quartz, also called Low Quartz, at 573°, yielding the stable low temperature mineral. It is tetartohedral, showing polarity along the c axis and is divisible into Right Hand Quartz and Left Hand Quartz

(E) CHALCEDONY - a cryptocrystalline, or very finely fibrous mineral, which has not been successfully located in the thermal equilibrium diagram. Heating to 725-850° usually results in an alteration to tridymite, which thereafter acts as normal tridymite. Chalcedony is usually found as a deposit from solutions, and may be a mixture of glass and quartz, or more probably an intermediate product in the dehydration of the opal colloid. Various subdivisions of chalcedony have been made on optical grounds.

- Chalcedony - biaxial, positive, elongation positive.
 Chalcedonite - biaxial, negative.
 Lussatite - biaxial, positive, parallel elongation.
 Quartzine - biaxial, positive, negative elongation
 pseudochalcedonite, Lutecite.
 Jenzschite - differently soluble, but of same S. G. as chalcedony.
 Melanophlogite - possibly impure chalcedony.
 Sulfuricin - probably a chalcedony rich in sulphur.

(F) COLLOIDAL SILICA - is usually hydrous, and is commonly described under opal. Silicon occurs in nature combined with oxygen in various forms of silica and silicates. Silicates have complex structures consisting of SiO₄ tetrahedral structural units

incorporated to a number of metals. Silicon is never found in nature in free elemental form. Among all elements silicon forms the third largest number of compounds after hydrogen and carbon. There are well over 1000 natural silicates including clay, mica, feldspar, granite, asbestos, and hornblende. Such natural silicates have structural units containing orthosilicates, SiO_4^{4-} , pyrosilicates $\text{Si}_2\text{O}_7^{6-}$, and other complex structural units, such as, $(\text{SiO}_3)_n^{2n-}$ that have hexagonal rings arranged in chains or pyroxene $(\text{SiO}_3^{2-})^n$ and amphiboles, $(\text{Si}_4\text{O}_{11})^{6-}$ in infinite chains. Such natural silicates include common minerals such as tremolite, $\text{Ca}_2\text{Mg}_5(\text{OH})_2\text{Si}_8\text{O}_{22}$; diopside, $\text{CaMg}(\text{SiO}_3)_2$; kaolin, $\text{H}_8\text{Al}_4\text{Si}_4\text{O}_{18}$; montmorillonite, $\text{H}_2\text{Al}_2\text{Si}_4\text{O}_{12}$; talc, $\text{Mg}_3[(\text{OH})_2\text{SiO}_{10}]$; muscovite (a colorless form of mica), $\text{H}_2\text{KAl}_3(\text{SiO}_4)_3$; hemimorphite, $\text{Zn}_4(\text{OH})_2\text{Si}_2\text{O}_7 \cdot \text{H}_2\text{O}$; beryl, $\text{Be}_3\text{Al}_2\text{Si}_6\text{O}_{18}$; zircon, ZrSiO_4 ; benitoite, $\text{BaTiSi}_3\text{O}_9$; feldspars, KAlSi_3O_8 ; zeolites, $\text{Na}_2\text{O} \cdot 2\text{Al}_2\text{O}_3 \cdot 5\text{SiO}_2 \cdot 5\text{H}_2\text{O}$; nephrite, $\text{Ca}(\text{Mg,Fe})_3(\text{SiO}_3)_4$; enstatite, $(\text{MgSiO}_3)_n$; serpentine, $\text{H}_4\text{Mg}_3\text{Si}_2\text{O}_{10}$; jadeite, $\text{NaAl}(\text{SiO}_3)_2$; topaz, $\text{Al}_2\text{SiO}_4\text{F}_2$; and tourmaline, $(\text{H,Li,K,Na})_3\text{Al}_3(\text{BOH})_2\text{Si}_6\text{O}_{19}$. silica, the other most important class of silicon compounds, exists as sand, quartz, flint, amethyst, agate, opal, jasper, and rock crystal.



สถาบันวิทยบริการ
จุฬาลงกรณ์มหาวิทยาลัย

3.6 MCM-41

3.6.1 General feature of MCM-41

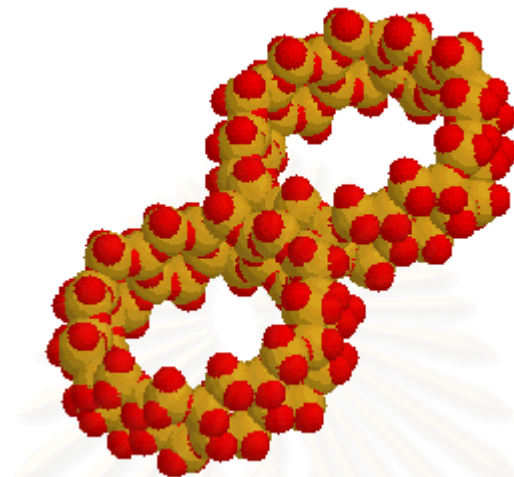


Figure 3.1 Two hexagonal channels of MCM41, linked to its 3D structural pdb file.

The most striking fact about the material MCM-41 is that, although composed of amorphous silica, it displays an ordered structure with uniform mesopores arranged into a hexagonal, honeycomb-like lattice. In this figure one looks directly inside the uniform mesopores, which are separated from each other by thin walls of amorphous silica, approximately 1 - 1.5 nm thick. The mesopores are not necessarily running in a straight way through the silica matrix, but they can be slightly curved, thereby retaining the hexagonal ordering. From the micrographs it is apparent that MCM-41 has a very large void fraction, due to the presence of the mesopores, and concomitantly a rather low density. As a result MCM-41 displays a very large specific surface area of approximately $1,000 \text{ m}^2 \text{ g}^{-1}$. This property makes MCM-41 very interesting to be used as a support material for heterogeneous catalysts. Moreover, because MCM-41 exclusively contains mesopores it can both provide access to large molecules and alleviate diffusion problems, which are frequently encountered in microporous materials such as zeolites. It should be noted, however, that the one-dimensional nature as well as the relatively large length of the mesopores (usually extending over several hundreds of nanometers) could also give rise to transportation limitations.

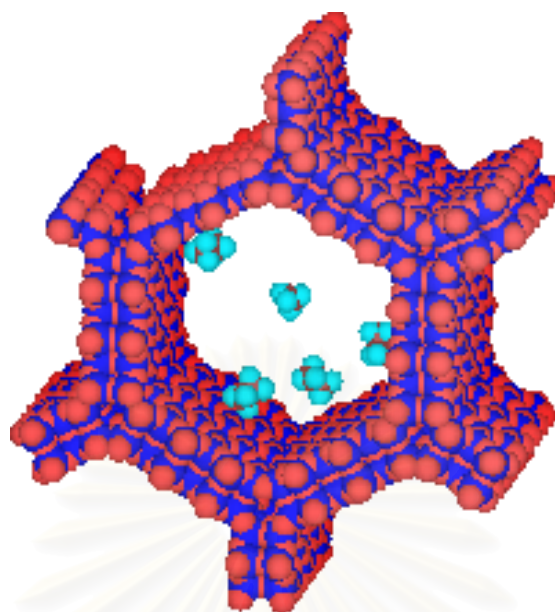


Figure 3.2 Methane and ethane inside one of the hexagonal pores of molecular sieve MCM-41 (of about 3 nm pore diameter). Red = oxygen, Blue = silicon, Light Blue = hydrogen, Brown = carbon.

Despite the advantages mentioned above there is one eminent drawback associated with MCM-type materials, viz. the rather limited stability, which is a result of the very thin, amorphous pore walls. Because of the very large mesopore surface area the pore walls are extremely reactive towards a number of agents, resulting in the collapse of the thin walls upon exposure to these agents. From a viewpoint of application the instability of silica support materials towards steam (either co-fed as a diluent or produced during catalysis), resulting in the chemical evaporation of silica, makes silicasupported catalysts inappropriate for a rather large range of processes. Furthermore, there is a notable instability of MCM-41 towards mineralizing agents, i.e. hydroxide and fluoride ions, because these agents dissolve silica. As a result the stability of MCM-41 in aqueous solutions is limited to pH values ≤ 7 . Moreover, the chemical affinity of the pore surface towards precursors of catalytically active phases sometimes also results in the collapse of the hexagonal framework structure. An example of this behavior is the reaction with aqueous impregnation solutions containing common molybdenum precursors, viz. (poly)molybdate anions. Opposed to this behaviour towards molybdenum precursors, the interaction of the MCM-41 pore

surface with certain common nickel precursors is relatively weak, resulting in low dispersions of the active phase.

MCM-41 can be synthesised following a wide variety of preparation procedures. However, there is one thing all these procedures have in common next to the obvious presence of a source of silica, viz. a templating agent. A template is a structure-directing agent, which is usually a relatively simple molecule or ion, around which a framework is built up. The most common templates are quaternary ammonium ions with short alkyl chains, which are used for the syntheses of a large number of zeolites. For the synthesis of MCM-41 similar quaternary ammonium ions are frequently used, albeit with one important modification: at least one of the short alkyl chains is replaced by a long alkyl chain, generally a hexadecyl group. This slight modification has an enormous impact on the behaviour of the template in aqueous solutions, however. Due to the large hydrophobic alkyl chain the template ions will aggregate together in order to minimise energetically unfavourable interactions of the apolar alkyl chains with the very polar water solvent molecules. Although unfavourable from an entropic point of view, this is exactly the same behaviour as displayed by soaps upon dissolution in water. The resulting aggregates of ions are denoted micelles. It follows that these micelles have a hydrophobic core, containing the large alkyl chains, and a hydrophilic surface, due to the ionic character of the ammonium head groups.

The energetically most favourable form of micelles is spherical, because in this geometry the surface energy is minimised most efficiently. Moreover, this conformation allows the largest number of micelles to be formed out of a certain amount of template, which is attractive considering the entropy of the system. Nevertheless, it is observed that at increasing amounts of template in water a different micelle geometry evolves: the spherical micelles gradually transform into long tubes, often denoted as rod-like micelles. Increasing the template concentration even further results in aggregation of the rod-like micelles into a hexagonal liquid crystalline structure, resembling the MCM-41 structure. If the template concentration is increased further this hexagonal liquid crystalline phase first transforms into a cubic liquid crystalline phase and eventually, at the highest template concentrations, into a lamellar liquid crystalline phase. (J.S. Beck *et al.*, 1992; G.D. Stucky *et al.*, 1994; Q. Huo *et al.*, 1996) The cubic liquid crystalline phase resembles the structure of mesoporous MCM-

48, whereas the lamellar phase is the structural analogue of MCM-50 (an unstable material, which consists of platelets of amorphous silica). Because of the resemblances between the liquid crystalline phases and the MCM structures it is often assumed that the liquid crystalline structures are the actual templates of MCM-41 and MCM-48. In the case of MCM-48 this is indeed the most likely templating mechanism. However, in a large number of studies that were devoted to the elucidation of the mechanism of MCM-41 formation the hexagonal liquid crystalline phase was initially not observed in the synthesis gels, although MCM-41 was formed. (C-Y. Chen *et al.*, 1993; A. Monnier *et al.*, 1993) These findings imply that another mechanism can be operative as well in the formation of MCM-41. In this alternative mechanism the rod-like micelles assemble not prior to but during the generation of the MCM-41 structure. A convincing explanation for this behaviour is that the aggregation of the rod-like micelles into a liquid crystalline structure is thought to be energetically unfavourable, due to the electrostatic repulsions between the positively charged surfaces of the micelles (electrical charges are a result of the presence of the ionic head groups). During synthesis of MCM-41 the electrostatic repulsions decrease as a result of the formation of a monolayer of silica around the micelles, thereby facilitating the subsequent aggregation of the micelles into close-packed hexagonal structures.

Next to a structure-directing agent and water as a solvent two more ingredients are required for the synthesis of MCM-41: a source of silica and a mineralising agent. Various sources of silica can be used for syntheses, viz. water glass, amorphous silica and Kanemite (a layered silicate structure consisting of anionic silica sheets with charge-compensating sodium ions present in the interlayers). Furthermore, organic silicon alkoxides are also frequently used. For the dissolution of the various silica sources a so-called "mineralising agent" is used. For this purpose sodium hydroxide or a concentrated ammonia solution are frequently used, although HF also finds application, despite the hazards associated with its use. Upon dissolution of silica by the mineralising agent small silicon oxy-anions are produced. In the presence of the rod-like template micelles the silicate anions diffuse towards the surfaces of the micelles as a result of electrostatic attractions. Therefore the concentration of silicate anions at the surface of the micelles rapidly increases, as do the electrostatic repulsions between the individual silicate ions. In order to alleviate these repulsive interactions the silicate ions start to condense with each other, thereby forming a monolayer of

amorphous silica around the micelles. Charge compensation of the ionic headgroups of the template is still brought about by deprotonated silanol groups of the silica monolayer. At this stage the silica "coated" micelles can start to cluster together by condensation reactions between the silica layers of individual micelles, thus generating the MCM-41 framework. As a result of these processes the pore walls of MCM-41 are amorphous and only 2-3 monolayers thick. (C-Y. Chen et al., 1993)

The processes described above can take place over a wide range of synthesis conditions, including gel composition, pH, timescale, temperature and pressure. However, once MCM-41 has been formed its pores are filled with template and in order to obtain a completely mesoporous support material the micelles must be removed. The most elegant solution to this demand is removal by means of (repeated) washing with (slightly acidified) mixtures of organic solvent and water, resulting in extraction of the template. The resulting solutions, containing the template, can be evaporated to dryness, which leads to recovery of the template. If the synthesis conditions were relatively mild the template will not have decomposed and can be re-used for a next synthesis. A simpler method for template removal is calcination. During this process template is decomposed into CO_2 , some NO_x and steam. Although MCM-41 is unstable with respect to steam, the quantities of steam produced during this process are too small to do any damage to the MCM-41 framework structure.

Some modifications to the synthesis procedure described above are possible. The first possibility is the incorporation of hetero-elements inside the pore walls of the MCM-41 structure. The most frequently incorporated elements are aluminium and titanium. The presence of aluminium inside the pore walls generates an excess negative framework charge (as in zeolites and amorphous silica-aluminas). When this charge is compensated by protons the resulting material is weakly Brønsted acidic. Compared to all-silica MCM-41 the physical properties of materials containing aluminium are generally a bit less well-developed and dealumination can take place during template removal (especially in the presence of steam during calcination). Incorporation of titanium inside the pore walls results in materials displaying interesting oxidation properties. A second adaptation that can be made to MCM-41 is "engineering" of the pore size. The most frequently used template for the synthesis of MCM-41 is hexadecyl (=cetyl) trimethyl ammonium bromide (or chloride), i.e. a

template with an alkyl chain containing sixteen $-CH_2-$ moieties. This template yields MCM-41 with a uniform pore size of approximately 2.7 nm (vide infra). Using templates with longer or shorter alkyl chains the pore size can be influenced. Nevertheless, due to the limited range of alkylammonium ions suitable for the preparation of MCM-41 the pore size can be adjusted to a small extent only. A more dramatic increase of pore size can be accomplished by the addition of so-called "auxiliary organics" to the synthesis gel. 1,3,5-trimethylbenzene (mesitylene). These organic molecules, which must be apolar, do not dissolve in water, but instead they are absorbed in the hydrophobic core of the template micelles. Due to this absorption the micelles swell, thus increasing the average size of the mesopores in MCM-41 up to values of approximately 8-10 nm in diameter. (J.S. Beck *et al.*, 1992; N.K. Raman *et al.*, 1996; O. Franke *et al.*, 1995)



สถาบันวิทยบริการ
จุฬาลงกรณ์มหาวิทยาลัย

CHAPTER IV

EXPERIMENTAL

This chapter consists of experimental systems and procedures used in this work which is divided into three parts consisting of catalyst preparation (4.1), catalyst characterization (4.2) and reaction study in CO hydrogenation (4.3).

The samples were prepared and analyzed by means of X-ray diffraction (XRD), transmission electron spectroscopy (TEM), and temperature-programmed reduction (TPR). The reaction study was performed in order to measure activity and product selectivity toward CO hydrogenation at 220°C and 1 atm.

4.1 Catalyst preparation

4.1.1 Chemicals

The details of chemicals used in this experiment are shown in Table 4.1

Table 4.1 Chemicals used in the preparation of catalysts.

Chemical	Supplier
Cobalt (II) nitrate exahydrate ($\text{Co}(\text{NO}_3)_2 \cdot 6\text{H}_2\text{O}$)	Aldrich
Boric acid (H_3BO_3)	Aldrich
Silicon dioxide (SiO_2), larg pore	Stream Chemicals
Cetyltrimethyl ammonium bromide (CTABr)	Aldrich
Colloidal silica ludox AS 40%	Aldrich
Sodium hydroxide (NaOH)	Merck
Ammonia solution 25% (NH_3)	BDH
Acetic acid (CH_3COOH)	Carlo erba

4.1.2 Preparation of MCM-41 supports

Pure silica MCM-41 with 3 nm pore diameters was prepared in the same manner as that of Cho et al. (D.H. Cho et al., 2000) using the gel composition of CTABr:0.3 NH₃:4 SiO₂: Na₂O:200 H₂O, where CTABr denotes cetyltrimethyl ammonium bromide. Briefly, 20.03 g of colloidal silica Ludox AS 40% (Merck) was mixed with 22.67 g of 11.78% sodium hydroxide solution. Another mixture comprised of 12.15 g of CTABr (Aldrich) in 36.45 g of deionized water, and 0.4 g of an aqueous solution of 25% NH₃. Both of these mixtures were transferred into a Teflon lined autoclave, stirred for 30 min, then heated statically at 100 °C for 5 days. The obtained solid material was filtered, washed with water until no base was detected and then dried at 100 °C. The sample was then calcined in flowing nitrogen up to 550 °C (1–2 °C/min), then in air at the same temperature for 5 h, and is referred to in this paper as small pore MCM-41.

4.1.3 Preparation of the boron-modified MCM-41

A 1, 3, and 5 wt% of boron dispersed on the MCM-41 supports was prepared by the incipient wetness impregnation. A desired amounts of Boric acid (H₃BO₃) (Aldrich) was dissolved in deionized water and then impregnated onto the support obtained from 4.1.2. The sample was dried at 110°C for 12 h and calcined in air at 500°C for 4 h.

4.1.4 Preparation of the supported Co samples

A 5, 10, 15 and 20 wt% of boron dispersed on the boron-modified MCM-41 supports was prepared by the incipient wetness impregnation. A desired amounts of Cobalt (II) nitrate exahydrate [Co(NO₃)₂·6H₂O] (Aldrich) was dissolved in deionized water and then impregnated onto the boron-modified support obtained from 4.1.3. The sample was dried at 110°C for 12 h and calcined in air at 500°C for 4 h.

4.1.5 Sample nomenclature

The nomenclature used for the samples in this study is following:

SiB-a refers to the boron-modified silica support where:

a is the weight percents of boron

i-Co/SiB-a refers to the boron-modified silica supported cobalt catalyst where:

a is the weight percents of boron

i is the weight percent of cobalt

MB-a refers to the boron-modified silica support where:

a is the weight percents of boron

i-Co/MB-a refers to the boron-modified silica supported cobalt catalyst where:

a is the weight percents of boron

i is the weight percent of cobalt

4.2. Catalyst characterization

Various characterization techniques were used in this studied in order to clarify the catalyst structure and morphology, surface composition of various boron-modified supported cobalt catalyst.

4.2.1 N₂ physisorption

BET apparatus for the single point method

The reaction apparatus of BET surface area measurement consisted of two feed lines for helium and nitrogen using a Micromeritics Chemisorb 2750. The flow rate of the gas was adjusted by means of fine-metering valve on the gas chromatograph. The sample cell made from pyrex glass. The mixture gases of helium and nitrogen flowed through the system at the nitrogen relative of 0.3. The catalyst sample (ca. 0.2 to 0.5 g) was placed in the sample cell, which was then heated up to 200 °C and held at this temperature for 1 h. After the catalyst sample was cooled down to room temperature, nitrogen uptakes were measure as follows.

Step (1) Adsorption step: The sample that set in the sample cell was dipped into liquid nitrogen. Nitrogen gas that flowed through the system was adsorbed on the surface of the sample until equilibrium was reached.

Step (2) Desorption step: The sample cell with nitrogen gas-adsorption catalyst sample dipped into the water at room temperature. The adsorbed nitrogen gas was desorbed from the surface of the sample. This step was completed when the indicator line was in the position of base line.

Step (3) Calibration step: 1 ml of nitrogen gas at atmospheric pressure was injected through the calibration port of the gas chromatograph and the area was measured. The area was the calibration peak.

4.2.2 X-ray diffraction (XRD)

XRD were performed to determine the bulk phase of catalysts by SIEMENS D 5000 X-ray diffractometer connected with a computer with Diffract ZT version 3.3 program for fully control of the XRD analyzer. The experiments were carried out by using $\text{CuK}\alpha$ ($\lambda = 1.54439 \text{ \AA}$) radiation with Ni filter in the 2θ range of 20-80 degrees resolution 0.04° . The crystallite size was estimated from line broadening according to the Scherrer equation and $\alpha\text{-Al}_2\text{O}_3$ was used as standard.

4.2.3 Temperature programmed reduction (TPR)

TPR was used to determine the reducibility of catalysts using a Micrometric Chemisorb 2750:

1. The catalyst sample 0.2 g used in the sample cell.
2. Prior to operation, the catalysts were heated up to 200°C in flowing nitrogen and held at this temperature for 1 h.
3. After the catalyst sample was cooled down to room temperature, carrier gas (10 % H_2 in Ar) were ramping from 35°C to 800°C .
4. During reduction, a cold trap was placed to before the detector to remove water produced.

4.2.4 Scanning Electron microscopy

Scanning electron microscopy (SEM) and Energy dispersive X-ray spectroscopy (EDX) was used to determine the morphology and elemental distribution of the catalyst particles. Model of SEM: JEOL mode JSM-5800LV and EDX was performed using Link Isis Series 300 program at the Scientific and Technological Research Equipment Center, Chulalongkorn University (STREC).

4.2.5 Transmission Electron Microscopy (TEM)

The dispersion of cobalt oxide supports was determined using JEM-2100 transmission electron spectroscopy operated at 100 kV with 25 k magnification. The sample was dispersed in ethanol prior to the TEM measurement.

4.2.6 Hydrogen Chemisorption

Static H₂ chemisorption at 100 °C on the reduce catalysts was used to determine the number of reduce surface cobalt metal atoms and overall cobalt dispersion. The total hydrogen chemisorption was calculated from the number of injection of a known volume. H₂ chemisorption was carried out following the procedure described by CO- pulse chemisorption technique using a Micromeritics Chemisorb 2750 (pulse chemisorption system). Prior to chemisorption, the catalysts were reduced at 350 °C for 3 hours after ramping up at a rate of 1 °C/min.

4.3. Reaction study in CO hydrogenation

4.3.1 Materials

The reactant gas used for the reaction study was the carbon monoxide in hydrogen feed stream as supplied by Thai Industrial Gas Limited (TIG). The gas mixture contained 9.73 vol % CO in H₂ (22 cc/min). The total flow rate was 30 ml/min with the H₂/CO ratio of 10/1. Ultra high purity hydrogen (50 cc/min) and high purity argon (8 cc/min) manufactured by Thai Industrial Gas Limited (TIG) were used for reduction and balance flow rate.

4.3.2 Apparatus

Flow diagram of CO hydrogenation system is shown in Figure 4.1. The system consists of a reactor, an automatic temperature controller, an electrical furnace and a gas controlling system.

4.3.2.1 Reactor

The reactor was made from a stainless steel tube (O.D. 3/8 "). Two sampling points were provided about and below the catalyst bed. Catalyst was placed between two quartz wool layers.

4.3.2.2 Automation Temperature Controller

This unit consisted of a magnetic switch connected to a variable voltage transformer and a solid state relay temperature controller model no.SS2425DZ connected to a thermocouple. Reactor temperature was measured at the bottom of the catalyst bed in the reactor. The temperature control set point is adjustable within the rang of 0-800 °C at the maximum voltage output of 220 volt.

4.3.2.3 Electrical Furnace

The furnace supplied heat to the reactor for CO hydrogenation. The reactor could be operated from temperature up to 800 °C at the maximum voltage of 220 volt.

4.3.2.4 Gas Controlling System

Reactant for the system was each equipped with a pressure regulator and an on-off valve and the gas flow rates were adjusted by using metering valves.

4.3.2.5 Gas Chromatograph

The composition of hydrocarbons in the product stream was analyzed by a Shimadzu GC-14B (VZ10) gas chromatograph equipped with a flame ionization detector. A Shimadzu GC-8A (molecular sieve 5A) gas chromatograph equipped with a thermal conductivity detector was used to analyze CO and H₂ in the feed and product streams. The operating conditions for each instrument are show in the Table 4.2.

Table 4.2 Operating condition for gas chromatograph

Gas Chromatograph	SHIMADZU GC-8A	SHIMADZU GC-14B
Detector	TCD	FID
Column	Molecular sieve 5A	VZ 10
- Column material	SUS	-
- Length	2 m	-
- Outer diameter	4 mm	-
- Inner diameter	3 mm	-
- Mesh range	60/80	60/80
- Maximum temperature	350 °C	80°C
Carrier gas	He (99.999%)	N ₂ (99.999%)
Carrier gas flow	20 cc/min	-
Column gas	He (99.999%)	Air , H ₂
Column gas flow	20 cc/min	-
Column temperature		
- initial (°C)	60	70
- final (°C)	60	70
Injector temperature (°C)	100	100
Detector temperature (°C)	100	150
Current (mA)	80	-
Analysed gas	Ar, CO, H ₂	Hydrocarbon C ₁ -C ₄

4.3.3 Procedure

1. Using 0.2 g of catalyst packed in the middle of the stainless steel microreactor, which is located in the electrical furnace.

2. A flow rate of Ar = 8 cc/min, 9% CO in H₂ = 22 cc/min and H₂ = 50 cc/min in a fixed-bed flow reactor. A relatively high H₂/CO ratio was used to minimize deactivation due to carbon deposition during reaction.

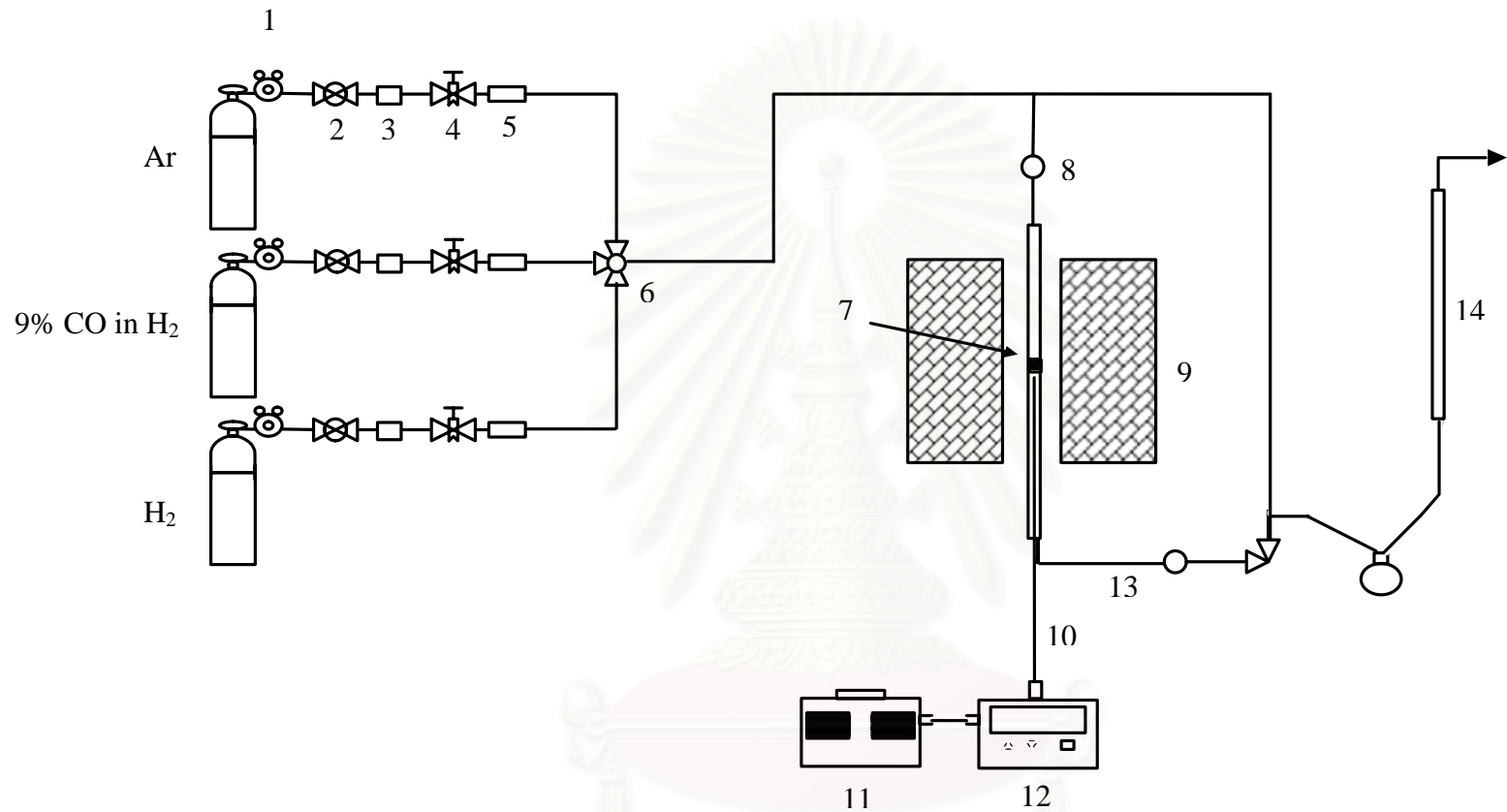
3. The catalyst sample was re-reduced *in situ* in flowing H_2 at $350^\circ C$ for 3 h prior to CO hydrogenation.

4. CO hydrogenation was carried out at $220^\circ C$ and 1 atm total pressure in flowing 9% CO in H_2 .

5. The effluent was analyzed using gas chromatography technique [Thermal conductivity detector (TCD) was used for separation of carbon monoxide (CO) and methane (CH_4) and flame ionization detector (FID) were used for separation of light hydrocarbon such as methane (CH_4), ethane (C_2H_6), propane (C_3H_8), etc.] In all cases, steady-state was reached within 5 h.

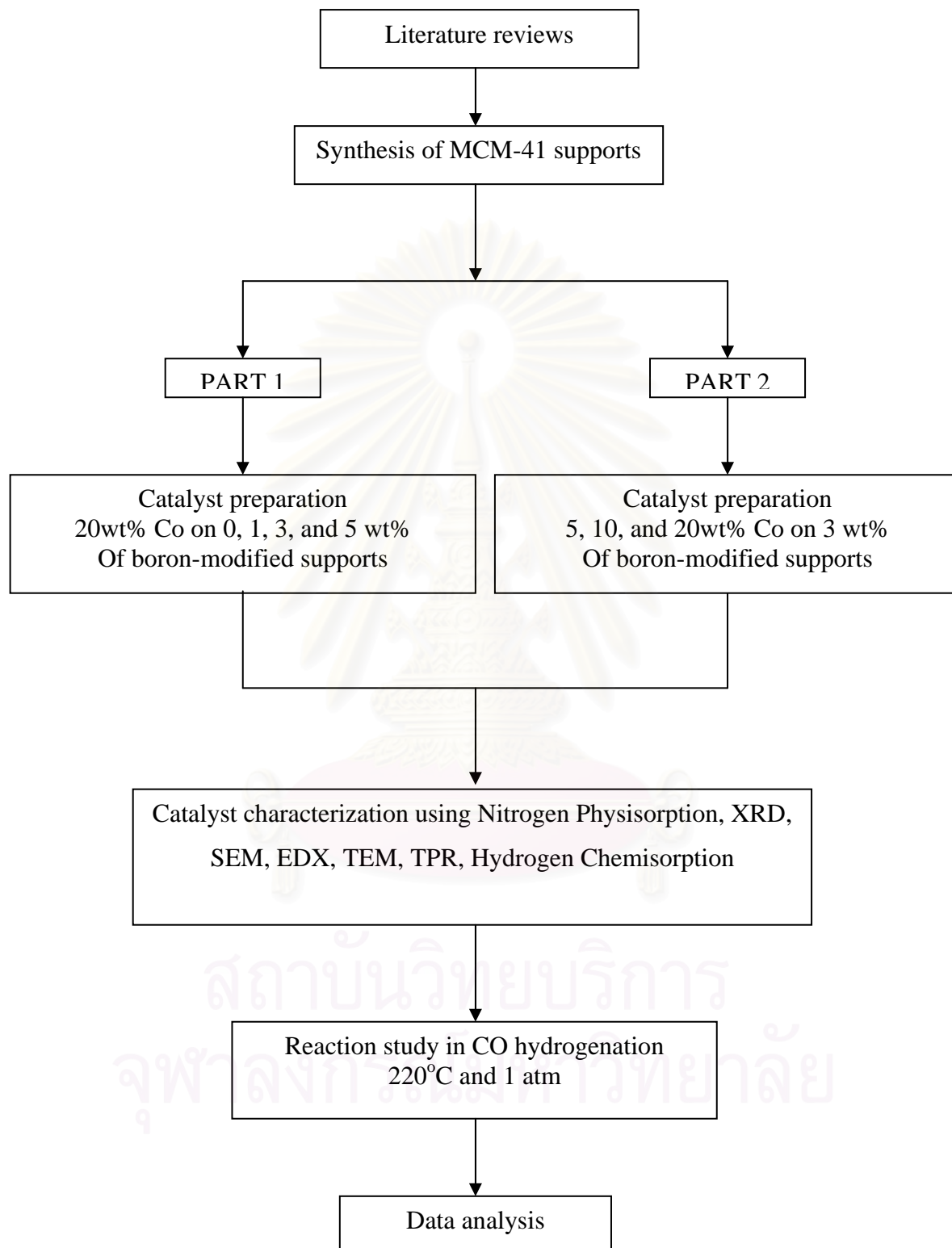


สถาบันวิทยบริการ
จุฬาลงกรณ์มหาวิทยาลัย



- | | | | |
|-----------------------|-----------------------|----------------------------------|----------------------------|
| 1. Pressure Regulator | 2. On-Off Value | 3. Gas Filter | 4. Metering Valve |
| 5. Back Pressure | 6. 3-way Valve | 7. Catalyst Bed | 8. Sampling point |
| 9. Furnace | 10. Thermocouple | 11. Variable Voltage Transformer | 12. Temperature Controller |
| 13. Heating Line | 14. Bubble Flow Meter | | |

Figure 4.1 Flow diagram of CO hydrogenation system

RESEARCH METHODOLOGY

CHAPTER V

RESULTS AND DISCUSSION

This chapter is divided into two sections. Section 5.1 described characteristics of 20 wt% cobalt (Co) dispersed on various boron-modified supports. Section 5.2 described characteristics and catalytic activity towards CO hydrogenation of various amounts of Co catalysts dispersed on 3 wt% of boron-modified supports.

5.1 Various boron loading of 20 wt% cobalt on boron-modified MCM-41 supported catalyst.

5.1.1 BET surface area

Table 5.1 BET surface area measurement of 20 wt% cobalt on boron-modified supported cobalt catalyst.

Supports	BET surface area (m ² /g)	Catalyst samples	BET surface area (m ² /g)
SiB-0	155	20-Co/SiB-0	142
SiB-1	165	20-Co/SiB-1	134
SiB-3	156	20-Co/SiB-3	136
SiB-5	147	20-Co/SiB-5	141
MB-0	510	20-Co/MB-0	450
MB-1	414	20-Co/MB-1	358
MB-3	391	20-Co/MB-3	319
MB-5	355	20-Co/MB-5	199

It was found that the surface areas of the modified and unmodified silica were 147-165 m²/g whereas those for MCM-41 were 355-510 m²/g. In fact, the surface areas decreased with boron modification and Co loading.

5.1.2 X-ray diffraction (XRD)

XRD patterns of the boron-modified supports before impregnation with the cobalt precursor are shown in **Figure 5.1**. It was observed that the pure SiO_2 and pure MCM-41 exhibited only a broad XRD peak assigning to the conventional amorphous silica. XRD patterns of the SiO_2 after B modification showed the XRD peak of B_2O_3 at 28° . XRD patterns of the MCM-41 after B modification also showed the XRD peak of B_2O_3 at 28° . After impregnation with the cobalt precursor, the catalyst samples were dried and calcined. The XRD patterns of the boron-modified supported Co catalyst are shown in **Figure 5.2**. Besides the observation of the characteristic peaks of the supports as shown in **Figure 5.1**, all calcined samples exhibited XRD peaks at 31° (weak), 36° (strong), and 65° (weak), which were assigned to the presence of Co_3O_4 . This indicated that the Co_3O_4 formed was highly dispersed.

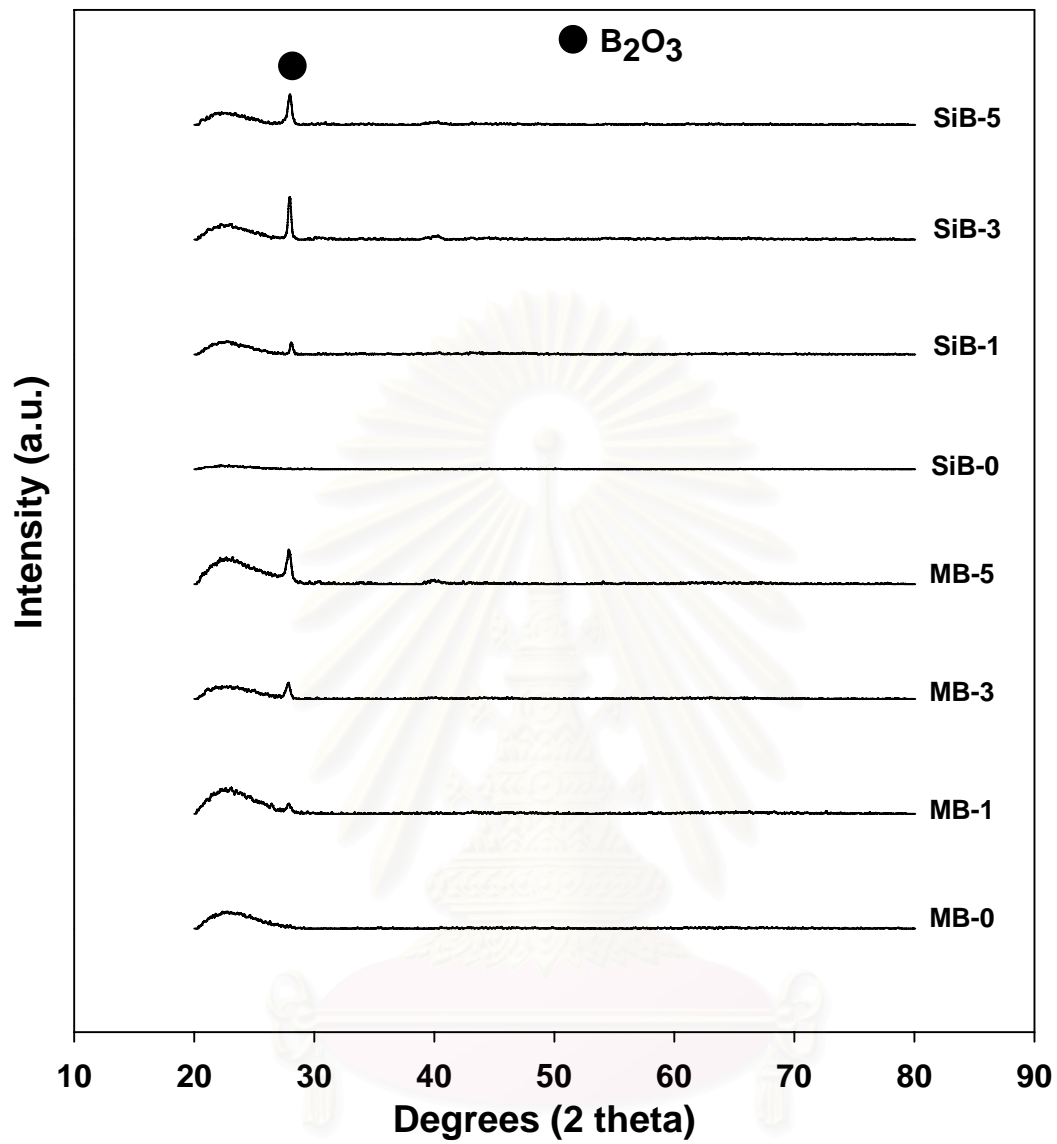


Figure 5.1 XRD patterns of the boron-modified supports before impregnation with the cobalt precursor.

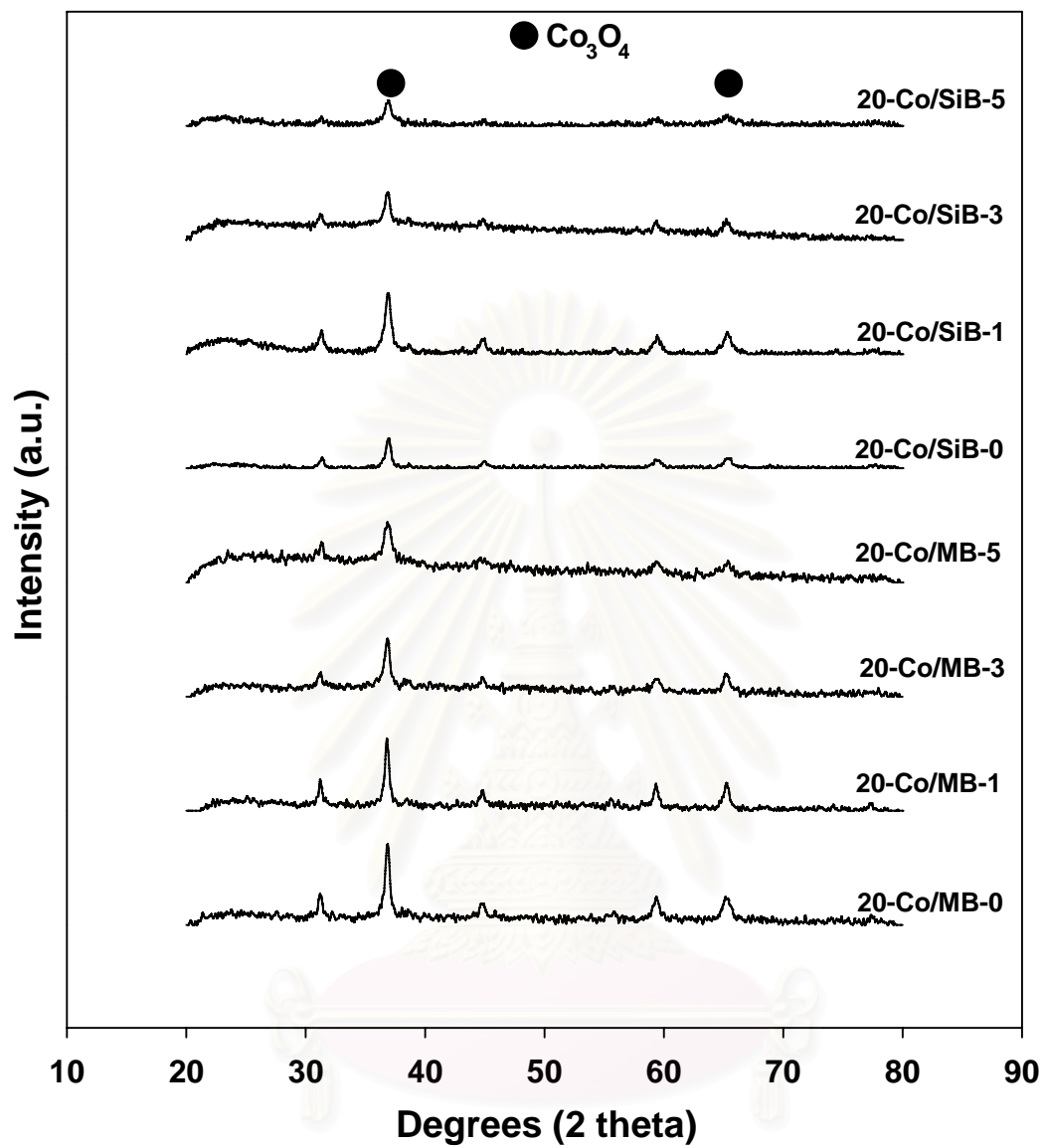


Figure 5.2 XRD patterns of the boron-modified-supported Co catalyst.

5.1.3 Scanning electron microscopy (SEM) and Energy dispersive X-ray spectroscopy (EDX)

SEM and EDX were also conducted in order to study the morphologies and elemental distribution of the samples, respectively. In general, there was no significant change in morphologies and elemental distribution of all catalyst samples after calcination. A typical SEM micrograph and EDX mapping for boron-modified-silica supported Co catalyst sample are illustrated in **Figure 5.3-5.6** and for boron-modified-MCM-41 supported Co catalyst sample are illustrated in **Figure 5.7-5.10**. It can be seen that the distribution of Co was well on the surface of the support.



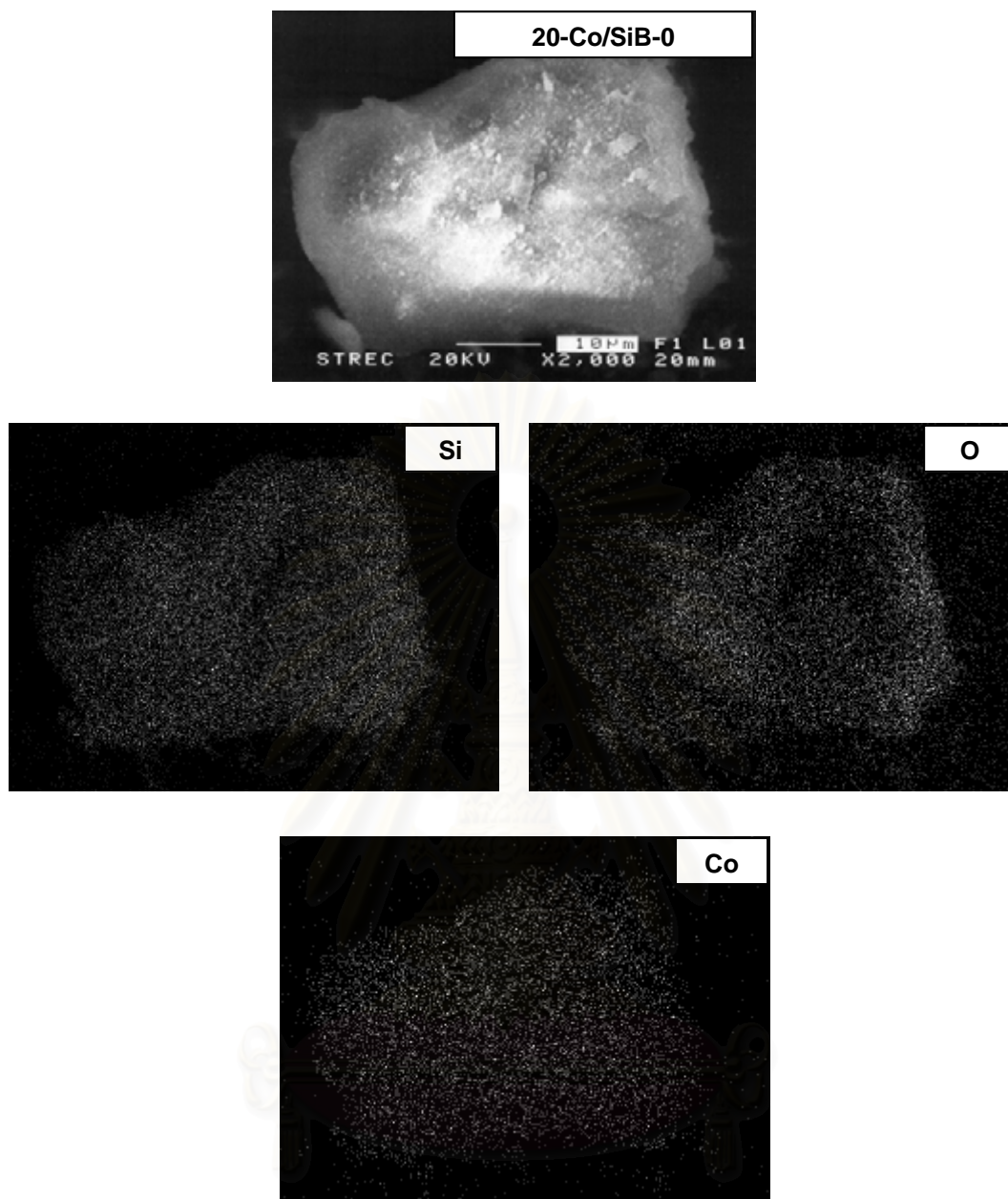


Figure 5.3 SEM micrograph and EDX mapping for 20-Co/SiB-0 catalyst granule.

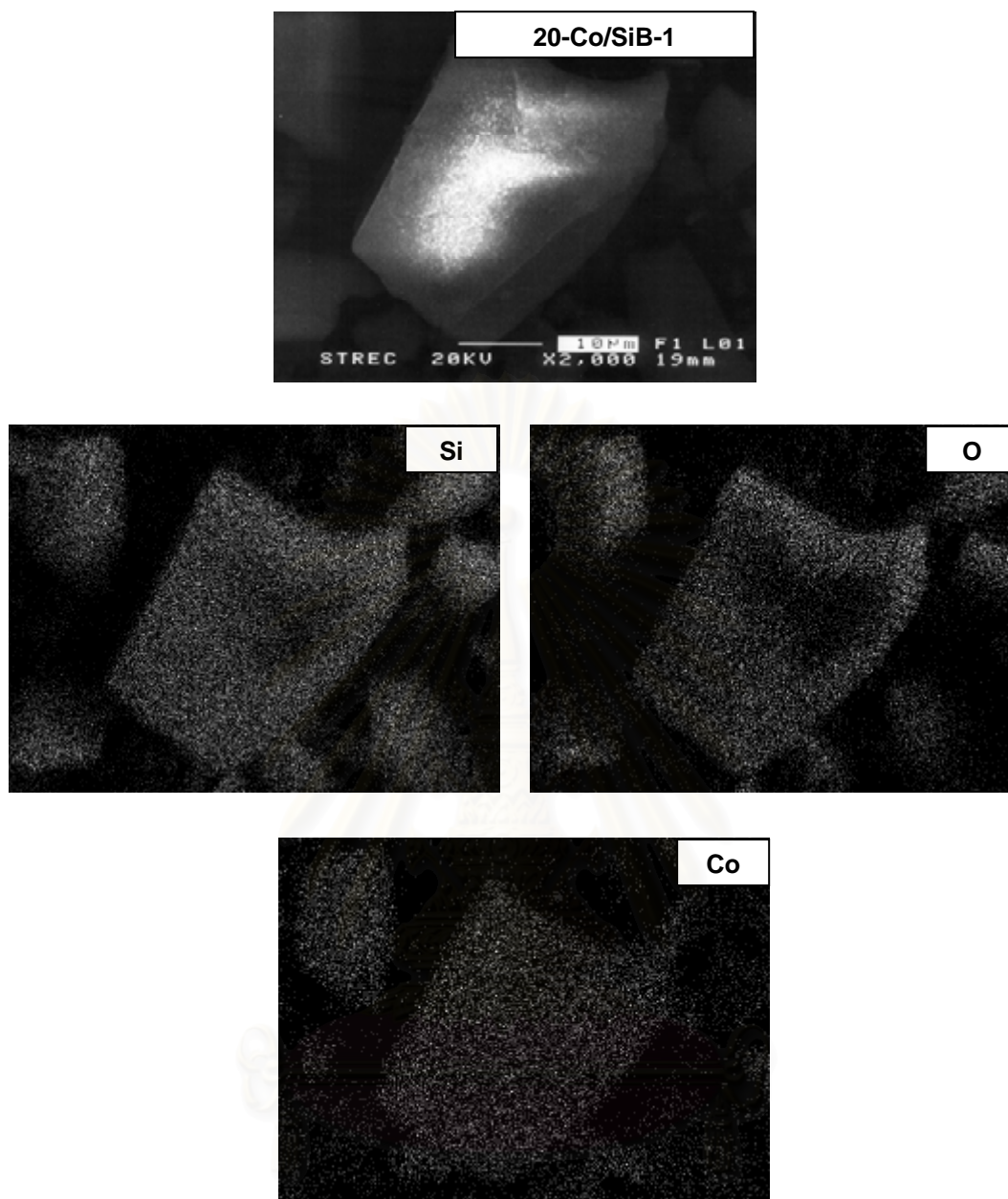


Figure 5.4 SEM micrograph and EDX mapping for 20-Co/SiB-1 catalyst granule.

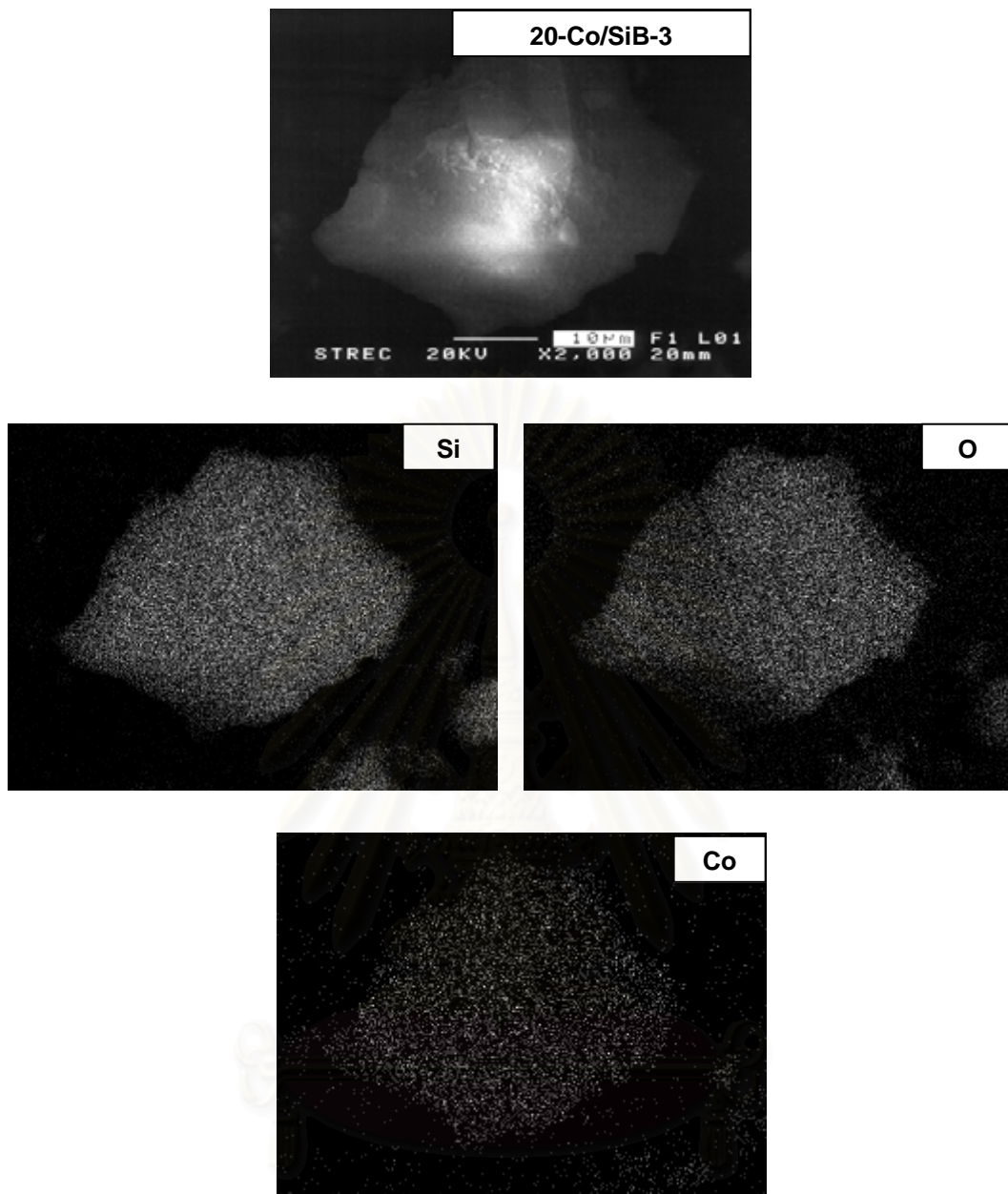


Figure 5.5 SEM micrograph and EDX mapping for 20-Co/SiB-3 catalyst granule.

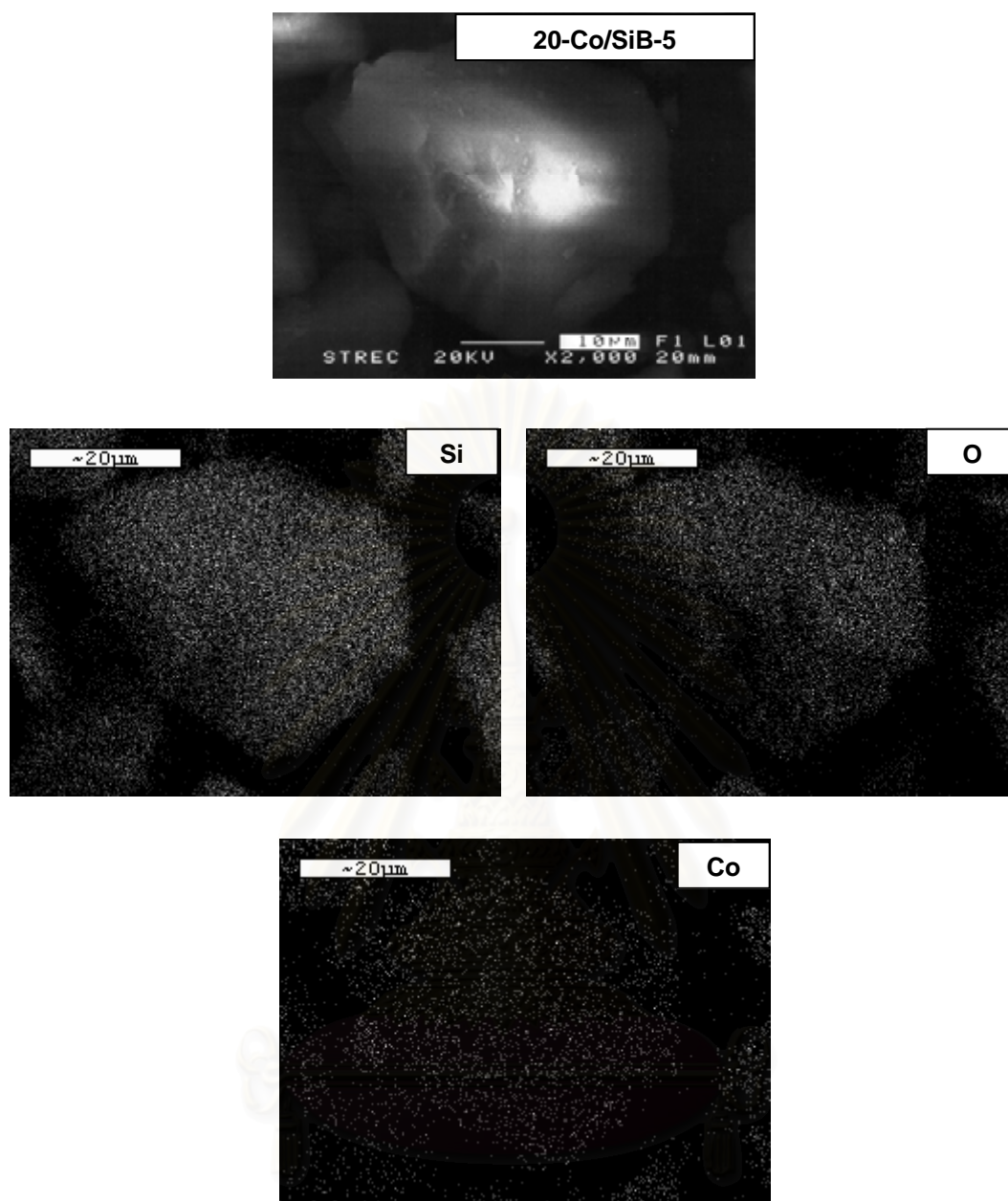


Figure 5.6 SEM micrograph and EDX mapping for 20-Co/SiB-5 catalyst granule.

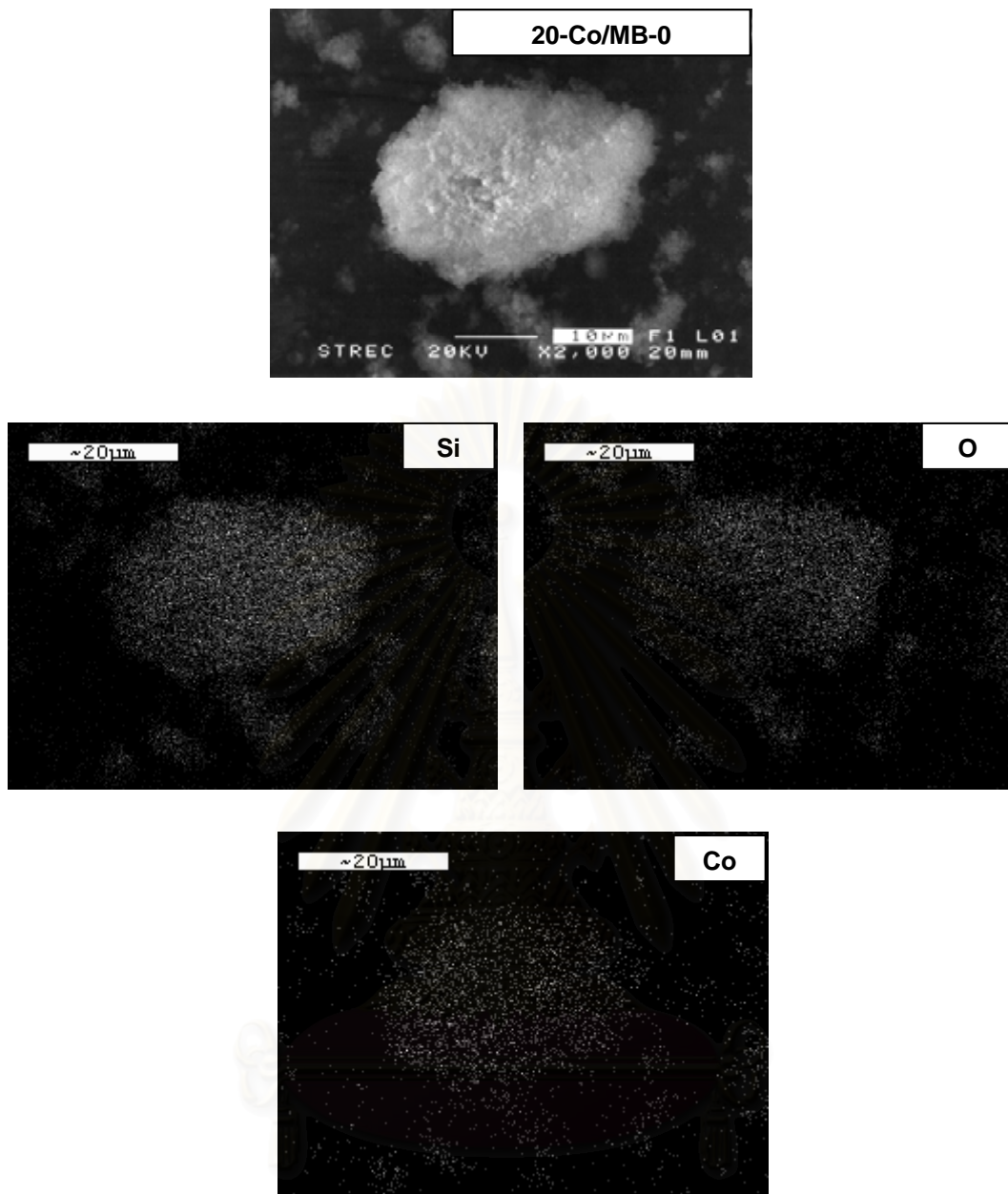


Figure 5.7 SEM micrograph and EDX mapping for 20-Co/MB-0 catalyst granule.

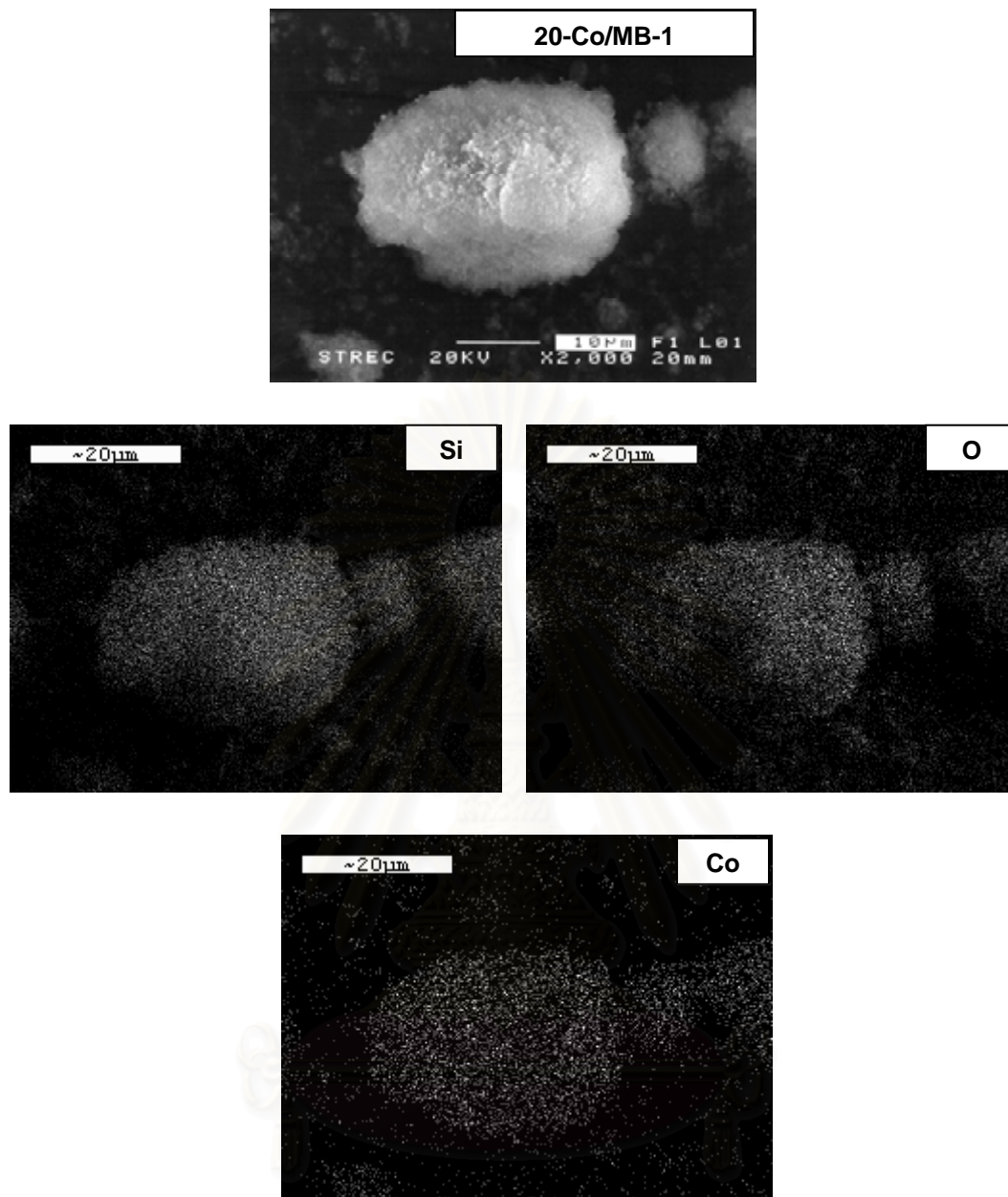


Figure 5.8 SEM micrograph and EDX mapping for 20-Co/MB-1 catalyst granule.

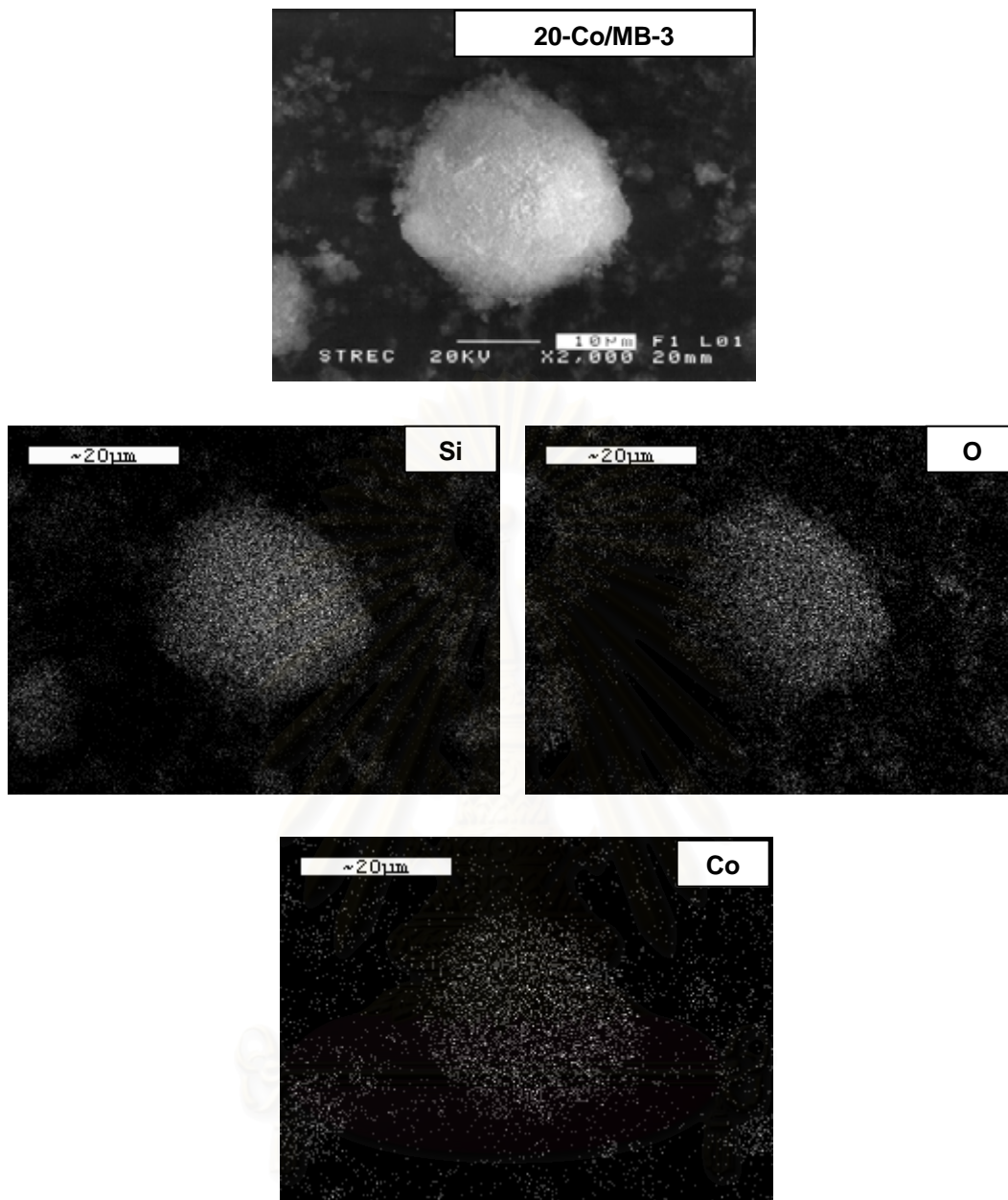


Figure 5.9 SEM micrograph and EDX mapping for 20-Co/MB-3 catalyst granule.

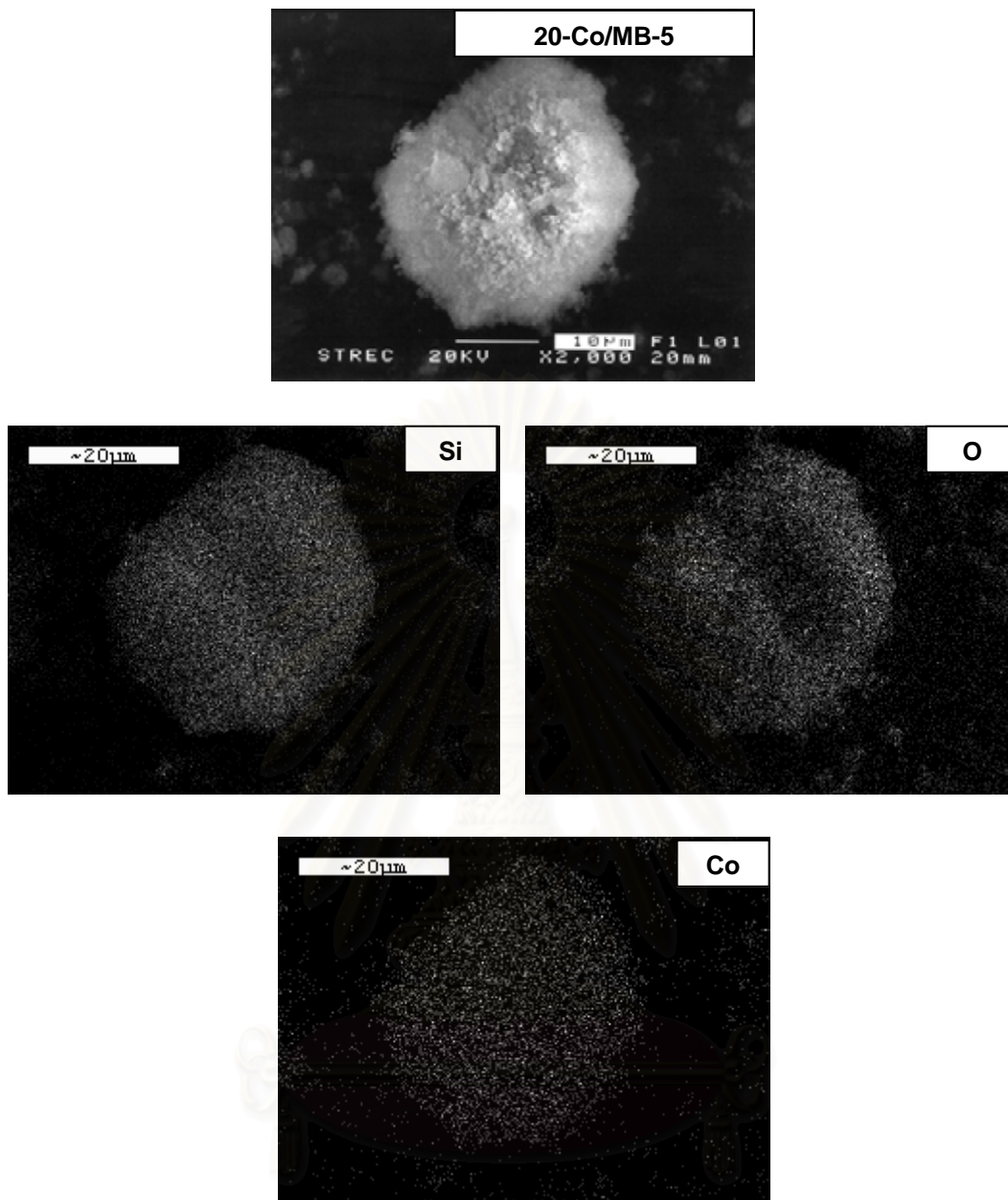


Figure 5.10 SEM micrograph and EDX mapping for 20-Co/MB-5 catalyst granule.

5.1.4 Transmission Electron Microscopy (TEM)

In order to determine the dispersion and crystallite size of Co oxides species dispersed on the supports employed, the high resolution TEM was used. The TEM micrographs for silica and MCM-41 supports are shown in **Figure 5.11** and structure of MCM-41 are shown in **Figure 5.12**. As seen in this Figure, pore sizes of MCM-41 are 3 nm (small pore MCM-41). The TEM micrographs for Co oxides species dispersed on silica supports with and without B modification are shown in **Figure 5.13** whereas those for MCM-41 supports are shown in **Figure 5.14**. As seen in both Figures, the dark spots represented the Co oxide species dispersed on the various supports. It can be seen from **Figure 5.13** that Co oxide species on the silica supports were well dispersed having the crystallite size of ca. 50 to 100 nm. Apparently, the crystallite size seemed to decrease with B modification. Similarly, the TEM micrographs as shown in **Figure 5.14** of Co oxide species on the MCM-41 supports were also well dispersed having the crystallite size of 100 to 200 nm. It can be seen that the crystallite size of Co oxide species on the silica supports was smaller than that on the MCM-41 supports indicating more agglomeration of Co oxide species.

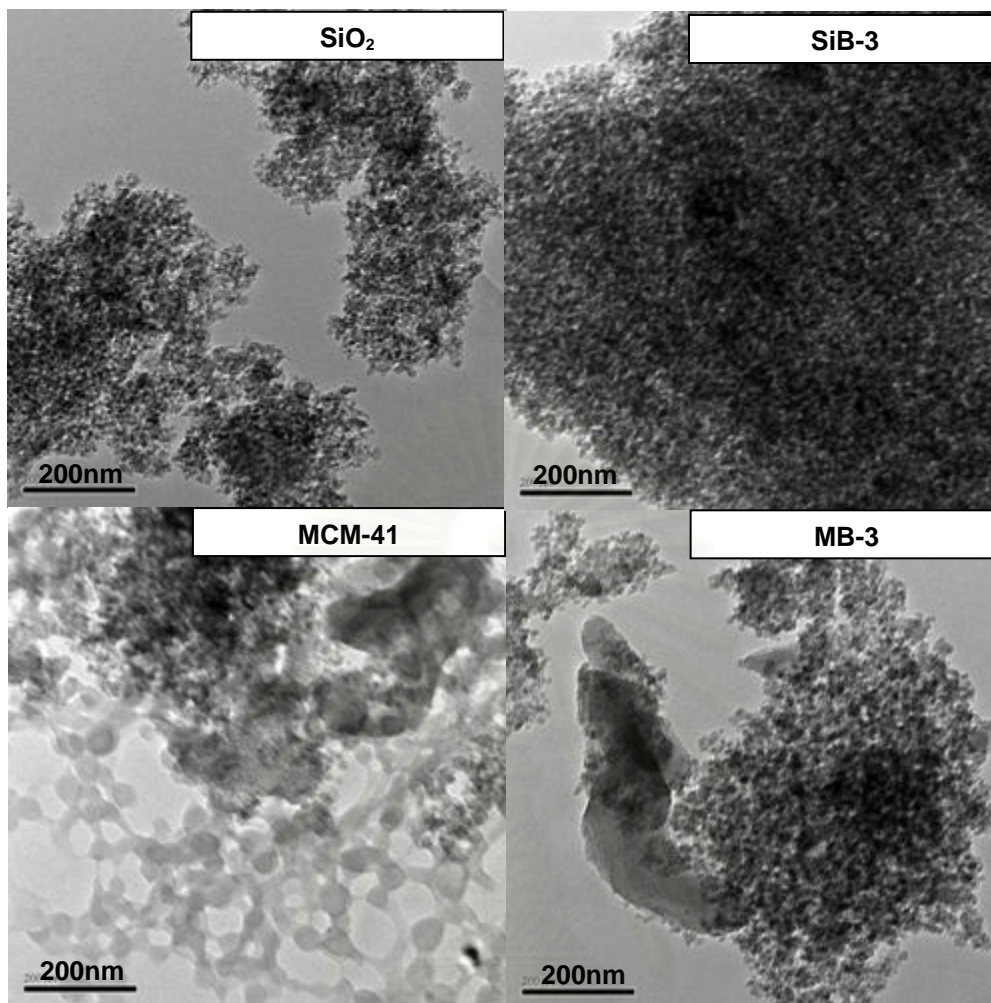


Figure 5.11 TEM micrographs of pure silica, pure MCM-41 and 3 wt% of boron-modified supports.

สถาบันวิทยบริการ
จุฬาลงกรณ์มหาวิทยาลัย

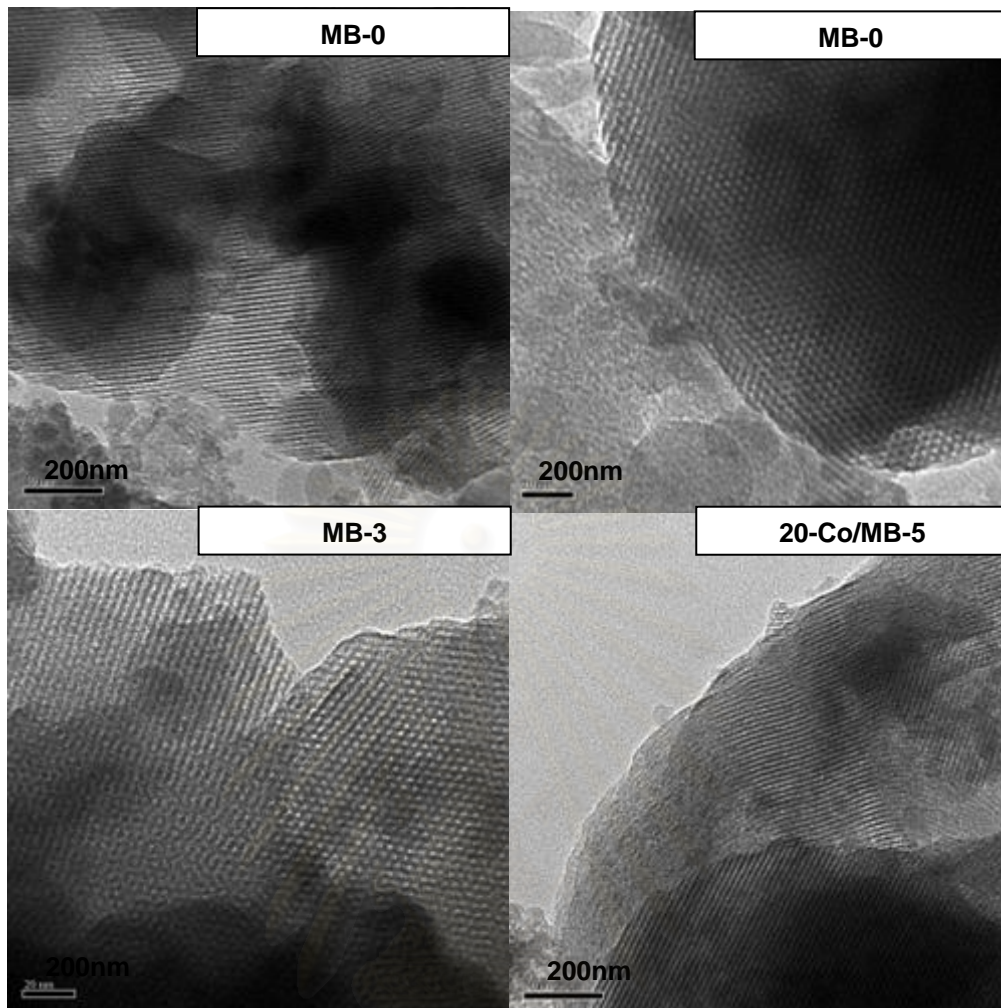


Figure 5.12 TEM micrographs of boron-modified MCM-41 supports and 5 wt% of boron-modified MCM-41 supported Co catalyst structure.

สถาบันวิทยบริการ
จุฬาลงกรณ์มหาวิทยาลัย

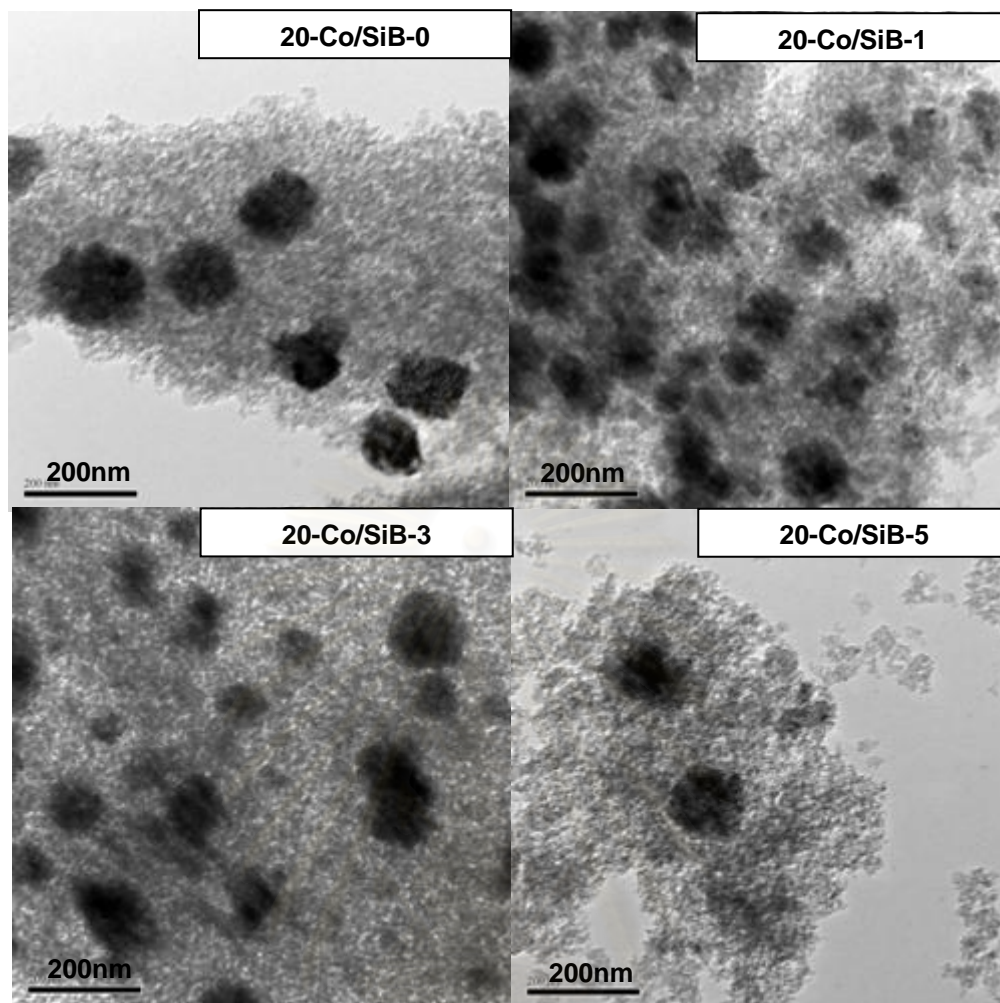


Figure 5.13 TEM micrographs for all cobalt dispersed on the boron-modified silica supports.

สถาบันวิทยบริการ
จุฬาลงกรณ์มหาวิทยาลัย

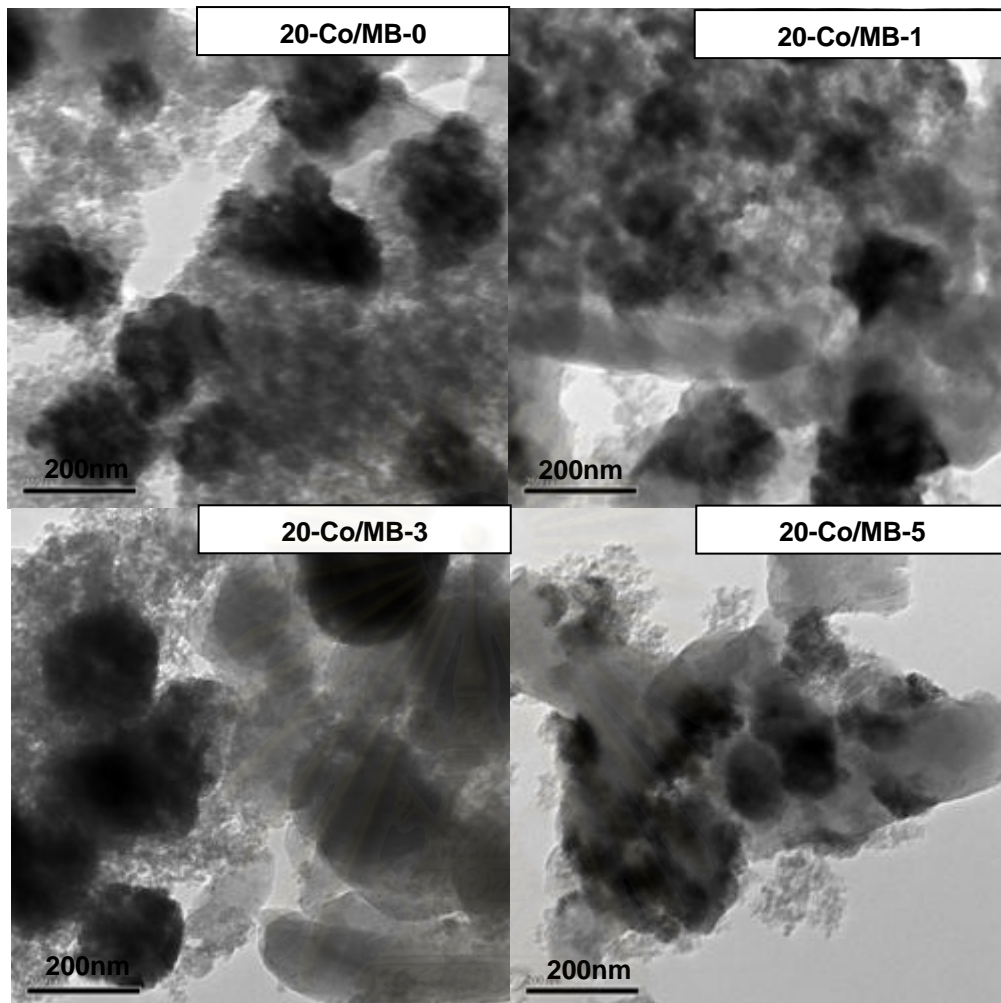


Figure 5.14 TEM micrographs for all cobalt dispersed on the boron-modified MCM-41 supports.

สถาบันวิทยบริการ
จุฬาลงกรณ์มหาวิทยาลัย

5.1.5 Temperature programmed reduction (TPR)

TPR was performed in order to determine the reduction behaviors of Co oxides species on various samples. The TPR profiles of Co supported on silica supports with and without B modification are shown in **Figure 5.15**. Basically, only two reduction peaks can be observed. The peaks can be assigned to the two-step reduction of Co_3O_4 to CoO and then to Co^0 (Y. Zhang *et al.*, 1999; D. Schanke *et al.*, 1995). Upon the TPR conditions, the two reduction peaks based on two-step reduction may or may not be observed. The TPR profile of the support with B modification showed no reduction peak. It appeared that the B modification resulted in higher degree of interaction between Co oxide species and the support indicating the shift of reduction temperature being higher with B modification. In addition, increased amounts of B modification caused in the increased degree of interaction between Co oxide species and the support. The TPR profiles of Co oxides supported on the MCM-41 with and without B modification are also shown in **Figure 5.15**. Apparently, the similar trend as mentioned for the silica supports was still observed. Essentially, B modification on silica and MCM-41 support resulted in higher degree of interaction, then being more difficult for such the Co oxide species to be reduced with the presence of B. However, when compared the reduction behaviors of Co supported on silica and MCM-41 supports. It seemed that the impact of B modification on the MCM-41 supports was more pronounced indicating the shift of reduction temperature to higher values. In fact, the effect of B source on the catalyst reducibility and Fischer-Tropsch synthesis activity of Co/TiO_2 catalysts was investigated by Coville *et al.* (N.J. Coville *et al.*, 2002). They reported that for all series of catalysts, at low B loadings (B wt% < 0.05), reaction rates increased with increasing B loading; at high B loadings (B wt% > 0.1%), there was a decrease in reaction rate. The results were in agreement with what we have found here regardless of the supports used. Thus, B modification consistently caused a decrease in reducibility of Co catalysts due to strong support interaction.

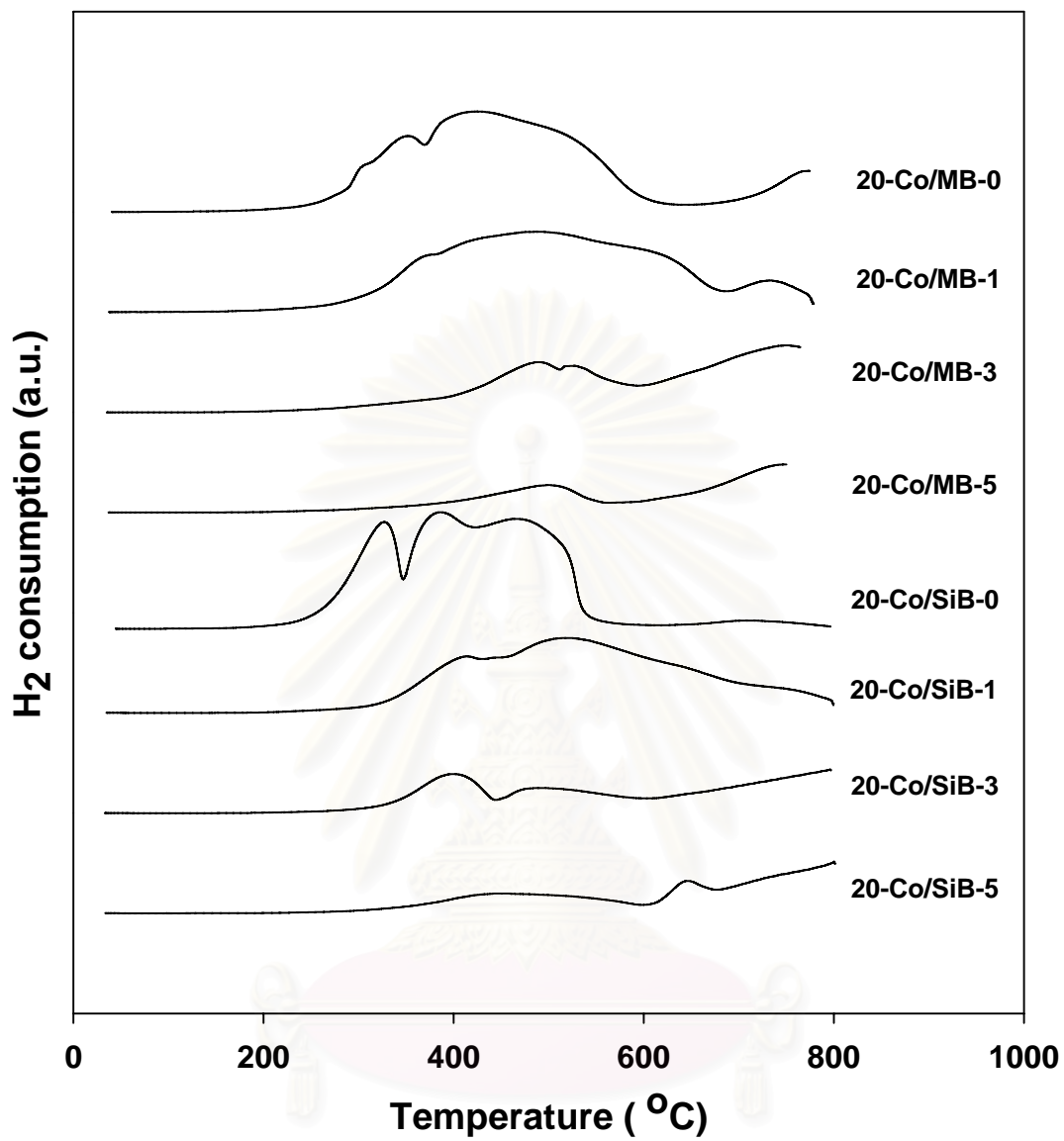


Figure 5.15 TPR profiles for the boron-modified-supported Co catalyst.

5.1.6 H₂ chemisorption

H₂ chemisorption was performed in order to measure the number of reduced cobalt metal surface atoms, which is related to the overall activity during CO hydrogenation. The resulted H₂ chemisorption is illustrated in **Table 5.3**. The amounts of H₂ adsorbed on the catalytic phase were in the range of 0.08 to 3.58 μmol/g of sample. It was found that the number of the reduced cobalt metal surface atoms was the largest for the cobalt dispersed on the 20 wt% of Co on 1 wt% of boron-modified MCM-41 support (20-Co/MB-1). It seemed that the use of 20 wt% of Co on boron-modified support consisting of lower amounts of boron.

5.1.7 Reaction study in CO hydrogenation

The reaction study under CO hydrogenation was also investigated in order to measure the activity and selectivity of catalysts. The reaction study results are listed in **Table 5.3**. It can be seen that for the silica supports, the modification of B resulted in lower activity of the catalysts. In fact, activities decreased with increasing the amounts of B modification. As known, upon the methanation, the majority of the product is methane. However, considering the selectivity, it can be observed that the selectivity to C₂-C₄ products apparently slightly increased with the B modification. The impact of B modification for the MCM-41 supports on the activities and selectivity is also listed in **Table 5.3** as well. Again, as seen from the modification on silica support, activities of Co supported on the MCM-41 essentially decreased with B modification. Even though decreased activities were observed with increased amounts of B modification, the degree of the decreased activities for Co/MB catalysts was less pronounced compared to those from Co/SiB catalysts. Besides, the selectivity to C₂-C₄ products obtained from the Co/MB without B and at low loading of B was slightly higher than that from the Co/SiB supports. Due to more strong support interaction occurred with the presence of B, it is suggested that the catalysts with B modification would be employed under the liquid phase system in order that the leaching of active species can be prevented. However, it should be noted that the strong support interaction also depends on the nature of active species and supports as well. Here, the interaction between the Co oxide species and silica as well as the MCM-41 supports

can be enhanced with the B modification. In order to better understanding different interactions upon various active species and supports, further studies should be investigated.

Table 5.3 Results of H₂ chemisorption, steady-state rate and selectivity to products

Samples	Total H ₂ chemisorption ($\mu\text{mol/g cat}$)	Steady-state Rate ($\times 10^2 \text{gCH}_2/\text{gcat.h}$)	Selectivity (%)	
			C ₁ compound	C ₂ -C ₄ compound
20-Co/SiB-0	2.59	37.4	99.4	0.5
20-Co/SiB-1	2.77	32.7	98.6	1.4
20-Co/SiB-3	0.10	14.8	98.2	1.8
20-Co/SiB-5	0.08	8.3	98.7	1.3
20-Co/MB-0	2.43	37.0	98.3	1.7
20-Co/MB-1	2.01	26.2	97.3	2.7
20-Co/MB-3	1.02	21.2	98.6	1.4
20-Co/MB-5	0.45	18.9	98.7	1.4

5.2 Various Co loading of 3 wt% boron-modified MCM-41 supported catalyst.

5.2.1 BET surface area

Table 5.4 BET surface area measurement of 3 wt% boron-modified supported cobalt catalyst.

Catalyst samples	BET surface area (m ² /g)	Catalyst samples	BET surface area (m ² /g)
5-Co/SiB-3	138	5-Co/MB-3	337
10-Co/SiB-3	151	10-Co/MB-3	325
15-Co/SiB-3	143	15-Co/MB-3	297
20-Co/SiB-3	136	20-Co/MB-3	319

The BET surface areas for different Co loading catalysts are listed in Table 5.4. It was found that Co/MB had higher surface areas than those of Co/SiB about two times.

5.2.2 X-ray diffraction (XRD)

XRD was performed in order to determine the bulk crystalline phases of the supports and catalysts. It can be observed that the XRD patterns for 5 wt% of cobalt loading exhibited only a broad XRD peak assigning to the conventional amorphous silica indicating highly dispersed cobalt. The XRD patterns of the boron-modified supported Co catalyst are shown in **Figure 5.16**, all calcined samples exhibited XRD peaks at 31° (weak), 36° (strong), and 65° (weak), which were assigned to the presence of Co₃O₄. This indicated that the Co₃O₄ formed was highly dispersed.

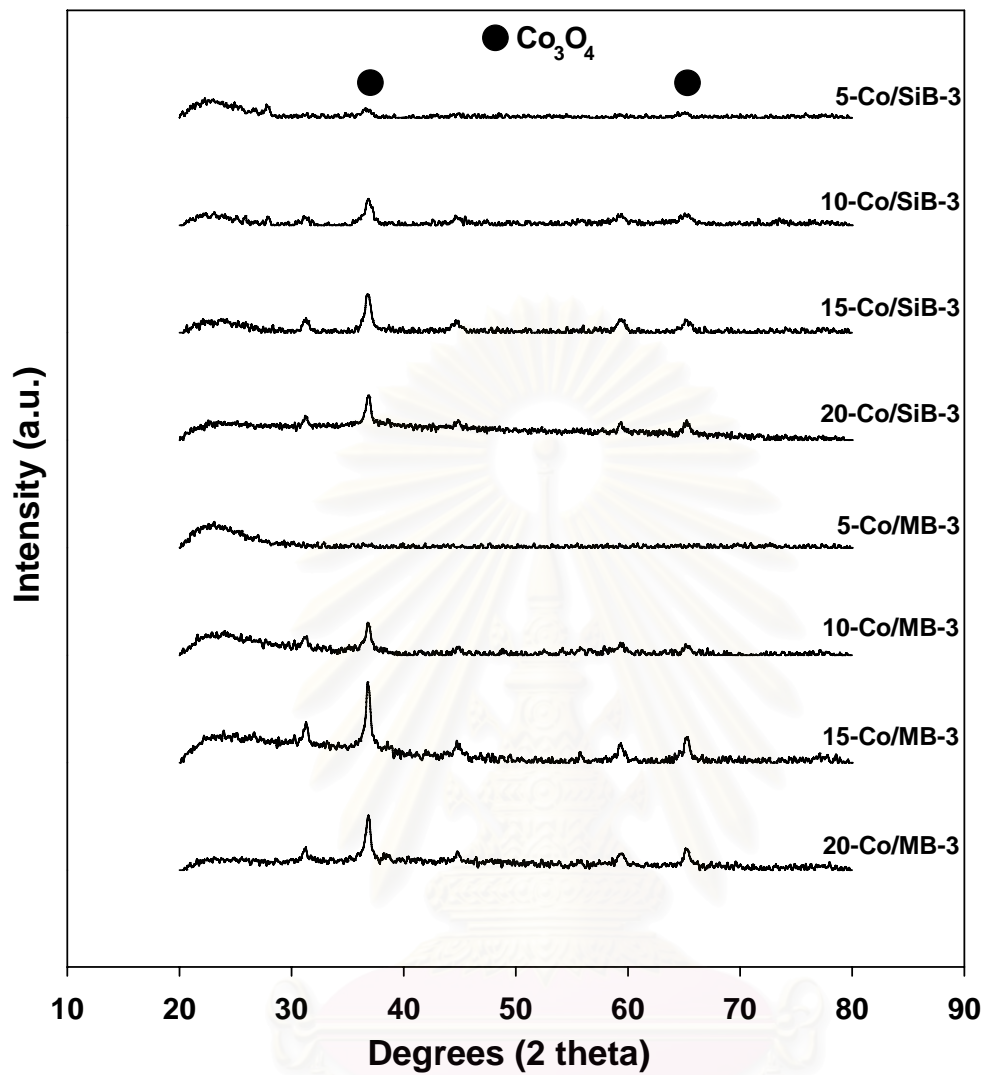


Figure 5.16 XRD patterns of the 3 wt% of boron-modified-supported Co catalyst.

สถาบันวิทยบริการ
จุฬาลงกรณ์มหาวิทยาลัย

5.2.3 Scanning electron microscopy (SEM) and Energy dispersive X-ray spectroscopy (EDX)

SEM and EDX were also conducted in order to study the morphologies and elemental distribution of the samples, respectively. Apparently, SEM micrographs and EDX mapping exhibited similar trends of morphologies and elemental (Co, Si, and O) distribution. The typical SEM micrograph along with the EDX mapping (for Si, O, and Co) of the 3 wt% of boron-modified supported Co catalysts are illustrated in **Figure 5.17-5.24** for 5-Co/SiB-3, 10-Co/SiB-3, 15-Co/SiB-3, 20-Co/SiB-3, 5-Co/MB-3, 10-Co/MB-3, 15-Co/MB-3 and 20-Co/MB-3 samples, respectively, indicating the external surface of the sample granule. It can be seen that the cobalt oxide species were well distributed (shown on EDX mapping) all over the sample granule.

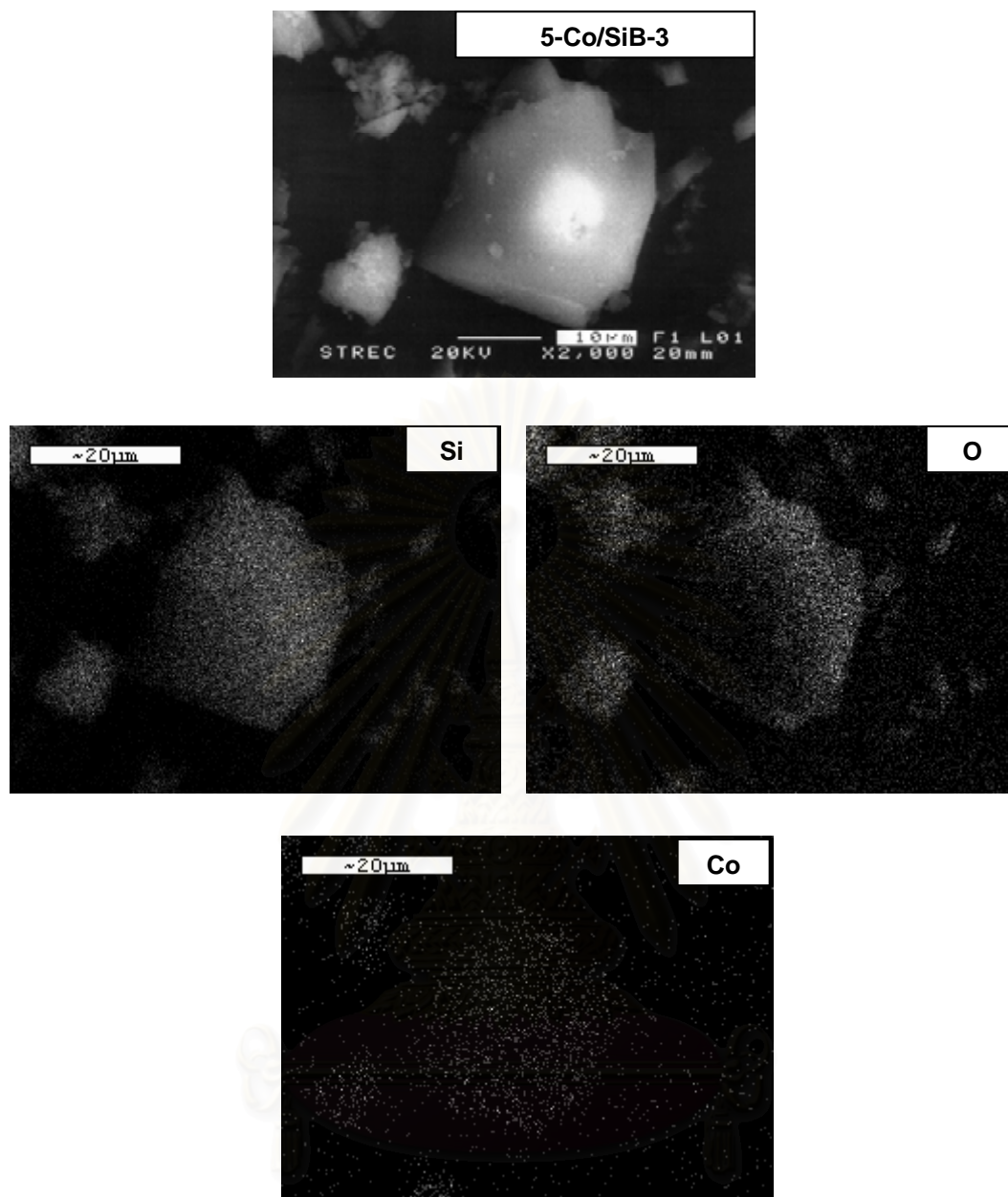


Figure 5.17 SEM micrograph and EDX mapping for 5-Co/SiB-3 catalyst granule.

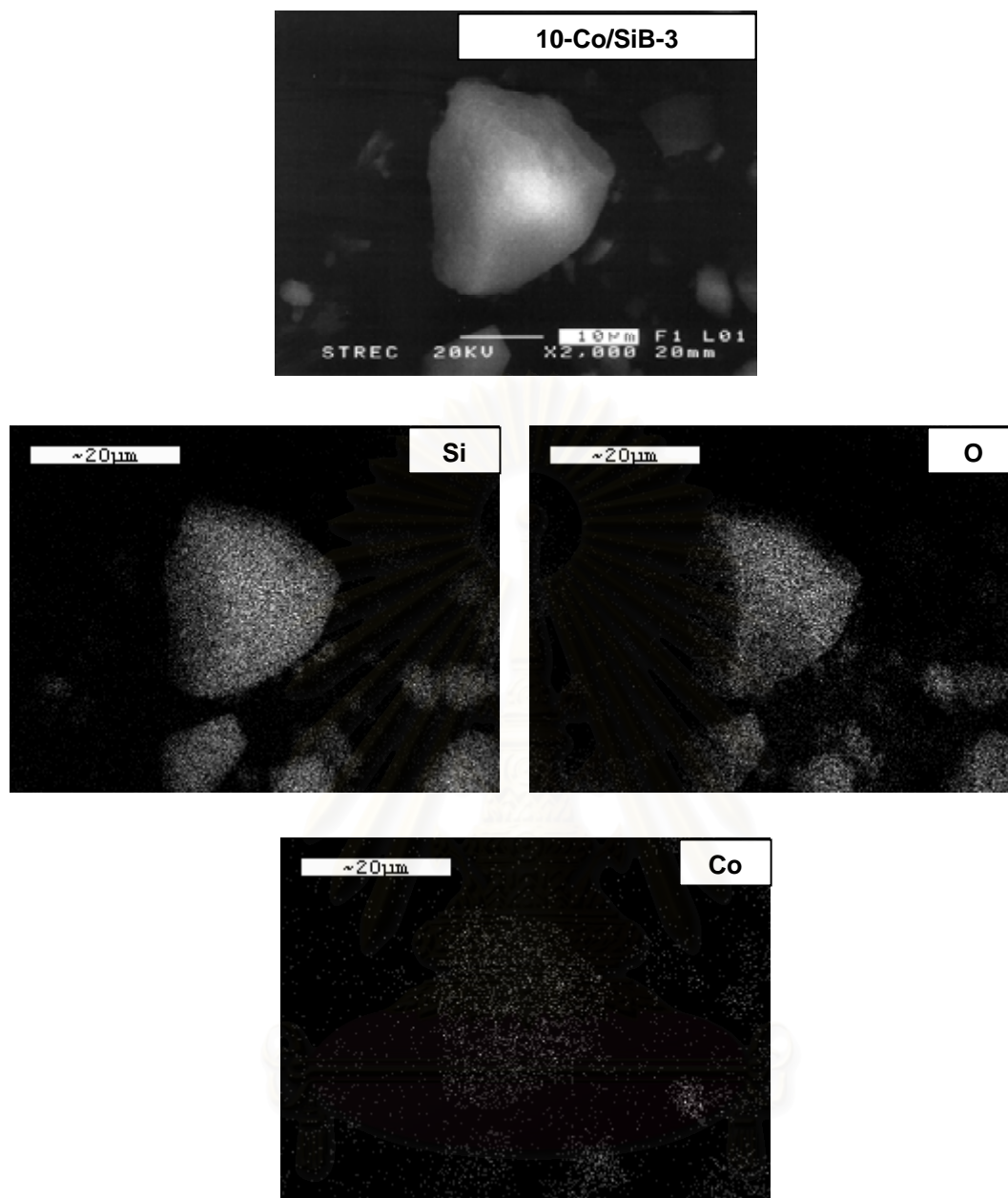


Figure 5.18 SEM micrograph and EDX mapping for 10-Co/SiB-3 catalyst granule.

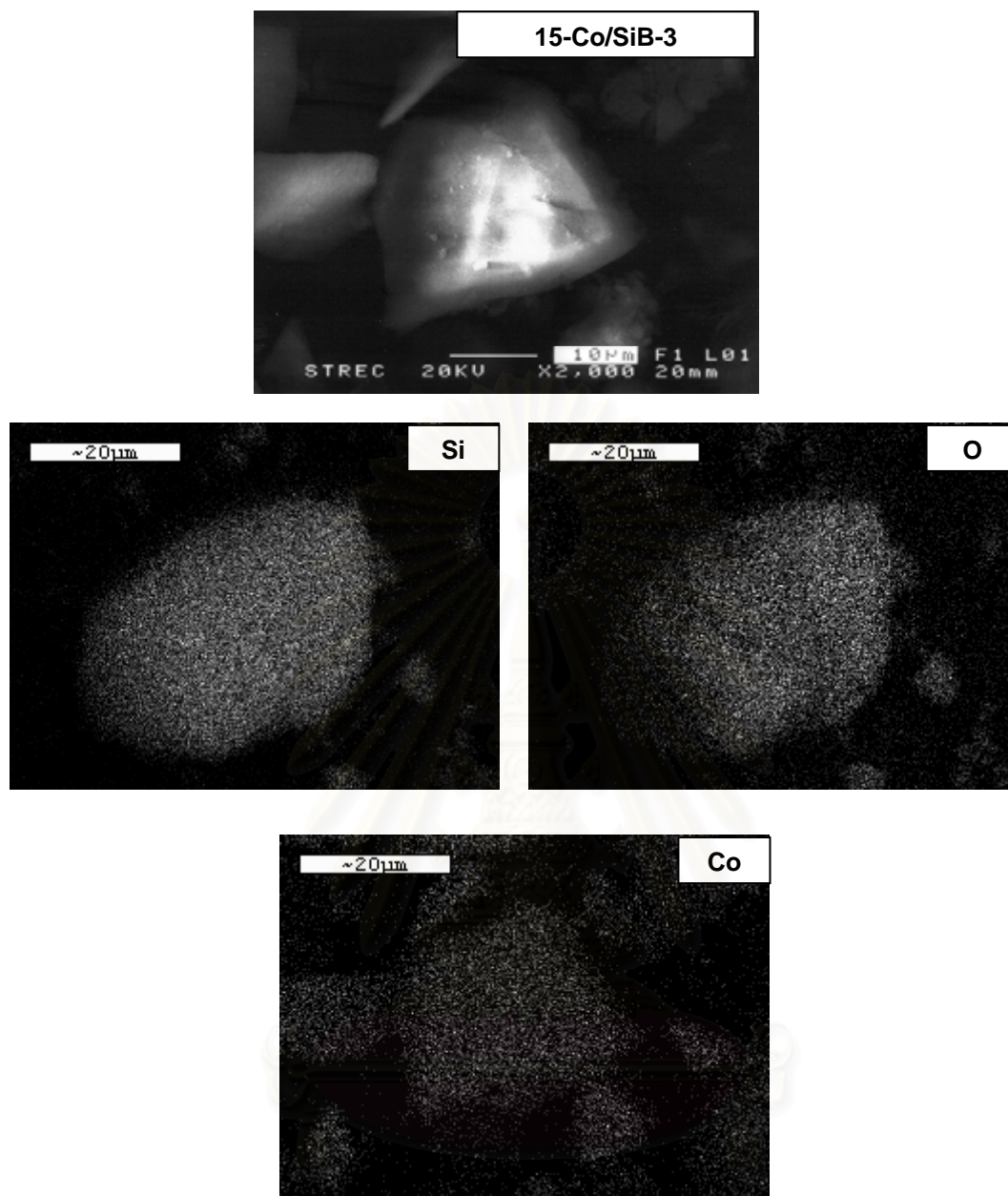


Figure 5.19 SEM micrograph and EDX mapping for 15-Co/SiB-3 catalyst granule.

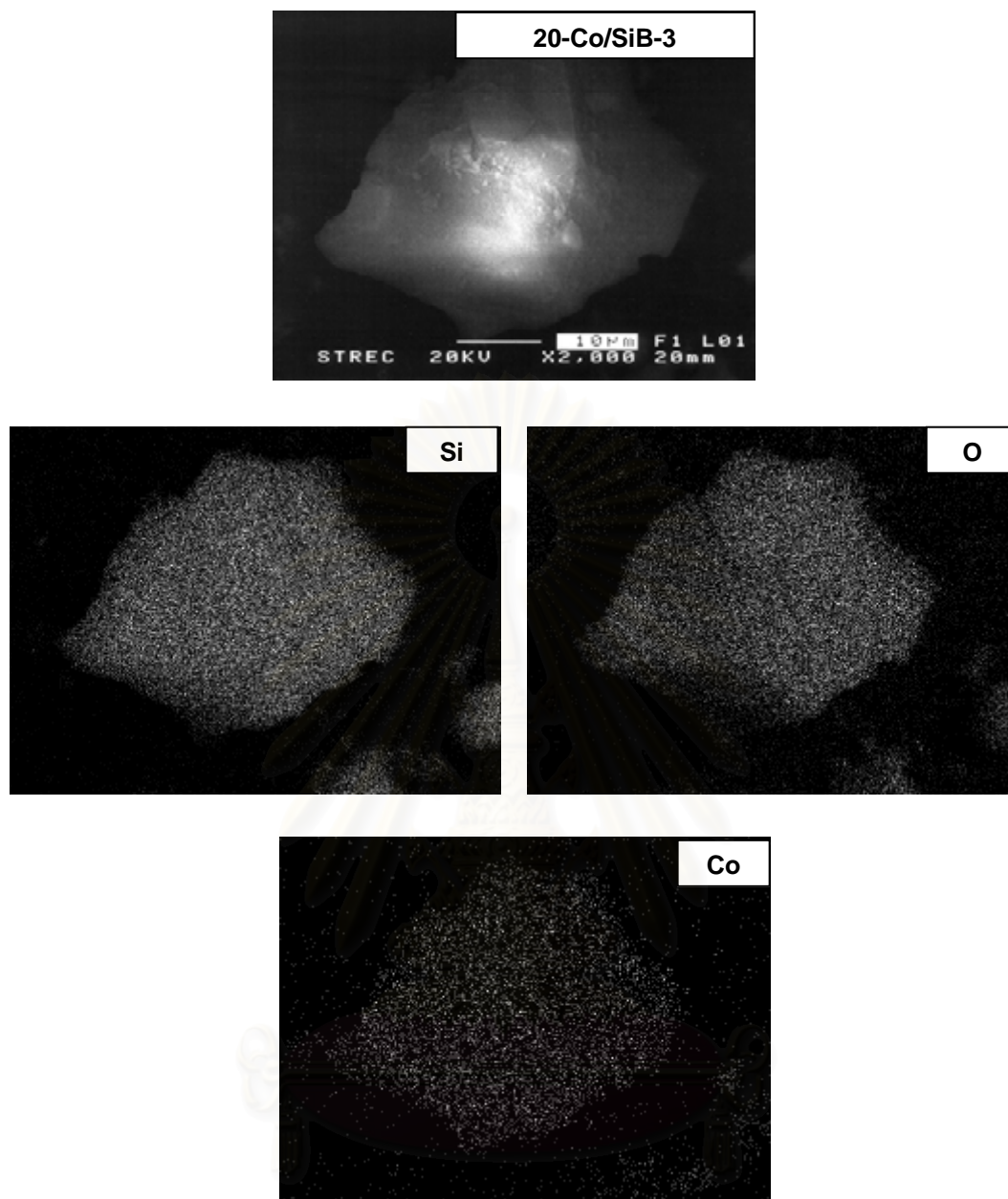


Figure 5.20 SEM micrograph and EDX mapping for 20-Co/SiB-3 catalyst granule.

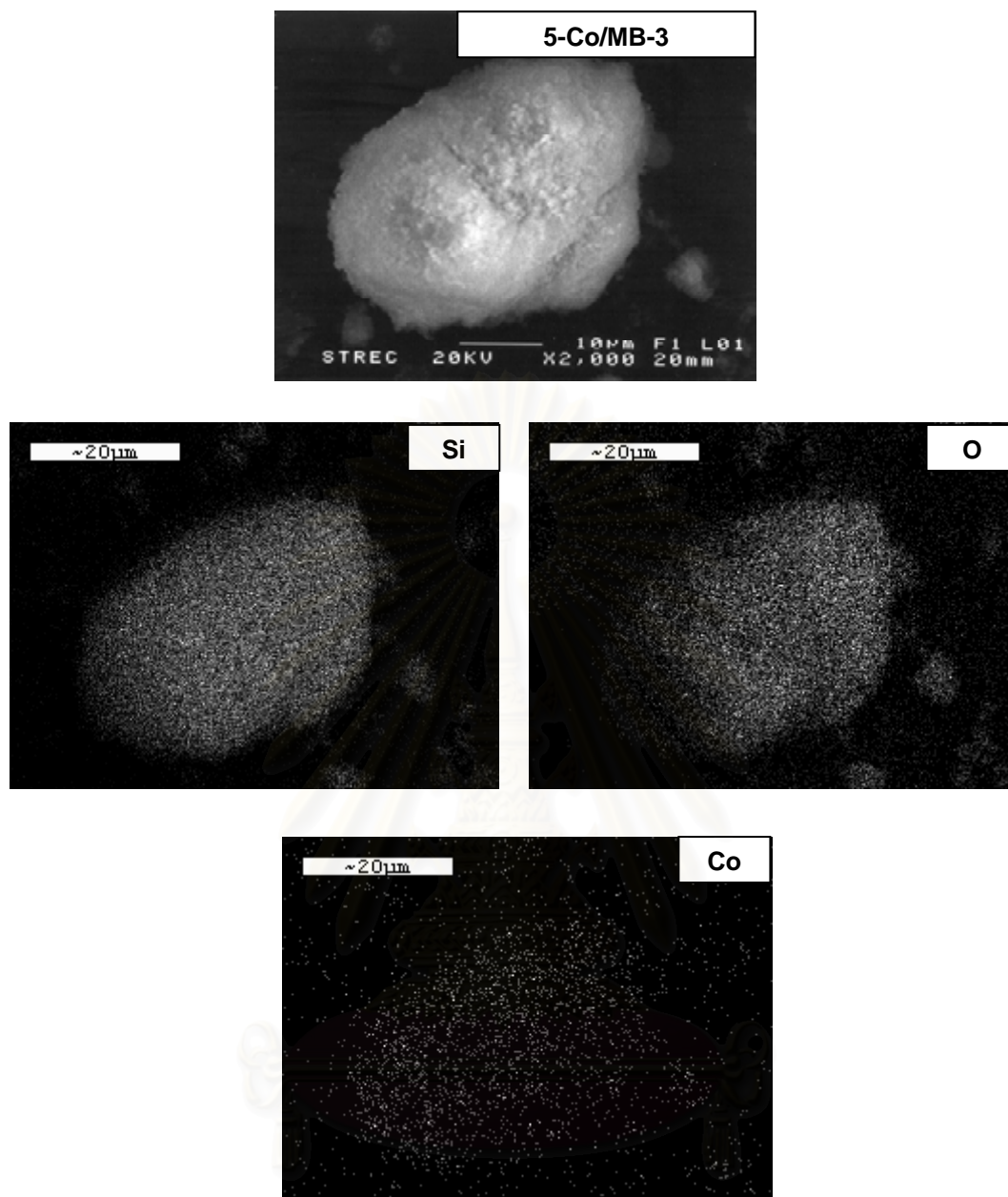


Figure 5.21 SEM micrograph and EDX mapping for 5-Co/MB-3 catalyst granule.

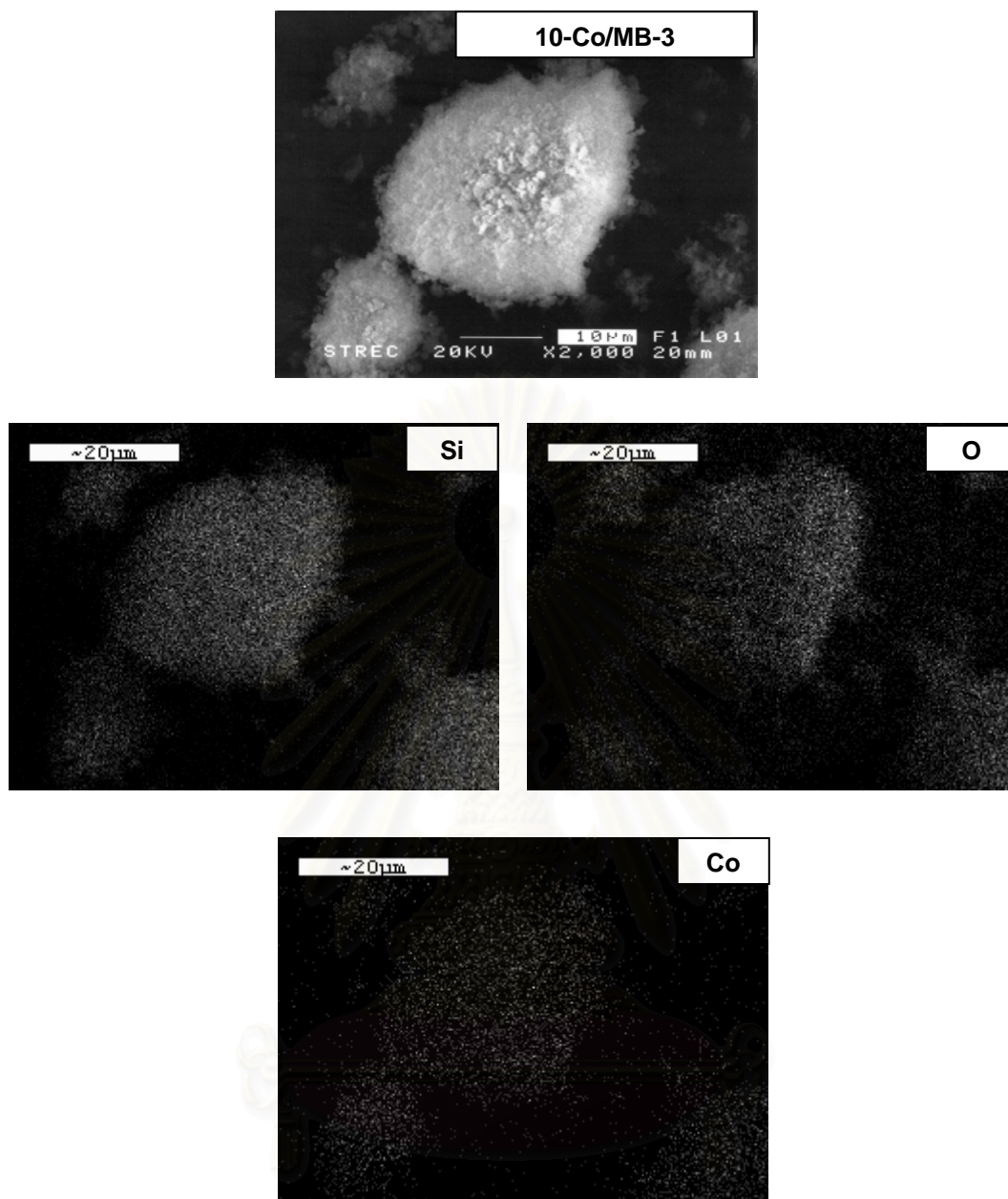


Figure 5.22 SEM micrograph and EDX mapping for 10-Co/MB-3 catalyst granule.

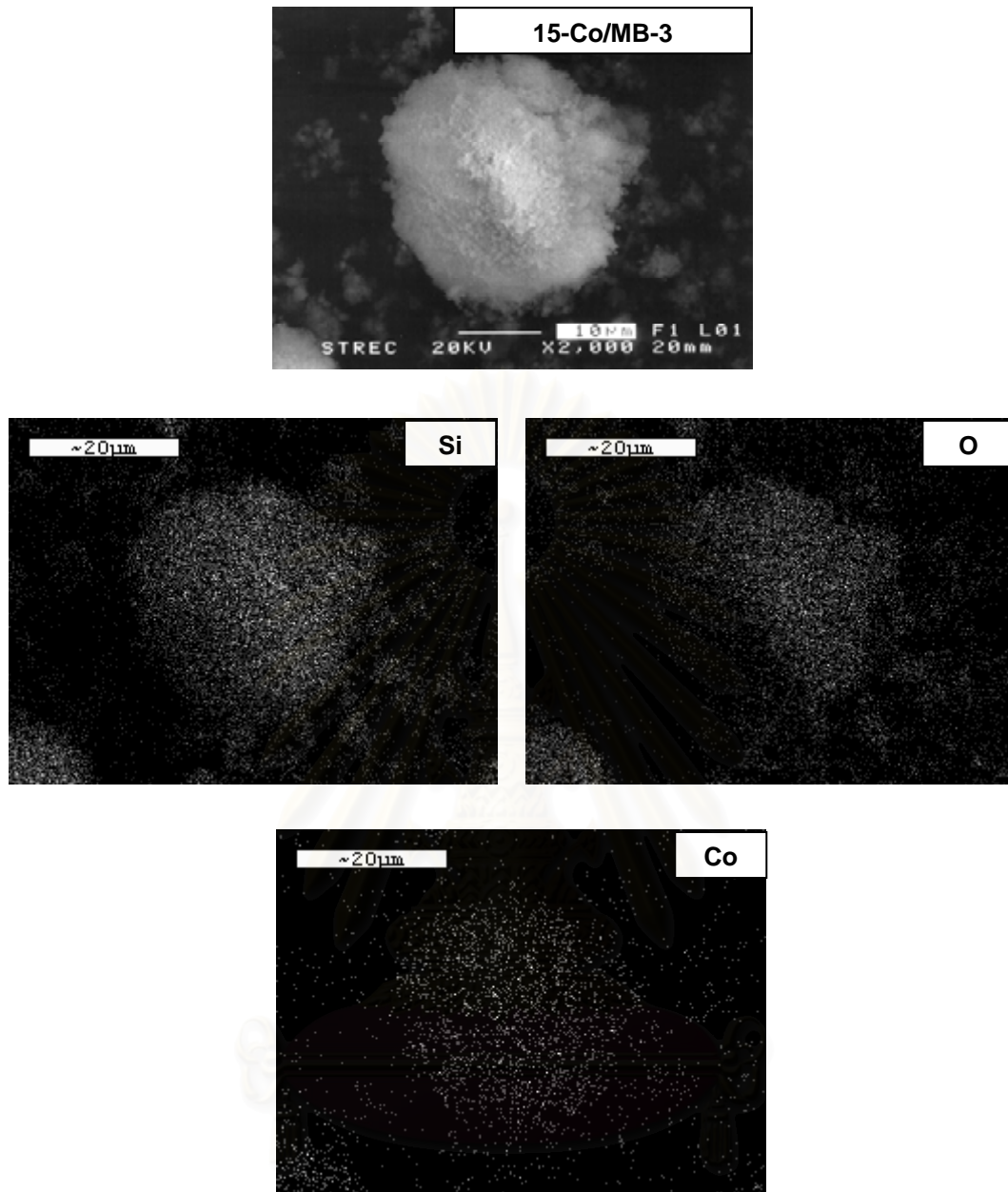


Figure 5.23 SEM micrograph and EDX mapping for 15-Co/MB-3 catalyst granule.

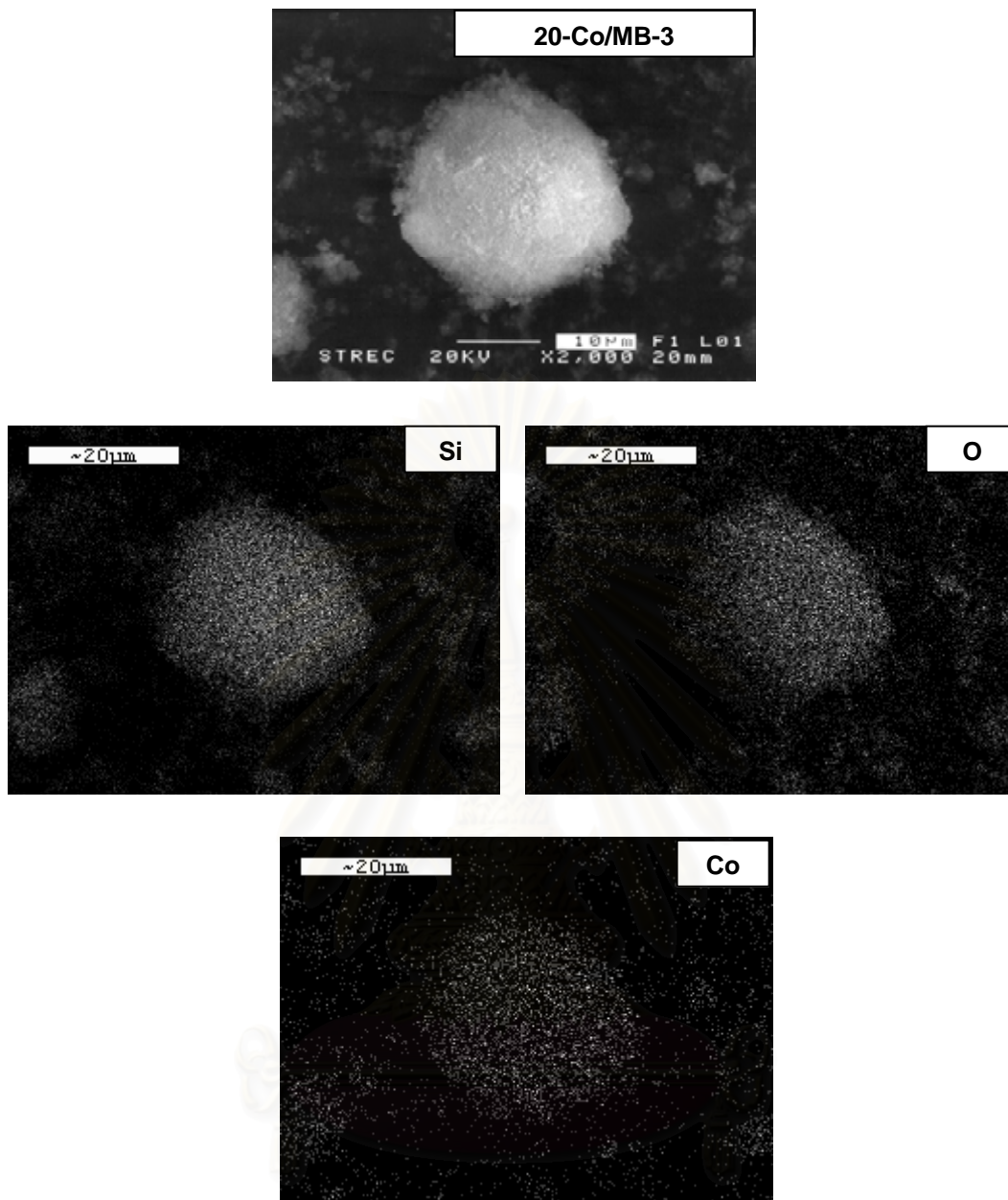


Figure 5.24 SEM micrograph and EDX mapping for 20-Co/MB-3 catalyst granule.

5.2.4 Transmission Electron Microscopy (TEM)

TEM was conducted in order to identify the crystallite size and dispersion of Co oxide species on the various supports. The TEM micrographs for the 3 wt% of boron-modified supported Co catalysts are shown in **Figures 5.25 and 5.26**, respectively. The TEM micrographs for Co oxides species dispersed on silica supports with 3 wt% of B modification are shown in **Figure 5.25** whereas those for MCM-41 supports are shown in **Figure 5.26**. As seen in both Figures, the dark spots represented the Co oxide species dispersed on the various supports. It can be seen from **Figure 5.25** that Co oxide species on the silica supports were well dispersed having the crystallite size of ca. 50 to 100 nm. Apparently, the crystallite size seemed to increase with increasing Co loading. Similarly, the TEM micrographs as shown in **Figure 5.26** of Co oxide species on the MCM-41 supports were also well dispersed having the crystallite size of 100 to 200 nm. It can be seen that the crystallite size of Co oxide species on the silica supports was smaller than that on the MCM-41 supports indicating more agglomeration of Co oxide species.

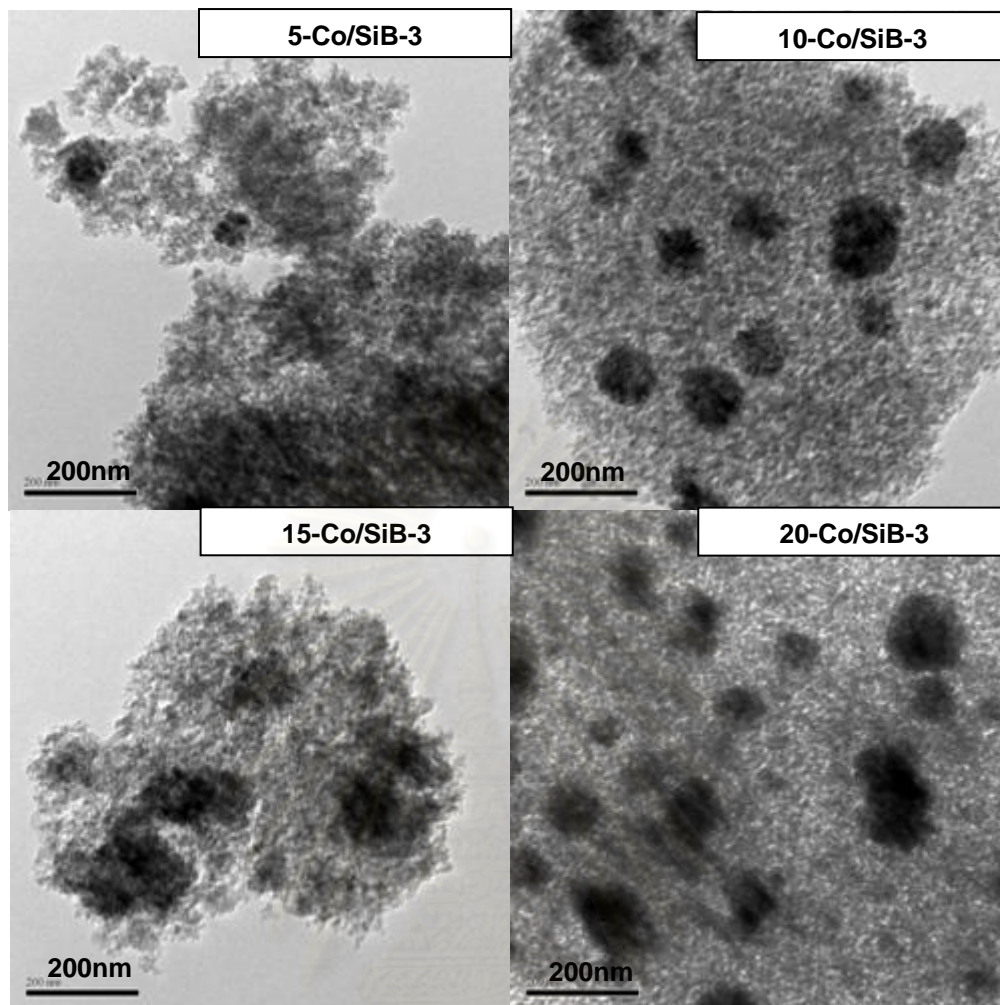


Figure 5.25 TEM micrographs of all cobalt dispersed on 3 wt% of boron-modified silica supports.

สถาบันวิทยบริการ
จุฬาลงกรณ์มหาวิทยาลัย

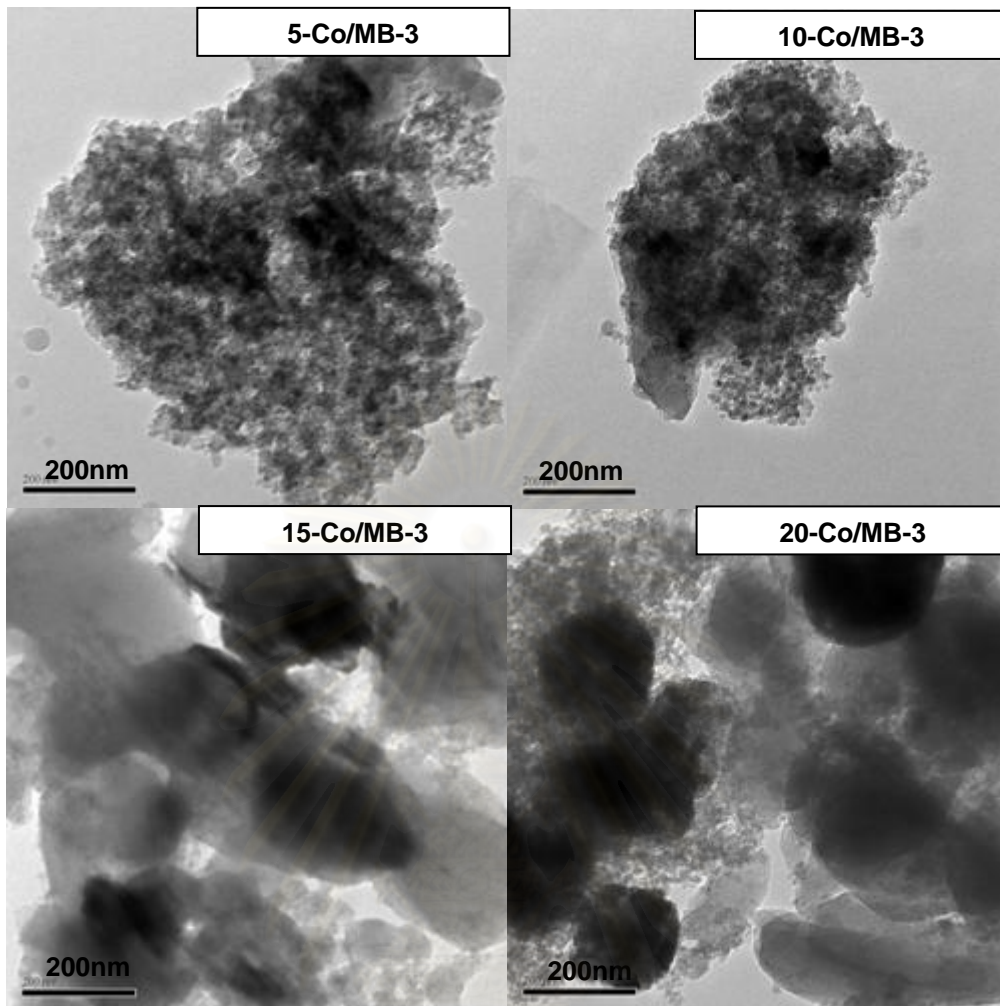


Figure 5.26 TEM micrographs of all cobalt dispersed on 3 wt% of boron-modified MCM-41 supports.

สถาบันวิทยบริการ
จุฬาลงกรณ์มหาวิทยาลัย

5.2.5 Temperature programmed reduction (TPR)

TPR was performed in order to determine the reduction behaviors of Co oxides species on various samples. The TPR profiles of Co supported on silica supports with 3 wt% of B modification are shown in **Figure 5.27**. Basically, only two reduction peaks can be observed. The peaks can be assigned to the two-step reduction of Co_3O_4 to CoO and then to Co^0 (Y. Zhang *et al.*, 1999; D. Schanke *et al.*, 1995). Upon the TPR conditions, the two reduction peaks based on two-step reduction may or may not be observed. The TPR profile of the support with B modification showed no reduction peak. It appeared that decreased Co loading resulted in higher degree of interaction between Co oxide species and the support indicating the shift of reduction temperature being higher with decreased Co loading. In addition, decreased amounts of cobalt loading caused in the decreased amounts of Co oxide species on the support. The TPR profiles of Co oxides supported on the MCM-41 with 3 wt% of B modification are also shown in **Figure 5.27**. Apparently, the similar trend as mentioned for the silica supports was still observed. Essentially, decreased in cobalt loading on silica and MCM-41 support resulted in decreasing cobalt oxide on supports, then being more difficult for such the Co oxide species to be reduced with the small amounts of cobalt loading. However, when compared the reduction behaviors of Co supported on silica and MCM-41 supports. It seemed that the impact of cobalt loading on the MCM-41 supports was more pronounced indicating the shift of reduction temperature to higher values.

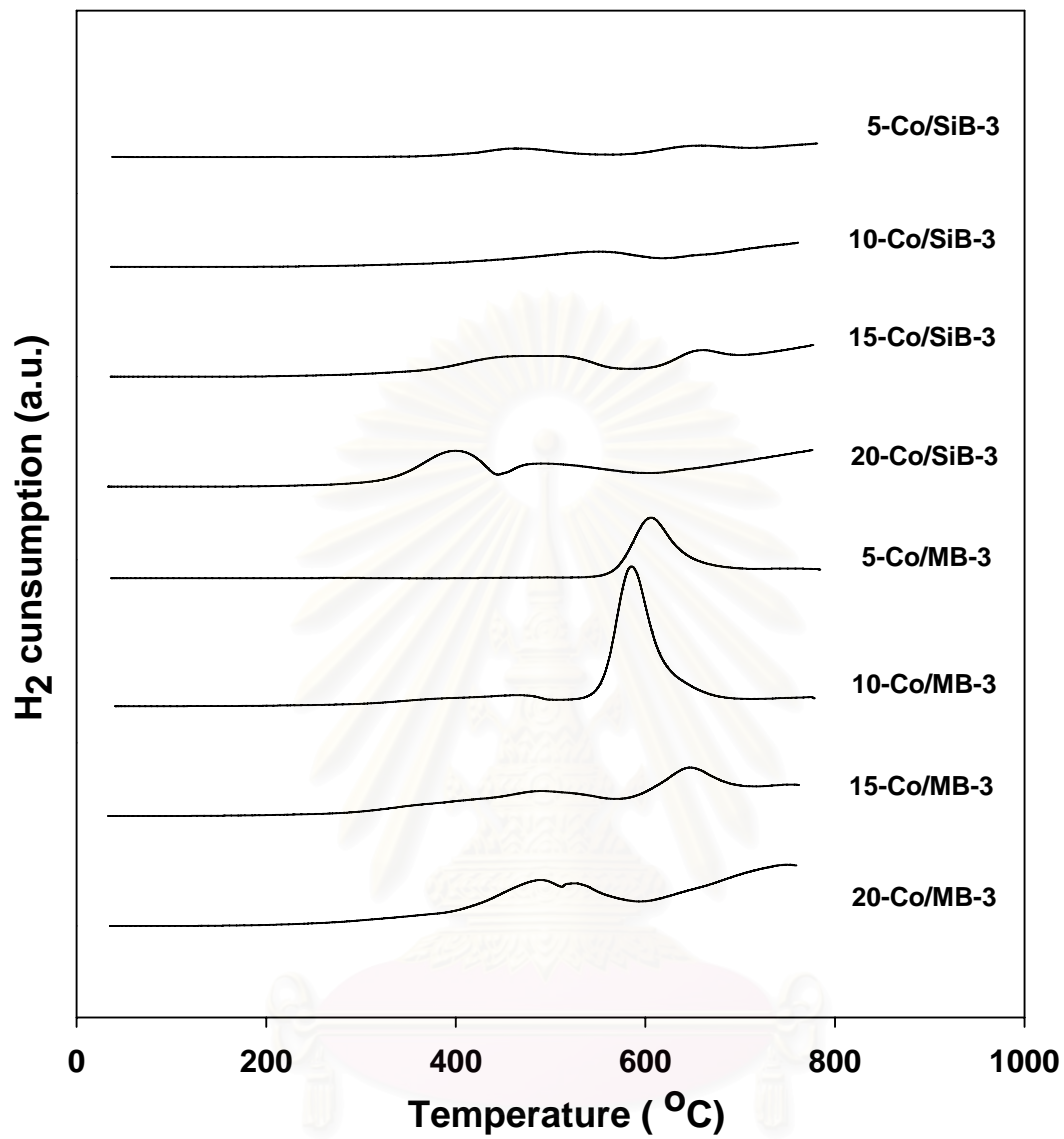


Figure 5.27 TPR profiles for the 3 wt% of boron-modified-supported Co catalyst.

5.2.6 H₂ chemisorption

H₂ chemisorption was performed in order to measure the number of reduced cobalt metal surface atoms, which is related to the overall activity during CO hydrogenation. The resulted H₂ chemisorption is illustrated in **Table 5.4**. The amounts of H₂ adsorbed on the catalytic phase were in the range of 0.02 to 1.09 μmol/g of sample. It was found that the number of the reduced cobalt metal surface atoms was the largest for the cobalt dispersed on the 15 wt% of Co on 3 wt% of boron-modified MCM-41 support (15-Co/MB-3).

5.1.7 Reaction study in CO hydrogenation

The reaction study under CO hydrogenation was also investigated in order to measure the activity and selectivity of catalysts. The reaction study results are listed in **Table 5.4**. It can be seen that for the 3 wt% of boron-modified silica supports, decreased cobalt loading apparently resulted in lower activity of the catalysts. Considering the selectivity, it can be observed that the selectivity to C₂-C₄ products apparently slightly changed with the decreasing cobalt loading. The impact of cobalt loading for the MCM-41 supports on the activities and selectivity is also listed in **Table 5.4** as well. Again, as seen from the modification on silica support, activities of Co supported on the MCM-41 essentially decreased with decreasing cobalt loading. Even though decreased activities were observed with decreased amounts of cobalt loading, the degree of the increased C₂-C₄ selectivity for Co/MB catalysts was more pronounced than those from Co/SiB catalysts.

Table 5.4 Results of H₂ chemisorption, steady-state rate and selectivity to products

Samples	Total H ₂ chemisorption ($\mu\text{mol/g cat}$)	Steady-state Rate ($\times 10^2 \text{gCH}_2/\text{gcat.h}$)	Selectivity (%)	
			C ₁ compound	C ₂ -C ₄ compound
5-Co/SiB-3	0.12	2.1	98.2	1.8
10-Co/SiB-3	0.20	7.7	98.9	1.1
15-Co/SiB-3	0.26	12.1	98.9	1.1
20-Co/SiB-3	0.66	14.8	98.2	1.8
5-Co/MB-3	0.15	0.1	100.0	0.0
10-Co/MB-3	0.58	3.9	98.3	1.7
15-Co/MB-3	0.99	10.5	98.4	1.6
20-Co/MB-3	1.02	21.2	98.6	1.4

สถาบันวิทยบริการ
จุฬาลงกรณ์มหาวิทยาลัย

CHAPTER VI

CONCLUSIONS AND RECOMMENDATION

This chapter is focused upon the conclusions of the experimental details of cobalt (Co) catalysts dispersed on various boron-modified MCM-41 for carbon monoxide (CO) hydrogenation reaction, and compared with those on the cobalt (Co) catalysts dispersed on various boron-modified silica which were described in section 6.1. In addition, recommendations for further study are given in section 6.2.

6.1 Conclusions

6.1.1 Various boron loading of 20 wt% cobalt on boron-modified MCM-41 supported catalyst.

The present study revealed the characteristics of cobalt dispersed on various boron-modified supports. It indicated that Co oxide species were in the highly dispersed on the various supports. There was no significant change in morphologies and elemental distributions of samples as seen from SEM/EDX. The presence of boron in the MCM-41 supports could result in the small amounts of active Co metal atoms as detected using H₂ chemisorption due to the strong support interaction. This resulted in decreased activity of the sample. However, the chain growth probability was found to slightly increase with the presence of the boron in the MCM-41 support.

6.1.2 Various Co loading of 3 wt% boron-modified MCM-41 supported catalyst.

Based on the present study, it can be concluded that the crystallite size of Co oxide species dispersed on a MCM-41 supports were bigger than those on silica supports. The support interaction, crystallite size and the nature of supports used were also the key to determine the number of active sites present. For the MCM-41 support, higher loading of cobalt dispersed on MCM-41 was more active. There was no significant change in morphologies and elemental distributions of samples as seen

from SEM/EDX. The small amounts of cobalt in the boron-modified MCM-41 supports could result in the small amounts of active Co metal atoms as detected using H_2 chemisorption due to the strong support interaction. This resulted in decreasing activity of the sample.

6.2 Recommendations

1. In order to investigate on different interactions, the MCM-41 having different pore sizes should be used for boron-modified supports.
2. Besides Co metal, other metals such as Ni, Pd, Fe and etc should be further investigated with MCM-41 modified supports.



สถาบันวิทยบริการ
จุฬาลงกรณ์มหาวิทยาลัย

REFERENCES

- Ali, S., Chen, B., and Goodwin, Jr., J.G. Zr promotion of Co/SiO₂ for Fisher-Tropsch Synthesis. J. Catal. 157 (1995): 35-41.
- Beck, J.S., Varturi, J.C., Roth, W.J., Leonowicz, M.E., Kresge, C.T., Schmitt, K.D., Chu, C.T.W., Olson, D.H., Sheppard, E.W., McCullen, S.B., Higgins, J.B., Schlenker, J.L. A new family of mesoporous molecular sieves prepared with liquid crystal templates. J. Am. Chem. Soc. 114 (1992): 10834-10843.
- Brady, R.C., Pettit, R.J., On the mechanism of the Fischer-Tropsch reaction. The chain propagation step. J. Am. Chem. Soc. 103 (1981): 1287-1289.
- Brik, Y., Kacimi, M., Verduraz, F.B., Ziyad, M. Characterization and Comparison of the Activity of Boron-Modified Co/TiO₂ Catalysts in Butan-2-ol Conversion and Oxidative Dehydrogenation of Ethane. J. Catal. 211(2002): 470-481.
- Chen, C-Y., Burkett, S.L., Li H-X and Davis M.E. Studies on mesoporous materials. II. Synthesis mechanism of MCM-41. Micropor. Mater. 2 (1993): 27-34.
- Cho, D.H., Chang, T.S., Ryu, S.K., Lee, Y.K. Characterization and catalytic activities of MoMCM-41. Catal. Lett 64 (2000): 227-232.
- Choi, J.G. Reduction of support cobalt catalysts by hydrogen. Catal Lett. 35 (1995): 291-296.
- Concepción, P., López, C., Martínez, A., Puentes, V.F. Characterization and catalytic properties of cobalt supported on delaminated ITQ-6 and ITQ-2 zeolites for the Fischer-Tropsch synthesis reaction. J. Catal. 228 (2004): 321-332.
- Corma, A., Martines, V., Soria, V.J. Hydrogenation of aromatics in diesel fuels on Pt/MCM-41 catalysts J. Catal. 169 (1997): 480-489.
- Cortés Corberán, V., Jia, M.J., El-Haskouri, J., Valenzuela, R.X., Beltrán-Porter, D., Amorós, P. Oxidative dehydrogenation of isobutane over Co-MCM-41 catalysts. Catal. Today 91-92 (2004): 127-130.
- Coville, N.J. and Li, J. Effect of boron source on the catalyst reducibility and Fischer-Tropsch synthesis activity of Co/TiO₂ catalysts Catal. Today 71(2002), 403-410.
- Curtis, V., Nicolaidis, C.P., Coville, N.J., Hildebrandt, D., Glasser, D. The effect of sulfur on supported cobalt Fischer-Tropsch catalysts. Catal. Today 49 (1999): 33-40.

- Dalai, A.K., Das, T.K., Chaudhari, K.V., Jacobs, G., Davis, B.H. Fischer-Tropsch synthesis: Water effects on Co supported on narrow and wide-pore silica. Appl. Catal. A 289 (2005): 135-142.
- Das, T.K., Conner, W.A., Li, J.L., Jacobs, G., Dry, M.E., Davis, B.H., Fischer-tropsch synthesis: Kinetics and effect of water for a Co/SiO₂ catalyst. Energy & Fuels 19 (2005): 1430-1439.
- Farrauto, R.J. and Bartholomew, C.H. Fundamentals of industrial catalytic processes. 1st ed. London: Chapman & Hall, 1997.
- Feller, A., Claeys, M., and Steen, E.V. Cobalt cluster effects in zirconium promoted. Co/SiO₂ Fischer-Tropsch Catalysts. J. Catal. 185 (1995): 20-130.
- Franke, O., Rathousky, J., Schulz-Ekloff, G. and Zukal, A. Stud. Surf. Sci. Catal. 91, (1995): 309.
- Iglesia, E. Design, synthesis, and use of cobalt-based Fischer-Tropsch synthesis catalysts Appl. Catal. A 161 (1997): 59-78.
- Jacobs, G., Das, T., Zhang, Y.Q., Li, J.L., Racoillet, G., Davis, B.H. Fischer-Tropsch synthesis: support, loading, and promoter effects on the reducibility of cobalt catalysts. Appl. Catal. A. 233 (2002): 263-281.
- Jacob, K., William, J.A., Jr., Ernest, G. Inorganic chemistry. Boston: D.C. Heath and company, 1960.
- Jentys, A., Pham, N.H., Vinek, H., Englisch, M., Lercher, J.A. Synthesis and characterization of mesoporous materials containing highly dispersed cobalt. Micropor. Mater. 6 (1996): 13-17.
- John, J.M. Chemical processing handbook. New York: Marcel Dekker, Inc., 1993.
- Jongsomjit, B., and Goodwin, Jr., J.G. Co-support compound formation in Co/Al₂O₃ catalysts: effect of reduction gas containing CO. Catal. Today 77 (2002): 191-204.
- Jongsomjit, B., Panpranot, J., and Goodwin, Jr., J.G. Co-Support Compound Formation in Alumina-Supported Cobalt Catalysts. J. Catal. 204 (2001): 98-109.
- Jongsomjit, B., Panpranot, J., and Goodwin, Jr., J.G. Effect of zirconia-modified alumina on the properties of Co/γ-Al₂O₃ catalysts. J. Catal. 215 (2003): 66-77.

- Jongsomjit, B., Sakdamnusun, C, and Goodwin, Jr., J.G., and Praserthdam, P. Co-Support Compound Formation in Titania-Supported Cobalt Catalyst. Catal. Lett. 94 (2004): 209-215.
- Jongsomjit, B., Sakdamnusun, C., Praserthdam, P. Dependence of crystalline phases in titania on catalytic properties during CO hydrogenation of Co/TiO₂ catalysts. Mater. Chem. Phys. 89 (2005): 395-401.
- Jongsomjit, B., Wongsalee, T., and Praserthdam, P. Study of cobalt dispersion on titania consisting various rutile: anatase ratios. Mater. Chem. Phys. 92 (2005): 572-577.
- Jongsomjit, B., Wongsalee, T., and Praserthdam, P. Characteristics and catalytic properties of Co/TiO₂ for various rutile: anatase ratios. Catal. Comm. 6 (2005): 705-710.
- Kogelbauer, A., Weber, J.C., and Goodwin, J.G., Jr. The formation of cobalt silicates on Co/SiO₂ under hydrothermal condition. Catal Lett. 34 (1995): 259-267.
- Kraum, M., and Baerns, M. Fischer-Tropsch synthesis: the influence of various cobalt compounds applied in the preparation of supported cobalt catalysts on their performance. Appl. Catal. A 186 (2002): 189-200.
- Kresge, C.T., Leonowicz, M.E., Roth, W.J., Vartuli, J.C., Beck, J.S. Ordered mesoporous molecular sieves synthesized by a liquid-crystal template mechanism. Nature 359 (1992): 710-712.
- Li, J. and Coville, N.J. The effect of boron on the catalyst reducibility and activity of Co/TiO₂ Fischer Tropsch catalysts. Appl. Catal. A.:General 181 (1999): 201-208.
- Li, J. and Coville, N.J. Effect of boron on the sulfur poisoning on Co/TiO₂ Fischer-Tropsch catalysts. Appl. Catal. A.:General 208 (2001): 177-184.
- Li, J., Jacobs, G., Zhang, Y., Das, T., Davis, B.H. Fischer-Tropsch synthesis: effect of small amounts of boron, ruthenium and rhenium on Co/TiO₂ catalysts. Appl. Catal. A. 223 (2002): 195-203.
- Monnier, A., Schüth, F., Huo, Q., Kumar, D., Margolese, D., Maxwell, R.S., Stucky, G.D., Krishnamurty, M., Petroff, P., Firouzi, A., Janicke, M. and Chmelka, B.F. Cooperative formation of inorganic-organic interfaces in the synthesis of silicate mesostructures. Science 261(1993): 1299-1303.
- Moradi, G.R., Basir, M.M., Taeb, A., and Kiennemann, A. Promotion of Co/SiO₂ Fischer-Tropsch catalysts with zirconium. Catal. Comm. 4 (2003): 27-32.

- Othmer, K. Encyclopedia of chemical technology. Vol. 6. 4 th ed. New York: A Wiley Interscience Publication, John Wiley&Son, 1991.
- Okabe, K., Li, X., Wei, M., Arakawa, H. Fischer–Tropsch synthesis over Co–SiO₂ catalysts prepared by the sol–gel method. Catal. Today 89(2004), 431-438.
- Oukaci, R., Singleton, A.H., Goodwin Jr., J.G. Comparison of patented Co F-T catalysts using fixed-bed and slurry bubble column reactors. Appl. Catal. A 186 (1999): 129-144.
- Panpranot, J., Goodwin, Jr., J.G., and Sayari, A. Synthesis and characteristics of MCM- 41 supported CoRu catalysts. Catal. Today 77 (2002): 269-284.
- Panpranot, J., Goodwin, Jr., J.G., and Sayari, A. CO Hydrogenation on Ru-Promoted Co/MCM-41 Catalysts. J. Catal. 211 (2002): 530-539.
- Panpranot, J., Kaewkun, S., Praserttham, P., Goodwin, Jr., J.G. Effect of cobalt precursors on the dispersion of cobalt on MCM-41. Catal. Lett. 91 (2003): 95-102.
- Panpranot, J., Pattamakomsan, K., Goodwin Jr., J.G., Praserttham, P. A comparative study of Pd/SiO₂ and Pd/MCM-41 catalysts in liquid-phase hydrogenation. Catal. Commun. 5 (2004): 583-590.
- Pradyot Patnaik, Ph.D. Handbook of inorganic chemicals. New York: McGraw-Hill, 2002.
- Raman, N.K., Anderson, M.T. and Brinker, C.J. Template-based approaches to the preparation of amorphous, nanoporous silicas. Chem. Mater. 8 (1996) 1682-1701.
- Reuel, R.C., and Bartholomew, C.H. The stoichiometries of H₂ and CO adsorption on cobalt: effects of support and preparation. J. Catal. 82 (1984): 63-77.
- Riva, R., Miessner, H., and Piero, G.D. Metal-support interaction in Co/SiO₂ and Ti/O₂. Appl. Catal. A 196 (2000): 111-123.
- Sales, L.S., Robles-Dutenhefner, P.A., Nunes, D.L., Mohallem, N.D.S., Gusevskaya, E.V., Sousa, E.M.B. Characterization and catalytic activity studies of sol-gel Co-SiO₂ nanocomposites. Mater. Char. 50 (2003): 95-99.
- Schanke, D., Vada, S., Blekkan, E.A., Hilmen, A., Hoff, A., Holmen, A. J. Catal. 156 (1995): 85.

- Schuth, F., Wingen, A., Sauer, J. Oxide loaded ordered mesoporous oxides for catalytic applications. Microporous Mesoporous Mater. 465-476 (2001): 465-476.
- Shinoda, M., Zhang, Y., Yoneyama, Y., Hasegawa, K., and Tsubaki, N. New bimodal pore catalysts for Fischer-Tropsch synthesis. Fuel Processing Tech. 86 (2004):73-85.
- Song, C.S., Reddy, K.M. Mesoporous molecular sieve MCM-41 supported Co-Mo catalyst for hydrodesulfurization of dibenzothiophene in distillate fuels. Appl. Catal. A 176 (1999): 1-10.
- Sun, S.L., Tsubaki, N. and Fujimoto, K. The reaction performances and characterization of Fischer-Tropsch synthesis Co/SiO₂ catalysts prepared from mixed cobalt salts. Appl. Catal. A. 202 (2000): 121-131.
- Suvanto, S., Pakkanen, T.A. Temperature programmed studies of Co on MCM-41 and SiO₂. J. Mol. Catal. A 164 (2000): 273-280.
- Vob, M., Borgmann, D., and Wedler, G. Characterization of alumina, silica, and titania supported cobalt catalysts, J. Catal. 212 (2002): 10-21.
- Withers Jr., H.P., Eliezer, K.F., Mitchell, J.W. Slurry-phase fischer-tropsch synthesis and kinetic studies over supported cobalt carbonyl derived catalysts. Ind. Eng. Chem. Res. 29 (1990): 1807-1814.
- Wongsalee, T., Jongsomjit, B., Praserttham, P. Effect of zirconia-modified titania consisting of different phases on characteristics and catalytic properties of Co/TiO₂ catalysts Catal. Lett. 108 (2006): 55-61.
- Young, R.S. COBALT: Its Chemistry, Metallurgy, and Uses. New York: Reinhold Publishing Corporation, 1960.
- Zhang, Y., Wei, D., Hammache, S., Goodwin Jr., J.G. Effect of water vapor on the reduction of Ru-promoted Co/Al₂O₃. J. Catal. 188 (1999): 281-290.



APPENDICES

สถาบันวิทยบริการ
จุฬาลงกรณ์มหาวิทยาลัย

APPENDIX A

CALCULATION FOR CATALYST PREPARATION

Preparation of boron-modified MCM-41 supports by the incipient wetness impregnation method are shown as follows.

- Reagent:
- Boric acid (H_3BO_3)
Molecular weight = 61.81 g
 - Pure SiO_2 support
 - Pure MCM-41 support

Example calculation for the preparation of 1 wt% of boron-modified MCM-41

Based on 100 g for support used, the composition of the support will be as follows:

$$\begin{aligned} \text{Boron} &= 1 \text{ g} \\ \text{MCM-41} &= 100 - 1 = 99 \text{ g} \end{aligned}$$

For 5 g of catalyst

$$\text{Boron required} = 5 \times (1/99) = 0.0505 \text{ g}$$

Boron 0.0505 g was prepared from boric acid (H_3BO_3) and molecular weight of boron is 10.81

$$\begin{aligned} \text{Boric acid (H}_3\text{BO}_3\text{) required} &= \frac{\text{MW of boric acid} \times \text{boron required}}{\text{MW of B}} \\ &= (61.81/10.81) \times 0.0505 = 0.289 \text{ g} \end{aligned}$$

Since the pore volume of the pure MCM-41 support is 0.868 ml/g for MCM-41. Thus, the total volume of impregnation solution which must be used is 4.34 ml for MCM-41 by the requirement of incipient wetness impregnation method, the de-ionized water is added until equal pore volume for dissolve Boric acid (H_3BO_3).

Preparation of 20%Co/MCM-41 catalysts by the incipient wetness impregnation method are shown as follows.

Reagent: - Cobalt (II) nitrate hexahydrate [$Co(NO_3)_2 \cdot 6H_2O$]

Molecular weight = 291.03 g

- Boron-modified SiO_2 support
- Boron-modified MCM-41 support

Example calculation for the preparation of 20%Co/MCM-41

Based on 100 g for catalyst used, the composition of the catalyst will be as follows:

$$\begin{aligned} \text{Cobalt} &= 20 \text{ g} \\ \text{MCM-41} &= 100-20 = 80 \text{ g} \end{aligned}$$

For 5 g of catalyst

$$\text{Cobalt required} = 5 \times (20/80) = 1.0 \text{ g}$$

Cobalt 1.0 g was prepared from $Co(NO_3)_2 \cdot 6H_2O$ and molecular weight of Co is 58.93

$$\begin{aligned} Co(NO_3)_2 \cdot 6H_2O \text{ required} &= \frac{MW \text{ of } Co(NO_3)_2 \cdot 6H_2O \times \text{cobalt required}}{MW \text{ of } Co} \\ &= (291.03/58.93) \times 1.0 = 4.94 \text{ g} \end{aligned}$$

Since the pore volume of the pure MCM-41 support is 0.868 ml/g for MCM-41. Thus, the total volume of impregnation solution which must be used is 4.34 ml for MCM-41 by the requirement of incipient wetness impregnation method, the de-ionized water is added until equal pore volume for dissolve Cobalt (II) nitrate hexahydrate.

APPENDIX B

CALCULATION FOR TOTAL H₂ CHEMISSORPTION AND DISPERSION

Calculation of the total H₂ chemisorption and metal dispersion of the catalyst, a stoichiometry of H/Co = 1, measured by H₂ chemisorption is as follows:

Let the weight of catalyst used	=	W	g
Integral area of H ₂ peak after adsorption	=	A	unit
Integral area of 45 μl of standard H ₂ peak	=	B	unit
Amounts of H ₂ adsorbed on catalyst	=	B-A	unit
Concentration of Co (by AAS)	=	C	%wt
Volume of H ₂ adsorbed on catalyst	=	45 × [(B - A) / B]	μl
Volume of 1 mole of H ₂ at 100°C	=	28.038	μl
Mole of H ₂ adsorbed on catalyst	=	[(B - A) / B] × [45 / 28.038]	μmole
Total H ₂ chemisorption			
	=	[(B - A) / B] × [45 / 28.038] × [1 / W]	μmole/g of catalyst
	=	N	μmole/g of catalyst
Molecular weight of cobalt			
	=	58.93	
Metal dispersion (%)			
	=	$\frac{2 \times H_{2_{tot}} / g \text{ of catalyst} \times 100}{No \mu mole Co_{tot} / g \text{ of catalyst}}$	
	=	$\frac{2 \times N \times 100}{No \mu mole Co_{tot}}$	
	=	$\frac{2 \times N \times 58.93 \times 100}{C \times 10^6}$	
	=	$\frac{1.179 \times N}{C}$	

Table B.1 H₂ chemisorption results for various boron-modified supported Co catalysts samples.

Sample	Total H ₂ chemisorption ($\mu\text{mol} / \text{g cat}$)	
	N	M
20-Co/SiB-0	2.59	6.69
20-Co/SiB-1	2.77	6.83
20-Co/SiB-3	0.66	3.89
20-Co/SiB-5	0.08	3.27
20-Co/MB-0	2.43	14.30
20-Co/MB-1	2.01	11.81
20-Co/MB-3	1.02	6.03
20-Co/MB-5	0.45	2.63
5-Co/SiB-3	0.12	0.71
10-Co/SiB-3	0.20	1.19
15-Co/SiB-3	0.26	1.52
5-Co/MB-3	0.15	0.91
10-Co/MB-3	0.58	3.42
15-Co/MB-3	0.99	5.87

APPENDIX C

CALIBRATION CURVES

This appendix showed the calibration curves for calculation of composition of reactant and products in CO hydrogenation reaction. The reactant is CO and the main product is methane. The other products are linear hydrocarbons of heavier molecular weight that are C₂-C₄ such as ethane, ethylene, propane, propylene and butane.

The thermal conductivity detector, gas chromatography Shimadzu model 8A was used to analyze the concentration of CO by using Molecular sieve 5A column.

The VZ10 column are used with a gas chromatography equipped with a flame ionization detector, Shimadzu model 14B, to analyze the concentration of products including of methane, ethane, ethylene, propane, propylene and butane. Conditions uses in both GC are illustrated in Table C.1.

Mole of reagent in y-axis and area reported by gas chromatography in x-axis are exhibited in the curves. The calibration curves of CO, methane, ethane, ethylene, propane, propylene and butane are illustrated in the following figures.

Table C.1 Conditions use in Shimadzu modal GC-8A and GC-14B.

Parameters	Condition	
	Shimadzu GC-8A	Shimadzu GC-14B
Width	5	5
Slope	50	50
Drift	0	0
Min. area	10	10
T.DBL	0	0
Stop time	50	60
Atten	0	0
Speed	2	2
Method	41	41
Format	1	1
SPL.WT	100	100
IS.WT	1	1

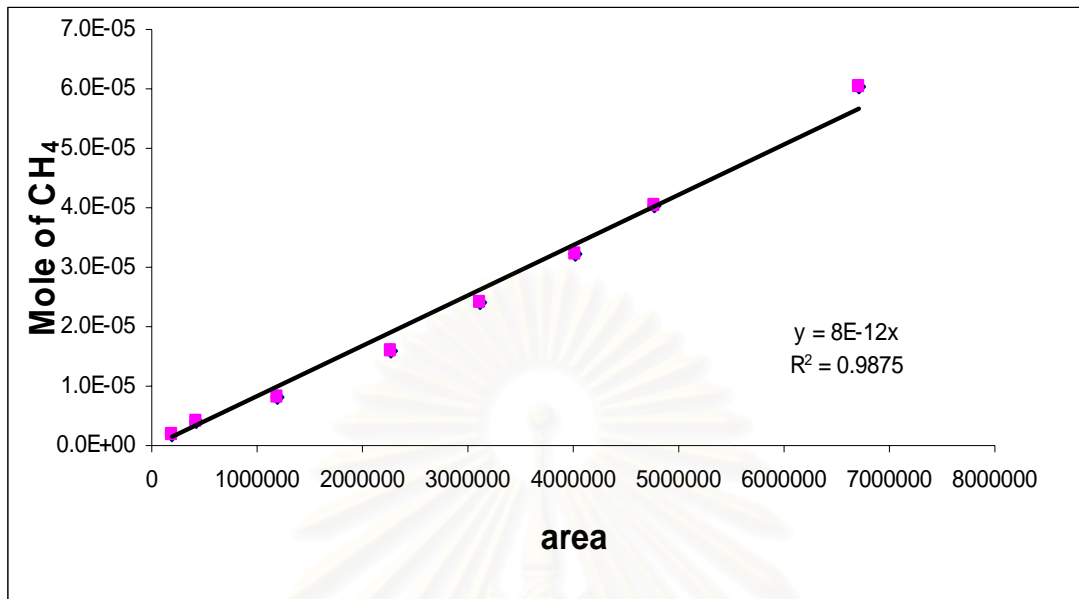


Figure C.1 The calibration curve of methane.

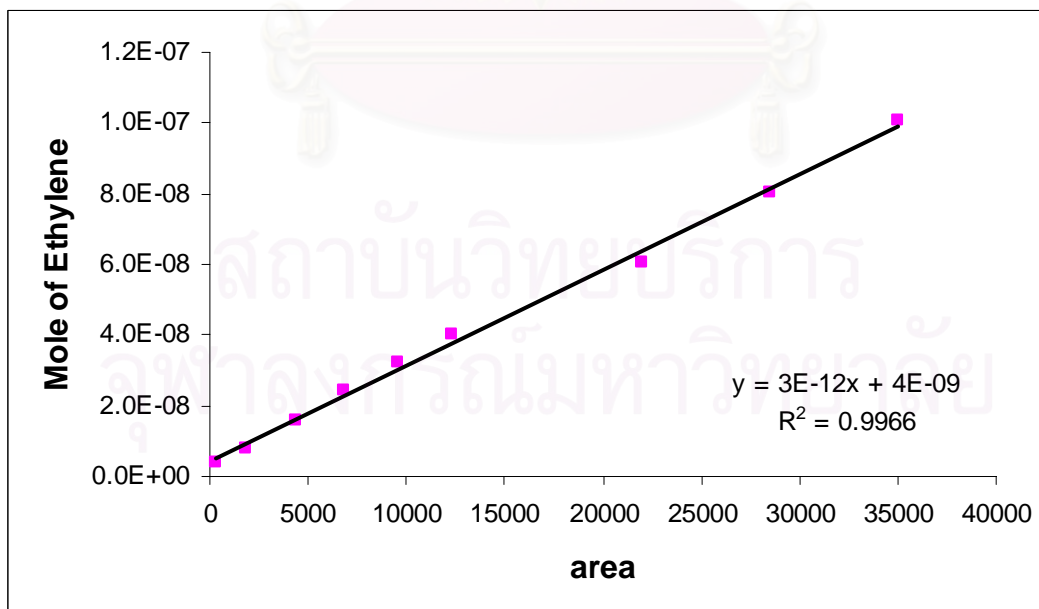


Figure C.2 The calibration curve of ethylene.

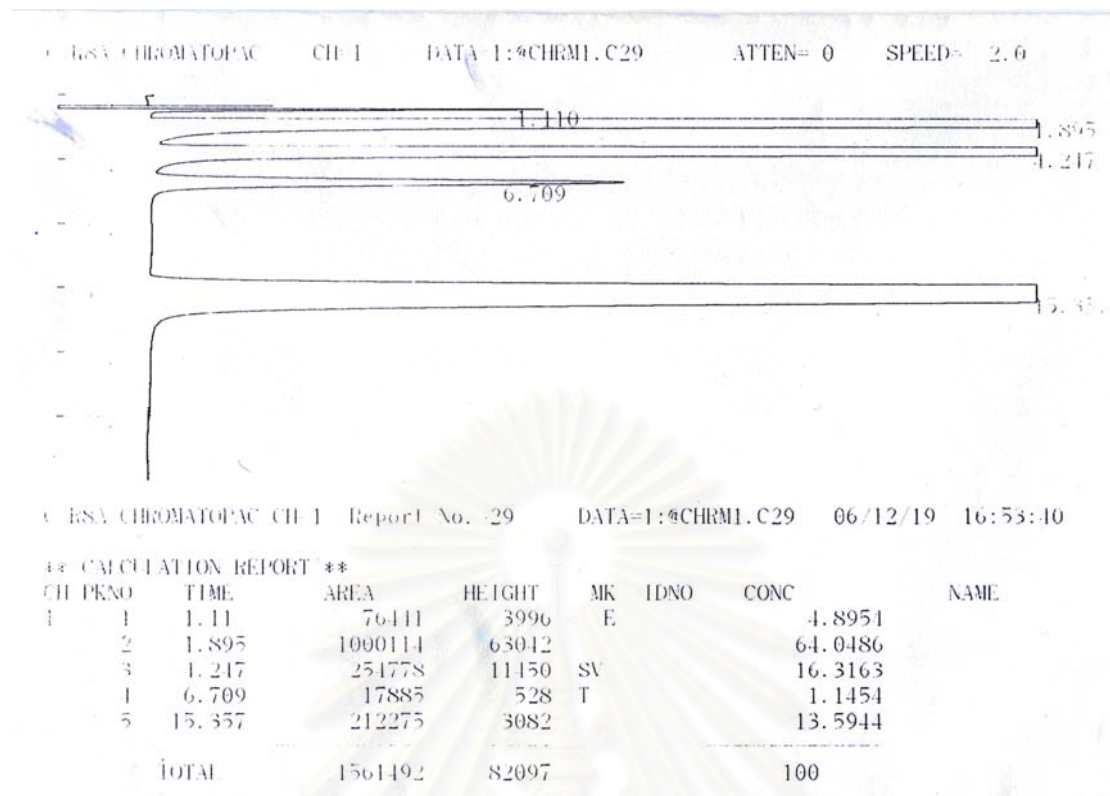


Figure C.3 The chromatograms of catalyst sample from thermal conductivity detector, gas chromatography Shimadzu model 8A (Molecular sieve 5A column).

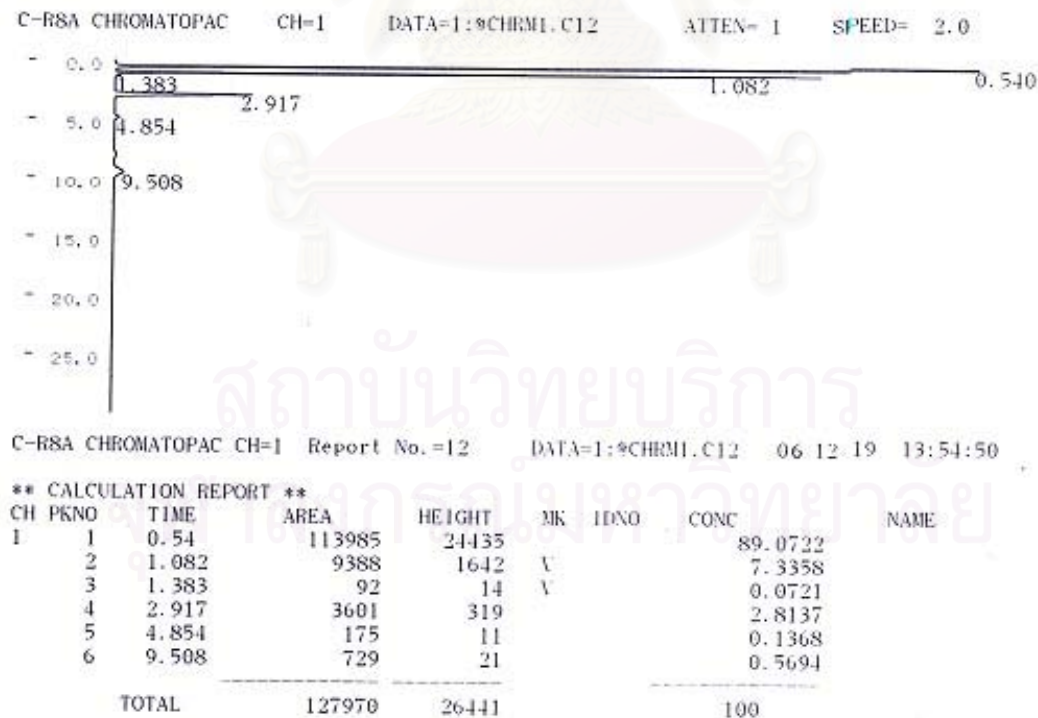


Figure C.4 The chromatograms of catalyst sample from flame ionization detector, gas chromatography Shimadzu model 14B (VZ10 column).

APPENDIX D

CALCULATION OF CO CONVERSION, REACTION RATE AND SELECTIVITY

The catalyst performance for the CO hydrogenation was evaluated in terms of activity for CO conversion rate and selectivity.

Activity of the catalyst performed in term of carbon monoxide conversion and reaction rate. Carbon monoxide conversion is defined as moles of CO converted with respect to CO in feed:

$$\text{CO conversion (\%)} = \frac{100 \times [\text{mole of CO in feed} - \text{mole of CO in product}]}{\text{mole of CO in feed}} \quad (\text{i})$$

Reaction rate was calculated from CO conversion that is as follows:

Let the weight of catalyst used	=	W	g
Flow rate of CO	=	2	cc/min
Reaction time	=	60	min
Weight of CH ₂	=	14	g
Volume of 1 mole of gas at 1 atm	=	22400	cc

$$\text{Reaction rate (g CH}_2\text{/g of catalyst)} = \frac{[\% \text{ conversion of CO} / 100] \times 60 \times 14 \times 2}{W \times 22400} \quad (\text{ii})$$

Selectivity of product is defined as mole of product (B) formed with respect to mole of CO converted:

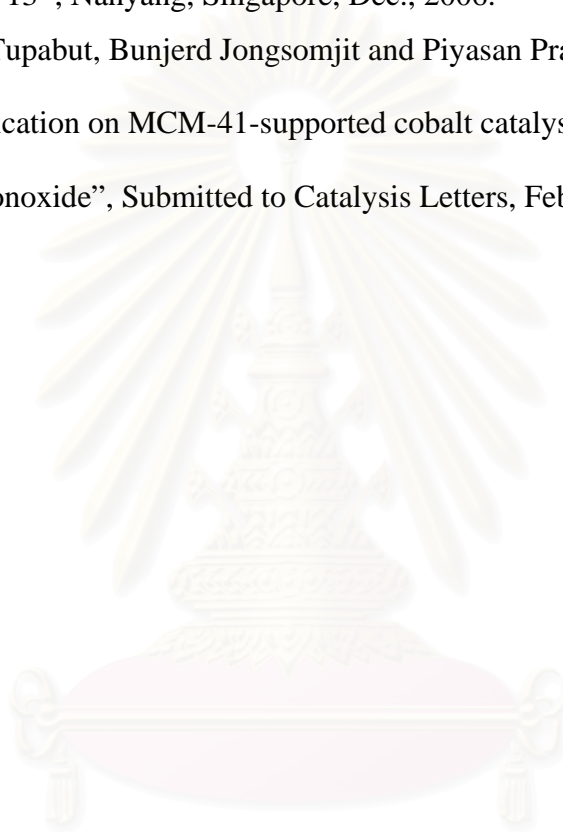
$$\text{Selectivity of B (\%)} = 100 \times [\text{mole of B formed} / \text{mole of total products}] \quad (\text{iii})$$

Where B is product, mole of B can be measured employing the calibration curve of products such as methane, ethane, ethylene, propane, propylene and butane

$$\text{mole of CH}_4 = (\text{area of CH}_4 \text{ peak from integrator plot on GC} - 14B) \times 8 \times 10^{12} \quad (\text{iv})$$

APPENDIX E**LIST OF PUBLICATIONS**

1. Pimchanok Tupabut, Bunjerd Jongsomjit and Piyasan Praserthdam, “Characterization of Co/SiO₂-B catalyst and catalytic properties during CO hydrogenation”, Proceedings of the Regional Symposium on Chemical Engineering 13th, Nanyang, Singapore, Dec., 2006.
2. Pimchanok Tupabut, Bunjerd Jongsomjit and Piyasan Praserthdam, “Impact of boron modification on MCM-41-supported cobalt catalysts for hydrogenation of carbon monoxide”, Submitted to Catalysis Letters, Feb., 2006.



สถาบันวิทยบริการ
จุฬาลงกรณ์มหาวิทยาลัย

VITAE

Mr. Pimchanok Tupabut was born on January 8th, 1983 in Singhaburi, Thailand. He finished high school from Bodindecha (Sing Singhaseni) 2 school, Bangkok in 2001, and received the Bachelor degree of Chemical Engineering from King Mongkut Institute of Technology Ladkrabang in March 2005. He continued his Master's study at the department of Chemical Engineering, Chulalongkorn University in 2006.



สถาบันวิทยบริการ
จุฬาลงกรณ์มหาวิทยาลัย